NASA
SPACE VEHICLE
DESIGN CRITERIA
(CHEMICAL PROPULSION)

NASA SP-8124

LIQUID ROCKET ENGINE
SELF-COOLED COMBUSTION CHAMBERS

SEPTEMBER 1977

NATIONAL AERONAUTICS AND SPACE ADMINISTRATION

FOREWORD

NASA experience has indicated a need for uniform criteria for the design of space vehicles. Accordingly, criteria are being developed in the following areas of technology:

Environment
Structures
Guidance and Control
Chemical Propulsion

Individual components of this work will be issued as separate monographs as soon as they are completed. This document, part of the series on Chemical Propulsion, is one such monograph. A list of all monographs issued prior to this one can be found on the final pages of this document.

These monographs are to be regarded as guides to design and not as NASA requirements, except as may be specified in formal project specifications. It is expected, however, that these documents, revised as experience may indicate to be desirable, eventually will provide uniform design practices for NASA space vehicles.

This monograph, "Liquid Rocket Engine Self-Cooled Combustion Chambers", was prepared under the direction of Howard W. Douglass, Chief, Design Criteria Office, Lewis Research Center; project management was by Harold Schmidt. This monograph was written by R. L. Ewen and H. M. Evensen, Aerojet Liquid Rocket Company and was edited by Russell B. Keller, Jr. of Lewis. To assure technical accuracy of this document, scientists and engineers throughout the technical community participated in interviews, consultations, and critical review of the text. In particular, C. D. Coulbert of the Jet Propulsion Laboratory, California Institute of Technology; John Campbell of the Rocketdyne Division, Rockwell International Corporation; A. R. Eberle of the Space Division, Rockwell International Corporation; T. F. Reinhardt of Bell Aerospace Company, Division of Textron Corporation; and W. G. Anderson of the Lewis Research Center individually and collectively reviewed the monograph in detail.

Comments concerning the technical content of this monograph will be welcomed by the National Aeronautics and Space Administration, Lewis Research Center (Design Criteria Office), Cleveland, Ohio 44135.

September 1977

GUIDE TO THE USE OF THIS MONOGRAPH

The purpose of this monograph is to organize and present, for effective use in design, the significant experience and knowledge accumulated in development and operational programs to date. It reviews and assesses current design practices, and from them establishes firm guidance for achieving greater consistency in design, increased reliability in the end product, and greater efficiency in the design effort. The monograph is organized into two major sections that are preceded by a brief introduction and complemented by a set of references.

The State of the Art, section 2, reviews and discusses the total design problem, and identifies which design elements are involved in successful design. It describes succinctly the current technology pertaining to these elements. When detailed information is required, the best available references are cited. This section serves as a survey of the subject that provides background material and prepares a proper technological base for the *Design Criteria* and Recommended Practices.

The *Design Criteria,* shown in italics in section 3, state clearly and briefly what rule, guide, limitation, or standard must be imposed on each essential design element to assure successful design. The *Design Criteria* can serve effectively as a checklist of rules for the project manager to use in guiding a design or in assessing its adequacy.

The Recommended Practices, also in section 3, state how to satisfy each of the criteria. Whenever possible, the best procedure is described; when this cannot be done concisely, appropriate references are provided. The Recommended Practices, in conjunction with the *Design Criteria,* provide positive guidance to the practicing designer on how to achieve successful design.

Both sections have been organized into decimally numbered subsections so that the subjects within similarly numbered subsections correspond from section to section. The format for the Contents displays this continuity of subject in such a way that a particular aspect of design can be followed through both sections as a discrete subject.

The design criteria monograph is not intended to be a design handbook, a set of specifications, or a design manual. It is a summary and a systematic ordering of the large and loosely organized body of existing successful design techniques and practices. Its value and its merit should be judged on how effectively it makes that material available to and useful to the designer.

CONTENTS

	Page
1. INTRODUCTION	1
2. STATE OF THE ART	3
3. DESIGN CRITERIA and Recommended Practices	61
APPENDIX A – Analytical Model for Gas Film Cooling	89
APPENDIX B – Analytical Model for Liquid Film Cooling	95
APPENDIX C – Conversion of U.S. Customary Units to SI Units	101
APPENDIX D – Glossary	103
REFERENCES	113
NASA Space Vehicle Design Criteria Monographs Issued to Date	121

SUBJECT	STATE OF THE ART		DESIGN CRITERIA	
ABLATIVE CHAMBERS	*2.1*	3	*3.1*	61
Thermochemical Design	*2.1.1*	6	*3.1.1*	61
Liner	*2.1.1.1*	6	*3.1.1.1*	61
Throat Insert	*2.1.1.2*	11	*3.1.1.2*	63
Insulation and Structural Shell	*2.1.1.3*	13	*3.1.1.3*	64
Structural Design	*2.1.2*	14	*3.1.2*	65
Throat Insert	*2.1.2.1*	14	*3.1.2.1*	65
Structural Shell	*2.1.2.2*	15	*3.1.2.2*	66
Attachments	*2.1.2.3*	16	*3.1.2.3*	67
Fabrication	*2.1.3*	19	*3.1.3*	68
Process Controls	*2.1.3.1*	21	*3.1.3.1*	68
Product Discrepancies	*2.1.3.2*	23	*3.1.3.2*	69
RADIATION-COOLED CHAMBERS	*2.2*	24	*3.2*	69
Thermal Design	*2.2.1*	24	*3.2.1*	69

SUBJECT	STATE OF THE ART		DESIGN CRITERIA	
Wall Materials	*2.2.1.1*	26	*3.2.1.1*	69
Wall Coatings	*2.2.1.2*	26	*3.2.1.2*	70
Wall Configuration	*2.2.1.3*	27	*3.2.1.3*	70
Structural Design	*2.2.2*	28	*3.2.2*	71
Chamber	*2.2.2.1*	28	*3.2.2.1*	71
Attachments	*2.2.2.2*	30	*3.2.2.2*	72
INTERREGEN AND HEAT-SINK CHAMBERS	*2.3*	33	*3.3*	73
Thermal Design	*2.3.1*	35	*3.3.1*	73
Wall Thickness and Film Cooling	*2.3.1.1*	35	*3.3.1.1*	73
Wall Contour	*2.3.1.2*	37	*3.3.1.2*	75
Hot Restart	*2.3.1.3*	38	*3.3.1.3*	76
Structural Design	*2.3.2*	38	*3.3.2*	76
Material Properties	*2.3.2.1*	38	*3.3.2.1*	76
Chamber Wall	*2.3.2.2*	39	*3.3.2.2*	77
Attachments	*2.3.2.3*	41	*3.3.2.3*	78
ADIABATIC-WALL CHAMBERS	*2.4*	43	*3.4*	79
Thermal Design	*2.4.1*	44	*3.4.1*	79
Materials	*2.4.1.1*	44	*3.4.1.1*	79
Structural Design	*2.4.2*	48	*3.4.2*	80
Chamber Wall	*2.4.2.1*	48	*3.4.2.1*	80
Attachments	*2.4.2.2*	49	*3.4.2.2*	81
Fabrication	*2.4.3*	49	*3.4.3*	81
HEAT TRANSFER TO THE CHAMBER WALL	*2.5*	51	*3.5*	82
Evaluation of Stanton Number	*2.5.1*	52	*3.5.1*	83
Film Cooling Analysis	*2.5.2*	56	*3.5.2*	86
Film Coolant Injection	*2.5.3*	58	*3.5.3*	88

LIST OF FIGURES

Figure	Title	Page
1	Typical design for an ablative chamber with throat insert	5
2	Material surface regression as a function of oxidizing potential of combustion products	9
3	Evolution of design for injector/chamber attachment for Apollo SPS	18
4	Two designs for attachment of ablative chamber to nozzle extension	20
5	Typical configurations for ablative-chamber fabric	21
6	Evolution of design for injector/chamber seal used on Apollo RCS engine	31
7	Injector/chamber attachment design providing thermal isolation of bipropellant valve	32
8	Injector/chamber attachment design providing thermal isolation of injector	32
9	Schematic of heat flow in an interegen chamber	34
10	Designs for attachment of beryllium chamber to injector and to nozzle	43
11	Corrosion characteristics of carbon with CTF oxidizer and various fuels at 6000°F and 500 psi	46
12	Four injector/chamber attachment designs for an adiabatic-wall chamber	50
13	Graph of heat-transfer data illustrating regions of reverse transition and laminarization	54
14	Effect of coolant/core-stream velocity ratio on coolant flow requirements	60
15	Parametric curves for determining wall thickness and coolant flow	74
16	Effect of acceleration on correlation coefficient for turbulent Stanton number	85
17	Entrainment fraction multiplier ψ_m as a function of area ratio (in expansion section)	87
A-1	Velocity-ratio correlation function f vs velocity ratio	92

Figure	Title	Page
A-2	Film-coolant effectiveness as a function of entrainment flow ratio	93
B-1	Liquid entrainment parameters A and a as functions of entrainment correlation parameter X_c	99

LIST OF TABLES

Table	Title	Page
I	Basic Features of Typical Operational Engines with Ablative Combustion Chambers	4
II	Typical Room-Temperature Properties of Three Different Phenolic Resins Reinforced with Silica Fabric	17
III	Typical Acceptance Limits for Properties of Representative Ablative Materials	22
IV	Basic Features of Typical Operational Engines with Radiation-Cooled Combustion Chambers	25
V	Properties of Refractory Metals and Alloys Used in Radiation-Cooled Chambers	29
VI	Basic Features of Operational Engines with Interegen and Heat-Sink Combustion Chambers	35
VII	Properties of Various Kinds of Bulk Graphite	41
VIII	Basic Features of R&D Engines with Adiabatic-Wall Combustion Chambers	45
IX	Typical Room-Temperature Properties of Fiber-Reinforced Graphite Composites	47

LIQUID ROCKET ENGINE

SELF-COOLED COMBUSTION CHAMBERS

1. INTRODUCTION

Self-cooled combustion chambers are chambers in which chamber wall temperature is controlled by methods other than fluid flow within the chamber wall supplied from an external source. In such chambers, adiabatic wall temperature may be controlled by use of upstream fluid components such as the injector or a film-coolant ring, or by internal flow of self-contained material; e.g., pyrolysis gas flow in charring ablators, and the flow of infiltrated liquid metals in porous matrices. (The use of infiltrated coolants is not considered to be within the present state of the art and is not treated herein.)

Five types of self-cooled chambers are considered in this monograph. The name identifying the chamber is indicative of the the method (mechanism) by which the chamber is cooled, as follows:

Ablative – A fiber-reinforced resin pyrolyzes endothermally within the chamber wall, releasing a gas and leaving a carbon matrix or char. The pyrolysis gas undergoes further reaction or cracking as it flows through the charred material to the inner surface, where it acts as a transpiration coolant.

Radiation Cooled – External radiation losses balance convective heating from the combustion products, thereby allowing the chamber wall to operate in thermal equilibrium.

Internally Regenerative (Interegen) – Heat is conducted away from the throat region and is absorbed by liquid film coolant over the forward part of the chamber.

Heat Sink – The heat capacity of the chamber wall limits surface temperatures (effective for a relatively short duration).

Adiabatic Wall – No self-cooling occurs; the chamber wall operates at the adiabatic wall temperature established by the combustion products and film coolant.

Except for the interegen and heat-sink concepts, each chamber type is discussed separately; these two chambers are considered jointly, since heat-sink chambers flown to date

physically are very similar to monolithic interegen designs. A separate and final section of the monograph deals with heat transfer to the chamber wall and treats Stanton number evaluation, film cooling, and film-coolant injection techniques, since these subjects are common to all chamber types. Techniques for analysis of gas film cooling and liquid film cooling are presented in Appendices A and B, respectively.

It must be noted that a particular type of chamber design can fall into more than one of the above cooling categories. For example, coated-columbium chambers can be purely radiation cooled, can be radiation cooled with adiabatic-wall temperature control, or can be operated as adiabatic-wall chambers with no dependence on radiation cooling. As noted, an interegen design can be physically similar to a film-cooled heat sink.

The primary problems in designing self-cooled chambers arise from the frequent need to use exotic high-temperature materials. For example, extensive use is made of composite and anisotropic materials, many of which undergo complex thermochemical reactions with significant changes in composition and state both at the surface and in depth. Only partially accomplished to date is the task of characterizing the dynamic thermochemical response of such materials and determining the properties required for this characterization. This monograph does not attempt to give a detailed description of the thermochemical behavior of these materials, but provides practical guides from the existing technology for material selection, chamber wall configuration, and mechanical and structural design.

The design of many self-cooled combustion chambers is intimately related to fabrication considerations, particularly in the case of the fiber-reinforced composite materials, since the material properties and chamber operating characteristics can be very sensitive to fabrication variables. As a result, some of the subject matter herein reflects this dependence on fabrication effects. The problem of attachment of high-temperature chambers to injectors and to nozzle extensions is treated in detail from the standpoint of its impact on the chamber design. However, the need to provide external thermal shielding for use in buried or clustered systems is considered secondary to the design of the chamber itself and is not discussed.

2. STATE OF THE ART

Self-cooled combustion chambers have been used primarily with chamber pressures less than 150 psi* and thrust levels less than 20 000 lbf*. These applications usually have featured multiple-firing duty cycles or continuous firings of limited duration, although continous firings of unlimited duration theoretically are possible with radiation-cooled, adiabatic-wall, and interegen chambers. Self-cooled chambers frequently are the only type suitable for low thrust levels because of the poor coolant flowrates per unit heat load and the fabrication difficulties associated with small fluid-cooled chambers. They are also favored when the propellants are poor coolants or when the feed system pressure is limited; and they are particularly suitable when fast response time and impulse accuracy are required, since there are no chamber coolant passages to fill or evacuate.

Among self-cooled chambers, ablative chambers are the most commonly used; applications range from small reaction-control engines to main propulsion systems. Radiation-cooled chambers have found wide application in spacecraft attitude-control engines that must operate for long accumulated durations in a pulsing mode. Tables giving typical applications of each type of chamber are presented in the appropriate sections that follow.

Present trends in the development of self-cooled combustion chambers include application at higher chamber pressures and thrust levels. New high-temperature materials are being developed, and more sophisticated use of injector film cooling and peripheral mixture-ratio control is providing better management of the thermal and chemical environment at the chamber wall; these developments are making practical chambers that are essentially adiabatic.

2.1 ABLATIVE CHAMBERS

Table I presents basic features of ablative chambers used in various engines with a range of thrust from 23 lbf to 21 500 lbf. Not all operational ablative-chamber engines are included, and not all of the listed engines are currently operational. No engine designed for service with fluorinated propellant has been included, since none has been sufficiently developed at this time to warrant inclusion. The selection of engines was made to include variations in size, duty cycle, materials, and design characteristics that are likely to arise in the design of new ablative-chamber engines.

In this monograph, an ablative material is defined as one that undergoes in-depth pyrolysis** of the resin. A number of resin systems fall into this category; however, the phenolics are used almost exclusively in ablative combustion chambers. To obtain sufficient structural strength for use in a combustion chamber, the phenolic resins must be reinforced. The

*Factors for converting U.S. customary units to the International System of Units (SI Units) are given in Appendix C.
**Terms, symbols, and materials are defined or identified in Appendix D.

Table I. – Basic Features of Typical Operational Engines with Ablative Combustion Chambers

Engine designation	Function	Propellants*	Thrust, lbf	Chamber pressure, psi	Chamber materials*
SE-7	Gemini OAMS	N_2O_4/MMH	23 79 94.5	135 126 133	SiC throat insert, silica/phenolic chamber liner, asbestos and glass overwrap, stainless steel shell.
SE-8	Apollo RCS	N_2O_4/MMH	91	137	JTA throat insert, silica/phenolic chamber liner, glass wrap, stainless steel shell.
Mira 150A	Surveyor Spacecraft vernier propulsion	MON/MMH	30 to 150	110	JTA throat insert, silica/phenolic chamber liner, titanium shell and skirt extension.
700800, SIVB	Saturn ACS	N_2O_4/MMH	147	101	Molybdenum throat insert with SiW coating, green Refrasil/phenolic chamber liner, glass wrap.
VTR-10	Apollo LEM descent engine	N_2O_4/A-50	9850	104	Silica/phenolic chamber liner, lightweight silica mat/phenolic insualtion, titanium shell.
Model 8258	Apollo LEM ascent engine	N_2O_4/A-50	3500	120	Green Refrasil/phenolic chamber liner, asbestos overwrap, aluminum shell.
AJ 10-137	Apollo SPS	N_2O_4/A-50	21 500	100	Rubberized silica/phenolic chamber liner, asbestos/phenolic insulation, glass wrap.
AJ 10-138	Titan III Transtage propulsion	N_2O_4/A-50	8100	108	Rubberized silica/phenolic chamber liner, asbestos/phenolic insulation, glass wrap.
XLR-66-AJ-2	Space throttling (development tested)	N_2O_4/A-50	9000	200	Silica/phenolic chamber and nozzle, glass wrap.
R-8D	Space RCS throttling (development tested)	N_2O_4/MMH	100	126	SiC-coated graphite chamber liner, silica/phenolic shell.
P8-1	Lance main propulsion	IRFNA/UDMH	—	—	SiC throat insert in central sustainer, silica/phenolic annular booster chamber liner.

*Identified in Appendix D

standard reinforcement is fibrous, consisting of either fiber-woven fabrics or chopped fibers of materials such as silica, graphite, or carbon. The in-depth pyrolysis of the resin, which drives off oxygen and hydrogen and leaves a carbon matrix, is endothermic. This characteristic provides a very effective means of thermal control that is especially well suited for high-performance, short-to-medium-duration duty cycles.

Ablative chambers perform well in pulse-mode operation and under throttleable conditions. They are, however, in general limited to total firing durations of less than 10 minutes. For longer durations, the required wall thicknesses exceed practical fabrication limits.

An ablative chamber usually consists of a flame liner (of reinforced phenolic resin), a structural shell, and provisions for attachment of the chamber to the injector and, in some cases, to a nozzle extension. In large chambers (> 1000 lbf thrust), the liner usually is overwrapped with additional reinforced phenolic that functions as insulation. In engines where throat erosion would exceed specified limits, "hard" throat inserts are incorporated. An example of an ablative chamber design is shown in figure 1.

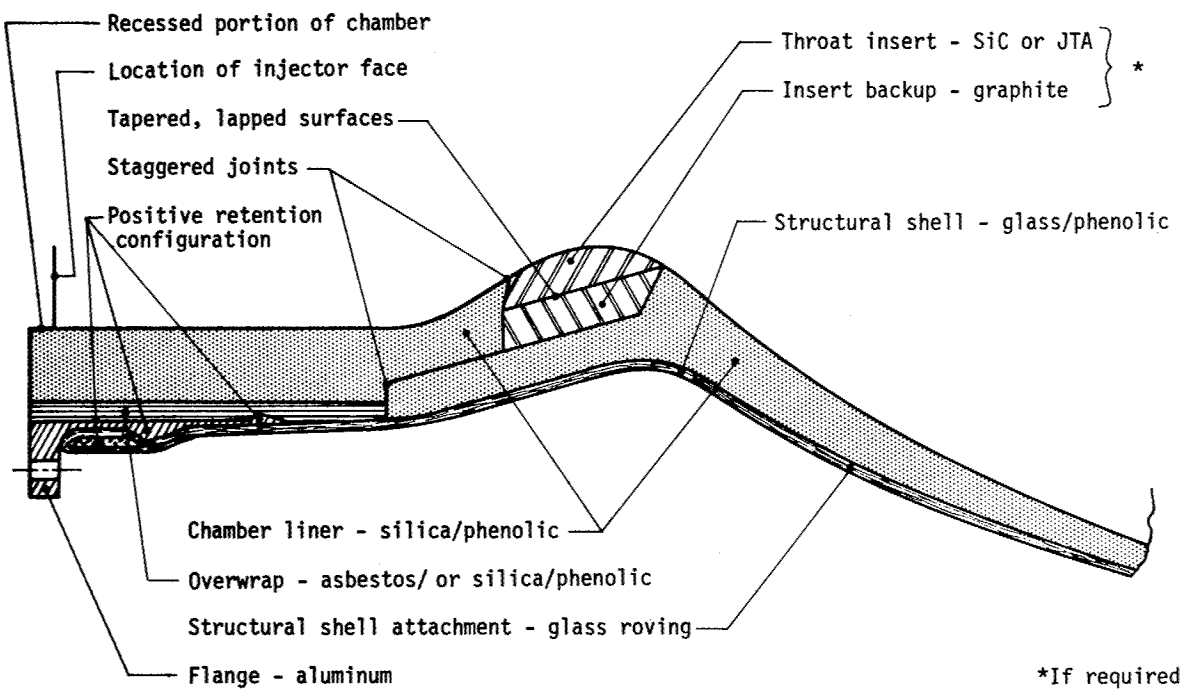

Figure 1. — Typical design for an ablative chamber with throat insert.

Ablative combustion chambers are assembled in so many different ways that only general practices can be presented. When several liner components are used, especially throat inserts, joints are staggered axially to prevent a direct leak path to the outer structural shell. Also, joints are located in areas where they are not likely to open up under imposed thermal or pressure loads. Differential thermal expansion of components is taken into account by selecting materials with comparable elastic moduli or by inserting crushable or flexible materials to allow expansion without the development of excessive strain-induced stresses.

2.1.1 Thermochemical Design

2.1.1.1 LINER

All ablative materials used for combustion-chamber liners are composites of fiber or fabric reinforcement in a resin matrix. When the constituents are altered, various characteristics of the composite material are changed. The resin system in particular is subject to modifications. For example, a modification used in the Apollo SPS system was the addition of acrylonitrile rubber to the basic phenolic system. This modification resulted in a reduction in density, thermal conductivity, and especially in elastic modulus. The thermal expansion, on the other hand, was increased appreciably, as was the permanent shrinkage after heating to above 300°F.

In addition to laminated chambers, in which the ablative material is used in tape or fabric form, molding compounds have been used in several (usually small) experimental engines. The molding compounds contain reinforcement (silica, carbon, etc.) in form of chopped fibers or chopped fabric. Since the reinforcement is randomly oriented relative to the chamber axis, molded components generally are subject to less uniform surface erosion than are laminated parts; sporadic spallation or chunking resulting from locally excessive internal stresses can and often does occur. This condition usually is not serious in that the performance is not measurably degraded and generally the thickness is adequate to prevent local burnthroughs.

The basic requirements for an ablative liner for a combustion chamber comprise chemical compatibility with the combustion gases, capability to withstand high temperatures, and structural strength. Chemical compatibility is especially important, since material surface regression due to reaction of the wall material constituents with the combustion gas species can be severe enough to make the material unacceptable as a liner. The combustion products of all the engines listed in table I, for example, contain large concentrations of water vapor. Graphitic materials and most refractory metals and alloys suffer excessive losses from oxidation when exposed to water vapor, and thus cannot be used in these engines unless the exposed surfaces are protected with oxidation-resistant coatings or the maximum wall surface temperature is kept below about 3000°F. Ablative liner materials that are most compatible with water vapor include glass, silica, quartz, asbestos, and magnesium

hydroxide. Silica is, by far, the reinforcement that has the widest usage in all operational engines. The commercial products generally consist of about 99 percent SiO_2, and the balance is made up of various other metal oxides, mainly TiO_2 and Al_2O_3. The glass reinforcement used in rocket nozzle applications consists of 55- to 65-percent SiO_2, with the balance primarily Al_2O_3, CaO, MgO, and B_2O_3. Glass softens at a temperature as low as 1500°F in comparison with about 3000°F for silica and quartz. The latter is a high-purity silica with about 99.9 percent SiO_2.

Even though asbestos and magnesium hydroxide are acceptable materials on the basis of chemical compatibility and melting points, they have other limitations that make their use less attractive. Both materials contain water of hydration and undergo considerable shrinkage during pyrolysis. As a consequence, the char that forms is relatively weak and is easily sloughed off, especially on restarts after complete cooldown. Reference 1 reports that magnesium hydroxide/phenolic chambers operating at 100 psi and 1000 lbf thrust could not be test fired for more than 100 seconds because of excessively high throat erosion rates. The propellants were N_2O_4/A-50 at a mixture ratio (MR) of 1.6.

Reference 2 reports that although magnesium hydroxide reinforcement performed well in low-velocity regions in the chamber and exhibited small char depths in comparison with silica/phenolic, its performance was poor (high erosion rate) under the high gas dynamic shear loads at the throat. The test vehicle utilized an Apollo SPS injector and operated with N_2O_4/A-50 at MR of 2.0 at 200 and 300 psi and 16 000 and 25 000 lbf thrust, respectively; the ablative chamber was made up of rings of various materials contained in a steel housing. In the same program, it was found that asbestos/phenolic shrank significantly on cooldown, especially in a direction perpendicular to the laminates. This characteristic is undesirable for chamber liner materials in engines requiring restarts after cooldown, since it may result in gas flow through gaps and potential burnthroughs. Asbestos/phenolic, however, is used successfully as a nozzle extension liner in the second-stage Titan engine. The delaminations and cracks that are plainly in evidence after completed duty cycles generally have not resulted in unacceptable performance.

Glass reinforcement has been used in experimental chambers and is in use in solid rocket nozzles intended for short-duration firing. The low melting point of glass, however, precludes its use in most liquid rocket engine applications. Both silica and quartz form structurally strong chars and have the advantage of forming tenacious surface layers when the reinforcement melts ($\approx$ 3100°F). Silica/phenolic combustion chambers designed for low pressures ($<$ 125 psi) have operated at wall temperatures exceeding 3100°F without suffering appreciable surface regression. At higher chamber pressures, gas shear forces tend to remove the molten silica layer from the surface.

2.1.1.1.1 Surface Regression

The primary regression problem, in the absence of a throat insert, is surface erosion at the throat. The mechanisms involved in regression are not yet understood to the extent that

they can be fully treated analytically. In addition, the local mass velocity and mixture ratio provided by the injector usually are not well known, although techniques described in references 3 and 4 can be used to estimate these variables. Mass loss occurs by chemical reaction between the ablative material and combustion gases and by mechanical means (erosion). The latter is primarily responsible for the uncertainty in predicting the surface recession of an ablative material with known boundary conditions. Mechanical erosion is affected by the environment (e.g., temperature, pressure, and gas velocity) and by material properties and characteristics such as melt temperature, strength of charred material, chemical reaction between the reinforcement and the charred matrix material, viscosity and tenacity of the surface melt layer, and surface roughness.

Analytical tools to predict surface recession have been developed (refs. 5 through 8), but the analytical results are not in good agreement with test data. The surface thermochemistry models include kinetically controlled reactions between the surface and the boundary layer, vaporization, sublimation, simulated mechanical erosion, and the homogeneous reactions in the boundary layer resulting from the injection of the products of these processes and of pyrolysis gas. The weakness of these models lies primarily in the kinetics models and parameters required for the heterogeneous reactions (although some carbon reactions have been characterized successfully) and in the representation of the surface failure mechanism for silica/phenolic. At temperatures above about 3000°F, a viscous layer of silica can form at the surface, at least if there is sufficient carbon depletion due to reaction of the carbon with the boundary layer and with the silica itself. Usually these chars are silica rich, so that the silica reaction does not prevent formation of the viscous layer. The effect of the gas shear forces on this layer has not been predicted adequately.

Since analytical techniques are not reliable, surface regression predictions must be based on empirical correlations. For char-forming materials, reference 9 recommends a surface temperature correlation of the form

$$\text{Regression rate} = a\, T_w^b \exp(-c/T_w) \qquad (1)$$

where a, b, and c are empirical constants and T_w is gas-side wall temperature. This expression (which was used in the design effort of ref. 10) yields regression rate in in./sec when T_w is expressed in °R. For silica/phenolic materials, reference 9 gives the following values for the empirical constants: a = 0.11, b = 2, and c = 10^5.

Hundreds of test firings have demonstrated that material regression is greatly dependent on the oxidizing potential of the combustion products, as shown in figure 2 for four materials (ref. 11). The oxidant value is defined as $\ln(1 + C_{ox})$, where C_{ox} is the concentration of oxidizing series in the combustion gases as computed from thermochemical data. At high oxidant values, the regression is caused primarily by chemical corrosion rather than by mechanical erosion. Experimental data have shown good correlation between regression rate and heat transfer coefficient. Since heat transfer coefficient is regarded as proportional to

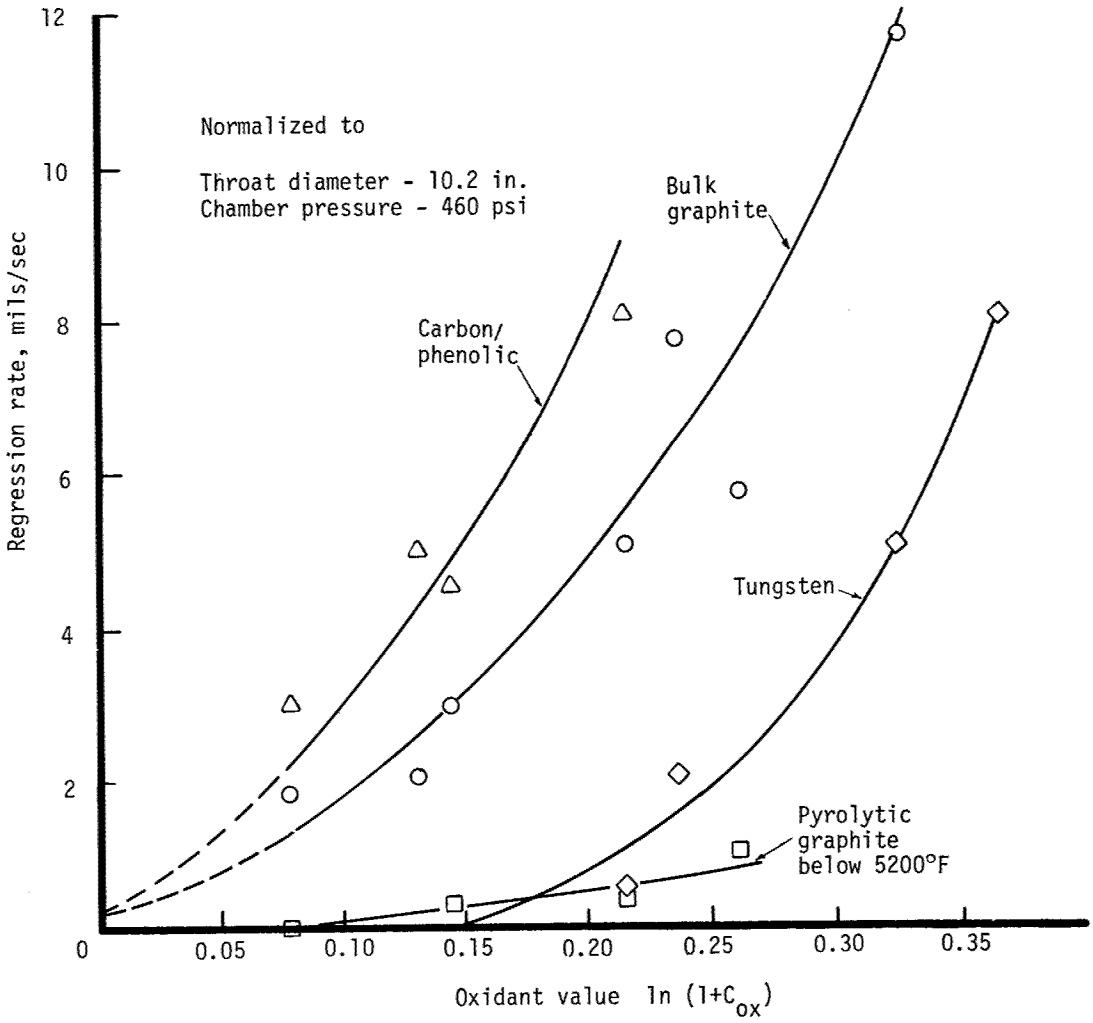

Figure 2. — Material surface regression as a function of oxidizing potential of combustion products.

$P_{ch}^{0.8}/D_t^{0.2}$ * (ref. 12), then for a given material and oxidant value, regression rate can be regarded as proportional to this same ratio.

Surface regression, in engines operating at low chamber pressures (< 125 psi), can be controlled at an acceptable low and uniform rate by film or barrier cooling that primarily affects the wall temperatures and secondarily the chemical environment in the boundary layer. Reference 13 reports throat regression of silica/phenolic was practically non-existent up to 3000°F, whereas significant regression occurred when the wall temperature was 3400°F. At temperatures higher than 3400°F, throat inserts are required at low as well as high chamber pressure. A program to develop and demonstrate a 300-psi, 3000-lbf-thrust, N_2O_4/N_2H_4 PBPS engine found that, even with temperatures controlled to less than 3000°F by use of barrier cooling, the silica/phenolic liner suffered excessive throat erosion after many restarts (ref. 14). The high chamber pressure caused sloughing off of the char layer that would have remained in place at lower pressures. The erosion problem was solved by incorporating a fiber-reinforced graphite composite (AGCarb-101) liner. Even though graphite is not compatible with the combustion products of N_2O_4/N_2H_4 (which contain a high concentration of water vapor), the N_2H_4 barrier cooling and the low wall temperatures prevented surface regression.

In a program designed to improve the performance of and extend the mission capability of the Apollo LEM descent engine, quartz-fabric/phenolic exhibited only half the throat regression of the standard silica-fabric/phenolic (ref. 15). This difference was attributed to the higher viscosity of the melt layer and the improved mechanical properties. An independent program also found that quartz-fabric throats performed better than the silica counterparts (ref. 16). However, quartz is more expensive than silica and appears to present a few fabrication problems (e.g., delamination) (ref. 17). Relative to variations in silica reinforcements, there is no evidence of difference in performance between standard silica fabric and green Refrasil or among silica fabrics from different suppliers. The type of weave, however, imparts different properties to the end product. Examples of commonly used fabric weaves are square and 8-harness satin. Among the carbon and graphite reinforcements, tensile strength and modulus vary over fairly wide ranges.

Ablative chambers generally are designed with ablative liner thicknesses sufficient to prevent the liner being charred completely through under the worst operating duty cycles, including heat soaks. The problem of determining the appropriate thickness for ablative materials is a difficult one, for ablative materials respond in a variable way when tested repetitively in identical environments. Char depths are calculated by computer programs (refs. 3 through 8) that account for resin decomposition and flow of the resultant pyrolysis gases through the char layer in addition to the basic heat conduction through the chamber wall. Since the char thermal conductivity and its temperature dependence are not well known or easily measured, it is essential that predictions of char depth be correlated with experimental data. Variations in material characteristics and in boundary conditions (due to injector streaking) must be accounted for by correlating analytical models with maximum char depths or by

*P_{ch} is chamber pressure and D_t is throat diameter

applying a safety factor to the predicted value. Typically, char depths vary by ± 25 percent in silica/phenolic liners with negligible surface regression. Duty-cycle effects can be accounted for by simple empirical correlations. For example, mean char depths for Apollo SPS, Transtage, Delta F, and a number of other low-pressure (90-125 psi) silica/phenolic applications are given by the expression

$$\text{Char depth, in.} = 0.04 \sqrt{\text{firing duration, sec.}} \tag{2}$$

The consequences of charring completely through an ablative liner may be disastrous, as evidenced in the Delta-Transtage development program, where a combustion-chamber liner was ejected as a result of a gas leak between the liner and its overwrap (ref. 18). The chamber liner was charred completely through in local areas upstream of the throat, and a delamination extended completely through the liner wall in an area downstream of the throat. The interface bond between liner and overwrap was degraded by excessive heating, and pressure differential was sufficient to induce a gas flow. It was postulated that the pressure load on the liner at the delaminated area propagated quickly around the periphery (the rubber-modified silica/phenolic has poor interlaminar shear strength) and resulted in complete separation.

Practically all ablative chambers in current use are of laminated construction, with laminate orientation varying from 6° to 60° relative to the chamber surface. No optimum angle has been established, since no universally accepted performance criteria can be formulated. Generally, the orientation selected is a compromise of a number of design and fabrication requirements. On the basis of regression rate only, tests of 30°, 45°, 60°, and 90° orientation to the chamber surface contour showed that 60° orientation was optimum (ref. 19). However, on the basis of considerations other than regression rate, reference 20 reports that 6° gave the best performance in an ACS chamber. A low angle results in low thermal conductivity in the radial direction, a condition that reduces the liner thickness required to maintain a given temperature at the liner interface with the structural shell or insulation.

2.1.1.2 THROAT INSERTS

Throat inserts are used in ablative chambers when throat erosion of the liner is great enough to reduce performance below tolerances. This condition occurs when the surface temperature is appreciably higher than the reinforcement melt temperature or when gas shear forces exceed the strength of the charred material. Inserts are, of necessity, made of material that can withstand high temperatures and still sustain low erosion even in oxidizing environments. This requirement has limited the material selection to refractory ceramics and graphite composites. Refractory metals generally are not used because of recrystallization and increased brittleness after initial thermal exposure to 2400°F or above. The increased brittleness makes them less suitable for applications requiring many restarts. The Saturn IVB attitude-control engine had a molybdenum throat insert with a SiW coating; however, the maximum temperature was believed to be less than 2400°F.

References 21 and 22 report on a comprehensive throat insert evaluation program that used both small (1.20 in. diam.) and relatively large (7.82 in. diam.) chambers with N_2O_4/A-50 propellants; reference 23 reports results of a design and testing program to evaluate improved throat inserts. The general conclusions from these reports were that oxides and carbides provided the best oxidation protection but were limited by sensitivity to thermal shock. Silicon carbide is the old standby; used as an insert, it usually is modified to render it less shock sensitive. The modification most frequently used is called KT silicon carbide; it contains 1.5% to 4% silicon. KT silicon carbide was used in attitude and reaction control engines such as SE-7 and SE-9 and also in the Lance sustainer engine. The inserts do crack; however, since they are retained by a taper, they remain in place. Another modification consists of uniformly dispersing graphite particles in the silicon carbide matrix to enhance its ductility and thereby improve its resistance to cracking from thermal shock; a type that has performed well as a solid rocket engine throat insert is GRB silicon carbide. Silicon carbide also is used as a coating on graphite substrates.

The selection of coating thickness and type of substrate has been the subject of many investigations. It was found (refs. 21 and 22) that a 0.050-in.-thick SiC coating pyrolytically deposited on a UT-6 graphite substrate cracked as a result of thermal stress, whereas a 0.030-in.-thick coating (deposited in the same manner and on the same substrate material) produced an adherent bond. Two other inserts of SiC pyrolytically deposited on SX-4 graphite with coating thicknesses of 0.023 and 0.037 in. also produced adherent bonds and prevented thermal stress failures. The SX-4 graphite substrate was chosen in an attempt to match the thermal expansion of the SiC coating during firing. SiC coatings applied by pack cementation were also tested. Although this process resulted in an improved bond due to diffusion of the coating into the substrate, the oxidation resistance was not as good as that of pyrolytically deposited coatings, probably because of the porosity of the pack cementation coatings. Best results were obtained with a vapor-deposited SiC coating (Marquardt RM005) on a graphite substrate (Le Carbone grade P2239) (ref. 24).

Some experimental work has been done with carbide coating on fibrous-graphite composite substrate instead of on bulk graphite (ref. 25). Improved adherence was obtained, but further development is required.

Since all carbides including silicon carbide (pure as well as modified) are essentially brittle, attempts have been made to find replacement materials. Composites of graphite and oxidation-resistant metals have shown most promise in experimental evaluation programs. A typical example is JTA, which consists of 48% graphite, 35% zirconium, 9% silicon, and 8% boron (nominal values). JTA throat inserts were used in the Apollo Command Module reaction control engine (SE-8) and in the Surveyor Spacecraft vernier propulsion engine (MIRA-150). JTA has the same temperature capability as silicon carbide (about 3600°F in an oxidizing environment), but suffers slightly higher erosion losses. Its advantage over silicon carbide is its improved thermal shock resistance. In the Apollo Command Module RCS engine, throat spalling occurred occasionally; it was usually associated with exposure to moisture prior to or during the firing sequence. The problem was resolved by imposing more stringent requirements on JTA processing and properties.

In high-temperature (> 3600°F) applications with oxidizing combustion gases, where neither JTA nor silicon carbide is adequate because of excessive surface regression, pyrolytic graphite (PG) and high-density carbon/carbon composites are the only materials sufficiently developed to be considered at the present time. PG has been used in many liquid and solid rocket propulsion engines, either in form of washers or wedges or as coatings deposited on graphitic substrates. Several design limitations result from the anisotropic properties of PG, as discussed further in section 2.1.2.1. Thermal conductivity in the plane of deposition (a-b plane) is about 100 times that in a direction normal to that plane (c-direction), whereas the thermal expansion in the c-direction is about 10 times that in the a-b direction. The greatest problem with PG coating, however, is its tendency to spall or crack. This tendency has been reduced by proper selection of coating thickness, substrate material, and coating process parameters (refs. 26 and 27).

A number of material systems for throat inserts in high-temperature (> 4000°F) environments are being developed and evaluated. They include various oxides, carbides, nitrides and diborides, composite and laminate structures, and coatings. These materials and related processes have not been developed sufficiently to be considered state-of-the-art materials or processes.

2.1.1.3 INSULATION AND STRUCTURAL SHELL

Chamber liners are designed primarily to inhibit surface regression, and they are not necessarily the best insulators. Therefore, ablative chambers typically include an insulative overwrap between the liner and the structural shell. Both fiberglass and metal support structures have been used. Examples of fiberglass structures are found in the Transtage and the Apollo SPS engines. In the Lance booster and LEM descent engines, metal structures of steel and titanium, respectively, were used. In the LEM ascent engine, the support structure was a combination of aluminum and fiberglass.

The fiberglass structures generally incorporate both fabric and roving reinforcement with a phenolic resin. These structures offer the advantage of being easily fitted to irregular combustion chamber shapes. Metal flanges and other reinforcements such as gimbal ring attachment brackets are wrapped into the fiberglass structure.

Metal structures of either steel or aluminum are relatively inexpensive and find wide usage in workhorse and development combustion chambers. They are especially well suited to chambers with sea-level (low-expansion-ratio) nozzles that require simple cylindrical or conical shapes. A relatively unique approach to chamber structural design was demonstrated in the LEM descent engine, which incorporated a "hot" structural member. The titanium case was designed to operate at temperatures in excess of 800°F, thereby permitting the flame liner and overwrap insulation to char completely through during the last burn. This design condition reduces the overall liner thickness and as a result the chamber weight is reduced.

The structural shells, especially those of fiberglass, are vulnerable to flow of hot gases from the combustion products and from resin pyrolysis. The shell is exposed to these hot gases if the liners contain delaminations through their entire thickness. This potentially serious condition is another reason for the use of flatwise insulation overwraps.

The selection of insulation material must take into account whether the insulation is load carrying. When the chamber incorporates throat inserts and also when the structural member is fiberglass, the insulation must be capable of transmitting imposed loads (mechanical and thermal) from the chamber liner to the structural shell. A typical example is the Apollo SPS combustion chamber, which incorporates asbestos/phenolic as an insulative, load-carrying overwrap. Asbestos/phenolic is an excellent material for this application, combining low thermal conductivity, high strength, and low cost. However, problems result from the high resin content and high volatile content of standard asbestos/phenolic. In thick sections, especially if the asbestos/phenolic is wrapped parallel with the surface, the volatiles from the resin cure encounter high resistance to flow along the plies and to diffusion through the plies. As a consequence, areas with high concentrations of residual volatiles may exist. In the Apollo SPS development program, blistering of the overwrap occurred in chambers exposed to long-duration firings. The cause of the blistering was deduced to be local concentrations of residual volatile matter that expanded when the overwrap was heated during firing or during subsequent heat soak (ref. 28). "Staging" of the material and re-orientation of the overwrap to facilitate volatile escape solved the problem. This problem, on the other hand, did not arise in the Titan III Transtage program, which utilized the same liner and overwrap materials. In the Transtage chamber, the asbestos overwrap was fairly thin (about 0.18 in.), whereas in the initial Apollo chamber the thickness exceeded 0.3 in.; the increased thickness resulted in increased resistance to flow of volatile gases by diffusion through the plies. In addition, the insulation in the initial Apollo chamber was wrapped parallel to the surface, thereby creating long flow paths for volatile escape along the plies.

Silica/phenolic also has been used as a load-carrying insulation. Standard-weight silica/phenolic (density about 1.73 gm/cm^3) is thermally more stable and has a lower resin content and lower volatile content than asbestos/phenolic. A lightweight silica/phenolic (density about 0.96 gm/cm^3) was used as a chamber insulation in an improved LEM ascent engine, successfully replacing a lightweight asbestos/phenolic (density about 1.28 gm/cm^3) (ref. 29). The primary problems with this material were variations in ply thickness and density; these problems were solved by fabrication and process controls instituted by the fabricator and the supplier of pre-impregnated materials.

2.1.2 Structural Design

2.1.2.1 THROAT INSERTS

Throat inserts have failed in the following modes:

(1) Spalling on the inside surface as a result of high biaxial compressive loads generated by the extreme thermal gradients that arise during the start phase of operation.

(2) Cracking of the insert by tensile stresses on the outside surface of the insert. Cracking usually occurs when the outside surface of the insert is still relatively cool and the bulk of the insert is hot. Internal pressure also contributes to this type of failure.

(3) Hoop compressive failure due to constraints placed on the insert by the material surrounding the insert.

(4) Axial compressive failure due to large axial thermal growths of the liner adjacent to the insert.

The question of whether to provide an external support for the insert or seal it in an ablative material that degrades during the firing can be answered only by analysis of each specific design. An external support may generate excessive compressive loads on the inner surface of the insert and result in spalling. Conversely, a flexible external structure may result in insert cracking as a result of excessive tensile loads on the insert outer surface. Both of these conditions have occurred in experimental and development programs.

Throat insert configurations vary considerably among different designs. Although some inserts are made with converging-diverging shapes, most inserts are designed with either a cylindrical or a conical outer contour. The conical insert (with the small end aft) is required in designs in which the insert is supported by an ablative material that is subject to thermal expansion and then subsequent shrinkage as the material chars. Without a conical interface, the insert would be loose, and the chamber would not be suitable for restarts. The bondline usually is filled with an elastomeric material (e.g., RTV-60 or Silastic). The filler acts both as a cushion for the insert and as a sealant to prevent gas leakage.

When pyrolytic graphite (PG) has been used as a stack of flat washers, it has been customary to allow for axial thermal expansion by incorporating crushable gaskets or spacers. In some applications, springs have been used (refs. 23 and 30); however, a spring system tends to become heavy and complex.

2.1.2.2 STRUCTURAL SHELL

The support structure in an ablative chamber has failed in the following modes:

(1) Failure of the structural shell as a result of axial loads generated by chamber pressure, vehicle accelerations, start transients, and thermal growth of the liner. When glass fabric is used as the structural material, unidirectional fabric generally is employed, the high-strength direction being made parallel to the chamber axis.

(2) Burst of the structural shell as a result of chamber pressure and radial expansion of the liner. Therefore, glass roving usually is wrapped over a fabric structure in the hoop direction.

(3) Shear/tension or compression failure of the glass shell as a result of bidirectional loading of the glass laminates.

Typical room-temperature properties of several silica/phenolics are given in table II.

Efficiently designed ablative chambers will operate with a liner-to-structure interface temperature above the degradation temperature of most adhesives. An adhesive joint between the liner and structure therefore is not depended on to transmit any loads. Generally the chamber configuration is designed to provide a mechanical joint to retain the liner; otherwise, flanges or shoulders are incorporated.

When metal shells, especially stainless steel shells, are used, allowance is made for differential thermal expansion of liner and shell; otherwise excessive compressive stresses in the liner may result from the elastic modulus of the shell being higher than that of the liner. Thermal expansion of the liner is not a problem with fiberglass shells, since thermal expansion coefficients and elastic moduli are comparable.

2.1.2.3 ATTACHMENTS

The injector usually is attached mechanically to an ablative chamber by a metal flange. This flange may be a continuation of the chamber's metal structure or it may be wrapped into the fiberglass structure. The flange-to-fiberglass interface usually incorporates both adhesive bonding and mechanical interlocks to provide a positive and, at times, redundant load transfer. A typical example is the Apollo SPS combustion chamber, which has a rubber-modified silica/phenolic liner with a laminate orientation of 45° relative to the chamber surface in the chamber region. Asbestos/phenolic with a parallel-to-axis orientation surrounds the liner. (Silica/phenolic overwrap was used in the prototype and Mod I designs.) The primary structural shell is glass fabric and roving, with the fabric laid up flatwise. Aluminum flanges are attached at both ends of the chamber.

The Apollo SPS chamber went through an evolution depicted in figure 3 in attempts to improve the forward flange attachment and accommodate the high thermal expansion and subsequent permanent shrinkage of the rubber-modified silica/phenolic liner. (The use of this material was justified on the basis of its good erosion resistance and relatively low thermal conductivity and low density.) The prototype chamber design (fig. 3(a)) resulted in separations of as much as 0.12 in. between the liner and injector because of the liner shrinkage. The Mod I design (fig. 3(b)) had the chamber nose better protected and an improved seal; in addition, a better locking of the glass fabric to the flange was achieved by

Table II. – Typical Room-Temperature Properties of Three Different Phenolic Resins Reinforced with Silica Fabric

Property	Resin		
	A	B	C
Density, gm/cm^3	1.45	1.76	1.73
Resin content, %	40 to 50	18 to 23	29 to 33
Compressive strength, psi, flatwise	5000	60 000	28 000
Compressive modulus, 10^6 psi, flatwise	--------	2.4	1.8
Compressive strength, psi, 45°	2600	25 600	16 000
Compressive modulus, 10^6 psi, 45°	0.02	1.64	1.0
Tensile strength, psi	4100	25 000	14 000
Tensile modulus, 10^6 psi	0.19	3.32	2.0
Flexural strength, psi	--------	30 000	20 000
Interlaminar shear, psi	620	2000	1600
Thermal expansion coefficient, 10^{-6} in./in.-°F (to 300°F)			
Parallel to plies	3.3	5.5	5.0
45° to plies	26.6	7.0	5.7
90° to plies	36.7	36.7	16.8
Thermal conductivity, Btu-in./hr-sq ft-°F 200° mean temperature	2.6	3.0	2.8
Specific heat, Btu/lbm-°F 200° mean temperature	0.33	0.27	0.27

Resin:
- A Elastomer-modified phenylsilane resin
- B Polyamide-modified phenolic (unfilled) resin
- C Filled phenolic resin

Data sources:
- Unpublished data – Apollo SPS engine program
- Reference 31
- Reference 32
- Vendor data

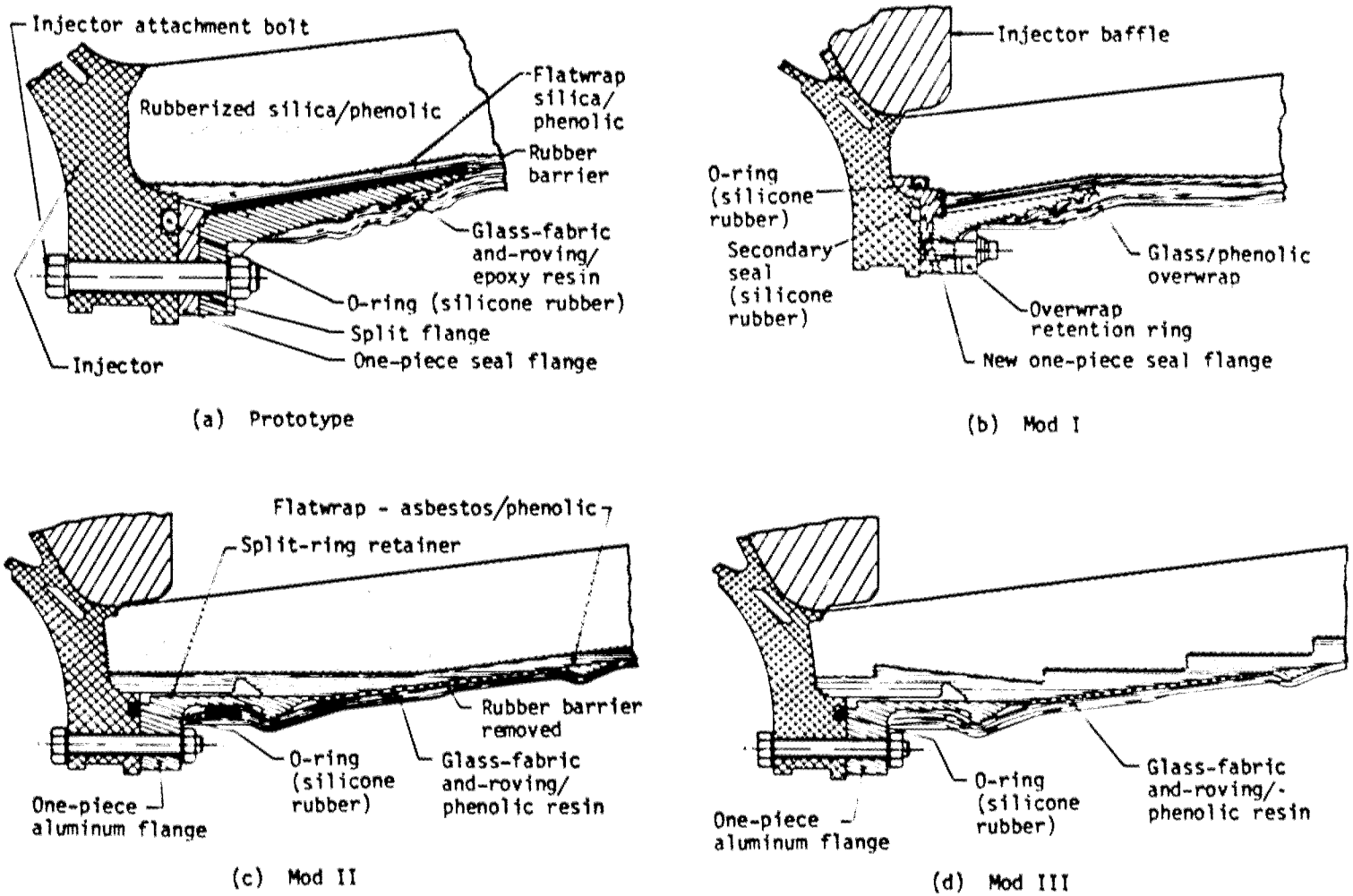

Figure 3. — Evolution of design for injector/chamber attachment for Apollo SPS.

carrying the fabric under the flange and clamping it to the flange by a separately bolted attachment. This design was not satisfactory for extended duty cycles. Excessive forward-flange temperatures and one flange burnthrough resulted from gas flow at the chamber-to-injector joint. The Mod II design (fig. 3(c)) incorporated a high-modulus overwrap (asbestos/phenolic) with a metal retaining ring positively locking it to the flange, an improved anchoring of the glass overwrap to the flange, an improved bond between liner and insulative overwrap (by removing the rubber barrier), and a lip extension on the injector to better protect the forward end of the liner. This design did not, however, prevent the liner from shrinking away from the injector face. The final design modification (fig. 3(d)) is representative of the qualified flight design. It incorporates steps at the liner to overwrap interface to restrain the liner mechanically. At the same time, as a consequence of the blistering problem referred to in section 2.1.1.3, the material was changed to a more highly staged phenolic resin, and parallel-to-axis (instead of parallel to outer surface) overwrap was used to facilitate escape of entrapped volatiles.

In the Apollo LEM descent engine, the early ablative face plate (installed between injector and chamber) was made of standard molded silica-reinforced phenolic. Occasionally fuel entrapped between the injector manifold and face plate would detonate, causing cracking and in one case ejection of a section of the face plate. Fuel had been entrapped in a gap between the two components that was opened by deflection (under firing loads) of the manifold. The ablative face plate was too stiff to deflect; a change to a rubber-modified silica/phenolic with a low modulus solved the problem.

The attachment of the nozzle extension generally requires joining a thin-walled, radiation-cooled nozzle extension to the ablative chamber. The joint normally is made by incorporating a metal flange on the chamber and bolting the nozzle extension to it. The bolts as well as the gas seal are such as to use the full thickness of the ablative chamber wall as protection from the combustion products, while simultaneously minimizing the thermal conductance and the radiation view factor from the hot nozzle extension. Figure 4 illustrates two such designs; the Apollo SPS aft flange of figure 4(a) could easily be moved forward relative to the hot radiating surface to reduce the view factor to the nozzle extension.

2.1.3 Fabrication

Ablative combustion chambers are fabricated from materials with variable properties by processes that are not well characterized. The properties and characteristics of the end product are, to a large degree, dependent on the fabrication method used.

Most ablative combustion chambers in current use are fabricated with woven-fabric reinforcement in a thermosetting resin. Tape-wrapping is the fabrication method most often used, since this method requires relatively inexpensive tooling, little material is wasted, and

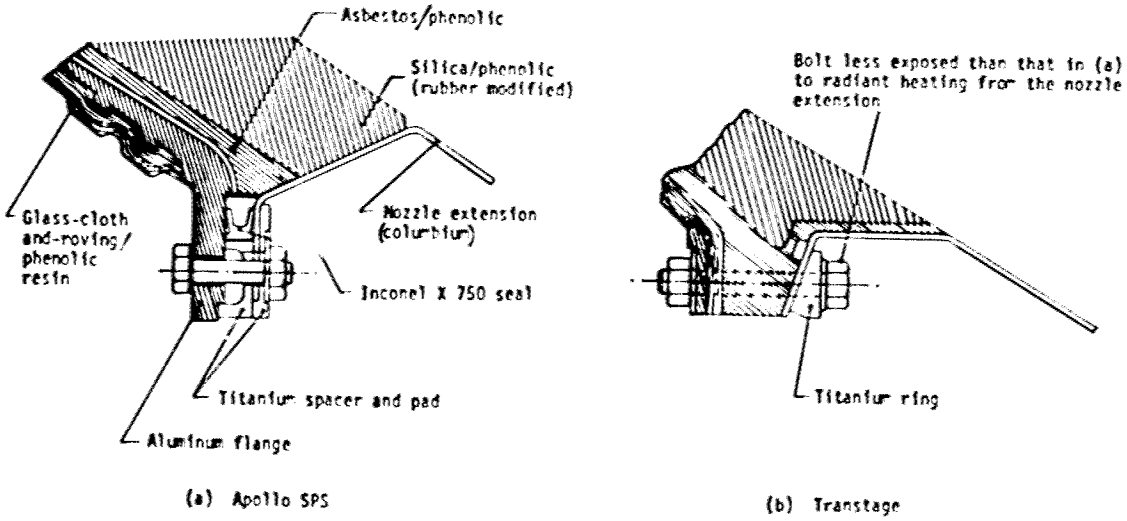

Figure 4. – Two designs for attachment of ablative chamber to nozzle extension.

the wrapping process is performed on semi-automatic machines. Small (< 4 in. diam.) thick-walled chambers generally lend themselves best to matched-die molding of precut patterns of fabric, laid up "coolie-hat" fashion to the desired laminate orientation. Other fabrication methods include fabric layup in a shingle or rosette pattern. This method is especially suitable for nozzle extensions in that it provides good axial strength and there is little material waste. Examples are the diverging portions of the combustion chambers in both the Apollo LEM ascent and descent engines. Figure 5 illustrates typical fabric configurations. The three-dimensional fabric configuration is shown for completeness, even though there are no components of this type in use at the present time.

To obtain satisfactory ablative performance and to meet structural requirements, the ablative component must be cured under pressure (⩾ 200 psi). Use of low pressure to obtain relatively-low-density (lightweight) cured materials has resulted in parts of inconsistent quality; a more successful method for achieving lighter weight is to substitute lightweight materials and add filler where performance requirements allow. Since the starting material, the fabric pre-impregnated with resin (prepreg), has a thickness about twice that of the final cured laminate, a considerable compaction and movement of the prepreg takes place. To avoid wrinkles and folds of the laminates in the cured product, it is important to achieve as high an as-wrapped density as possible prior to the pressure-cure process. This is especially important when the part is tape-wrapped on a male mandrel. One edge of the prepreg is in contact with the layup mandrel and cannot move. The balance of the prepreg undergoes an angular transition, the magnitude of which varies with the amount of debulking during the

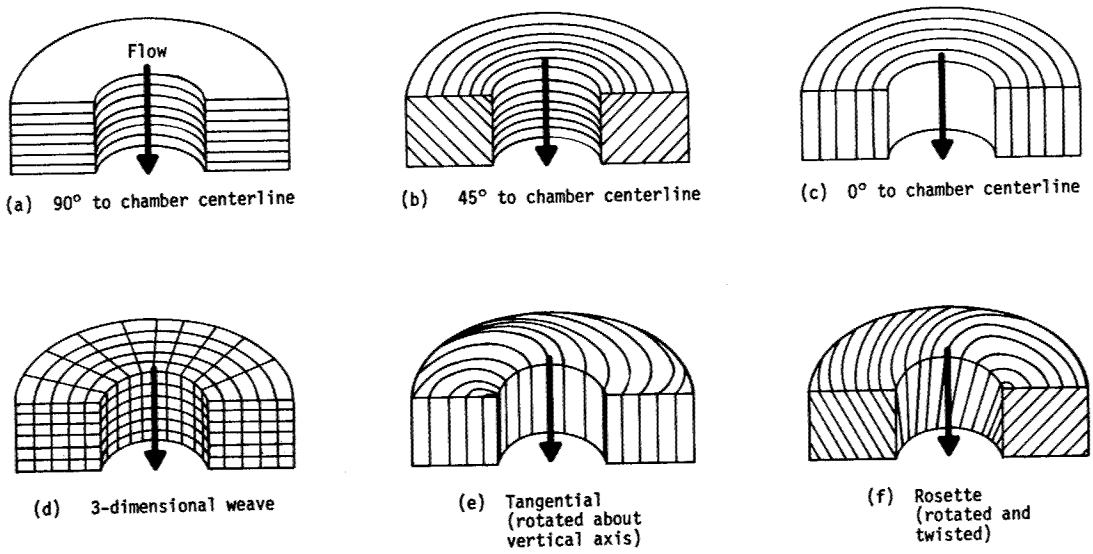

Figure 5. — Typical configurations for ablative-chamber fabric.

wrapping as well as with the location in the chamber. A high density will minimize this angular transition. The part is cured on the male mandrel with pressure exerted on the outer surface, which causes a reduction in the outer periphery; this reduction is minimized by debulking to achieve a high density prior to cure.

2.1.3.1 PROCESS CONTROLS

The designer of ablative chambers must specify and control the fabrication parameters to avoid or minimize areas of wrinkles or folds, since they are locations of potential failures, either by chunking or by rupture. The controls normally imposed include prepreg property limits (resin content, volatile content, and resin flow), process requirements that include wrapping parameters (e.g., tape temperature, tension, feed, and percent debulking prior to cure), cure-cycle specification, and end-product acceptance limits for density, hardness, and mechanical properties. Table III shows typical acceptance limits for properties of various ablative materials, including a carbon/phenolic and a graphite/phenolic, even though the latter is not used in production programs. Both prepreg and cured-composite properties are shown. The wide range in compressive strength is caused by variations in reinforcement as well as in resin type. It should be noted, however, that the limits shown are considered typical values. Differences in size and in processing produce different properties such that

Table III. – Typical Acceptance Limits for Properties of Representative Ablative Materials

Material*	Prepreg properties			Cured-composite properties				
	Resin content, %	Volatile content, %	Flow, %	Hardness, Rockwell R (min.)	Density, gm/cm^3 (min.)	Edgewise compressive strength, psi (min.)	Acetone extractables, % max.	Residual volatiles, % max.
A	40 to 50	2 to 6	—	—	1.44	2000	—	—
B	18 to 22	2 to 5	—	127	1.76	30 000	0.5	2.0
C	29 to 33	3 to 7	4 to 12	124	1.73	18 000	0.5	2.0
D	30 to 34	2 to 6	4 to 12	121	1.70	16 000	0.5	2.5
E	31 to 36	2 to 6	1 to 10	127	1.40	33 000	0.5	2.0
F	30 to 35	2 to 6	3 to 12	122	1.40	15 000	3.0**	2.5

*Material Description:

A Silica-reinforced elastomer-modified phenylsilane
B Silica-reinforced polyamide-modified phenolic
C Silica-reinforced filled phenolic
D Silica-reinforced unfilled modified phenolic
E Carbon-reinforced unfilled phenolic
F Graphite-reinforced phenylaldehyde

**Contains soluble acetone-extractable additive that does not polymerize.

the properties established for one component are not necessarily the same as those for another component even if they are made of the same material. The suppliers of ablative materials usually furnish data on mechanical and thermal properties (mostly room-temperature data). These properties generally are based on test results from laminates laid up and cured in a heated-platen press. These specimens are wrinkle-free and not representative of tape-wrapped material. Tensile and flexural strengths and moduli generally are considerably higher in the flat specimens than in actual components. In large production programs, the material acceptance and design properties usually are established from tag ends of actual components. Table II shows properties for three different types of silica/phenolic. Most of these properties were determined from actual components or from parts fabricated in the same manner as actual components.

2.1.3.2 PRODUCT DISCREPANCIES

The discrepancies that occur in ablative components generally are delaminations, wrinkles, folds, voids, and inclusions. Delaminations are common occurrences in ablative chamber liners. If the delaminations do not extend through the liner wall and if they are not too wide, they are not considred detrimental. There are, however, no firm rules of general applicability for the limits of delaminations. In some Apollo ACS engines (SE-8) that incorporated precharred chamber liners, excessive outer wall temperatures resulted when delamination exceeded previously established limits. Measured delaminations were 0.040 to 0.080 in. wide, penetrated to a depth of 0.050 in., and extended circumferentially through 240°. The outer wall temperatures exceeded the base-line temperature of the qualification unit by 45° to 100°F. The higher temperatures were attributed to surface roughness of the chamber wall that caused boundary-layer separation and thereby increased heat-transfer rates to the chamber wall.

The frequency and magnitude of delaminations are, to a large degree, dependent on material characteristics and on laminate orientation. Of general material characteristics, the thermal expansion in the through-ply direction and the resin shrinkage on charring are the greatest contributors to delaminations. The laminate orientation affects delamination primarily as a result of the large thermal expansion in the through-ply direction in comparison with that in the with-ply direction. The higher laminate angles (measured relative to the chamber axis) result in increased tendency to delaminate.

The other major discrepancy that occurs in fabrication of ablative chambers is wrinkling of the laminates. It is unrealistic to require and specify completely discrepancy-free parts, especially if the parts are tape-wrapped. References 33 and 34 report the results of studies on the influence of material and processing deviations on the performance of a graphite-fabric-reinforced composite and the effects of product discrepancies on nozzle performance reliability, respectively. Nozzle components were fabricated with deliberately introduced discrepancies and then evaluated in solid rocket motor firings. It was concluded

that discrepancies in the form of wrinkles, folds, voids and ply separation caused local effects such as gouging, chunking, or spalling, but that unless gas flow paths resulted, the effects on the overall performance of the component were negligible. When the ablative and structural analysis techniques were combined with a statistical analysis of variance, it was possible to establish accept/reject criteria for ablative nozzle components.

In many cases, minor defects such as delaminations can be repaired. For example, a silica/phenolic combustion-chamber liner that had broken in two (by interply delamination) was repaired by adhesively bonding the liner and overwrapping it with a glass/phenolic. The repair was possible because the liner charred only part way through at the repair location.

2.2 RADIATION-COOLED CHAMBERS

As the name indicates, radiation-cooled chambers depend primarily on heat loss by external radiation to control chamber wall temperatures. The relatively thin chamber walls typically are made of refractory metals, which are coated internally for oxidation resistance and externally for increased emissivity.

Radiation-cooled combustion chambers have found considerable use in small thrusters such as spacecraft attitude- or reaction-control engines that must operate for long accumulated durations in a pulsing mode. At low chamber pressures ($<$ 100 psi), radiation losses can reduce chamber wall temperature significantly below the local adiabatic wall temperature. Since the engines usually are mounted on the external surfaces of the vehicle, the radiant energy from the thruster is nondamaging; local insulation provides adequate protection of adjacent components or structures. Most radiation-cooled chambers in use today operate at chamber pressures from about 60 to 100 psi, with thrust levels from 5 to 200 lbf; however, the concept has been demonstrated at much higher thrust levels. Table IV presents basic features of some typical operational radiation-cooled engines (only bipropellant engines are covered in this monograph). The table is not intended to be complete; however, it does cover a range of operational and development engines and encompasses the three commonly used combustion-chamber materials: columbium, molybdenum, and 90Ta-10W. Only engines using earth-storable propellants are included, since other concepts are considered beyond the current state of the art. Section 2.4 provides a discussion of more advanced concepts such as adiabatic-wall chambers, which are quasi-radiation-cooled chambers.

2.2.1 Thermal Design

Because chamber wall temperatures usually must exceed 2200°F in order for the heat lost by radiation to balance convective heating from the combustion products, the basic problem in thermal design of radiation-cooled chambers is selection of the materials of construction. Wall materials must be selected from the refractory metals and their alloys. In addition, coatings are required to protect the inner wall from oxidation by the combustion products.

Table IV. – Basic Features of Typical Operational Engines with Radiation-Cooled Combustion Chambers

Engine designation	Function, status	Propellants*	Thrust, lbf	Chamber pressure, psi	Chamber materials*
Model 8348	Attitude control, development tested	N_2O_4/N_2H_4-MMH	5	60	C-103 columbium, silicide coated.
Model 8414	Lunar Manned Flying System, development tested	N_2O_4/A-50	100	80	SCb-291 columbium, silicide coated.
Model R-1A	Reaction control, flight tested	N_2O_4/N_2H_4-MMH	25	100	TZM molybdenum, silicide coated.
Model R-4D	Apollo reaction control, flight tested	N_2O_4/A-50	100	96	Unalloyed molybdenum, silicide coated (alternative: C-103 columbium)
Model 8250, unit I	Agena-Gemini secondary propulsion, flight tested	MON/UDMH	16	78	90 Ta-10W, aluminide coated. Pyrochrome emissivity coating.
Model 8250, unit II	Agena-Gemini secondary propulsion, flight tested	MON/UDMH	200	96	90 Ta-10W throat insert, Haynes 25 chamber liner (radiative/heat-sink combination)
Model TD-345 (C-1)	Apollo reaction control, flight tested	N_2O_4/A-50	100	93	90 Ta-10W, silicide coated.

*Identified in Appendix D.

2.2.1.1 WALL MATERIALS

With the well-developed silicide and aluminide coatings, the columbium alloys have emerged as the most suitable materials for radiation-cooled chamber walls. Frequent use of molybdenum and 90Ta-10W in the past was due to unavailability of the better columbium alloys, lack of adequate data on the temperature limits imposed by oxidation-resistant coatings, and underestimation of the seriousness of the effects of embrittlement on the refractory metals and alloys.

The alloy 90Ta-10W can withstand higher temperatures than can columbium. It is also almost twice as dense. At the present time, however, the high-temperature capability of 90Ta-10W cannot be utilized because suitable high-temperature coatings are not available. Some preliminary work has been done in evaluating improved coatings or claddings; however, none has been developed sufficiently to be considered state-of-the-art materials or processes.

Some columbium alloys are subject to embrittlement during the coating process. A program evaluating four coatings on three different columbium alloys found that both SCb-291 and C-129Y alloys exhibited brittle failures, whereas C-103 did not (ref. 35). The embrittlement was caused by the physical presence of the coating itself. It is possible that the tungsten alloying element may have contributed to the embrittlement. There is 10-percent tungsten in both SCb-291 and C-129Y and a negligible amount in C-103.

2.2.1.2 WALL COATINGS

All refractory metals and alloys require oxidation-resistant coatings for high-temperature use with the propellants listed in table IV. The coatings remain the limiting factor in determining chamber life and in establishing allowable wall temperatures. General requirements for an oxidation-resistant coating are as follows:

(1) The coating must be compatible with the propellants and the combustion products at the maximum wall temperatures for times required by the duty cycle.

(2) The coating must not detrimentally affect the mechanical or physical properties of the substrate or significantly alter the metallic characteristics of the substrate.

(3) The coating must be capable of being applied reproducibly in uniform density and in uniform thickness on all component surfaces.

(4) The coating should form a metallic bond with the substrate.

The most commonly used oxidation-resistant coatings are silicides and aluminides, which have been extensively evaluated (refs. 35 through 41). The silicides have higher temperature capabilities, being able to sustain operation up to 2800°F for one hour in comparison with 2400°F for aluminides. Aluminides, on the other hand, generally have less detrimental effects on the substrate properties and usually do not embrittle certain substrates as silicides do. Of the four coatings that were evaluated in the work reported in reference 35, three were silicides and one was aluminide. One of the silicides, R-512A, was slurry applied and vacuum fused to the surface, and two, Durak KA and Ti-Cr-Si, were applied by pack cementation; the aluminide coating was slurry applied. The program was limited in that the test matrix did not provide for evaluation of all coatings on all three substrates. The conclusions drawn from the program were that the C-103 substrate with the R-512A coating was the best material system and the C-103 with Durak KA was second best. The aluminide on C-103 failed in relatively short time in an oxy-propane torch test; at 2800°F, the coating burned through.

Other programs have reported satisfactory results with a R508C silicide coating on a C-103 columbium substrate (ref. 42) and with a R508C coating on a SCb-291 columbium substrate (ref. 43). No embrittlement of the substrate was reported.

Plasma-sprayed coatings also have been evaluated, but they have been found less desirable than slurry or pack-cementation coatings, primarily because they are more porous and do not form metallic bonds with the substrate. Plasma-sprayed coatings also are difficult to apply on the inside of small-diameter chambers.

Coating thicknesses vary from 0.0005 in. to 0.008 in., the thickness depending on type of application. No generally accepted thickness has been established; there is agreement in principle, however, that if the coatings are too thick they will spall or crack during thermal cycling. Failure of the coatings can also be caused by incomplete coverage (although small pinholes tend to be self healing) or by lack of adhesion to the substrate. The finish of the substrate surface is important in achieving a satisfactory coating; however, no generally acceptable criteria have been established. Suitable processes for cleaning and treating the substrate surface have been developed by the various coating suppliers to ensure reproducible bond conditions. These processes and the coating processes themselves generally are considered proprietary by the suppliers. Coatings usually are evaluated by means of high-velocity plasma torch applied to coated coupons. Coatings on finished components usually are inspected visually to determine completeness of coating; reference 44 reports a smoke test to detect uncoated areas. In this test, the coated component (combustion chamber) is placed in a furnace and heated; any uncoated areas will emit smoke.

Coatings also are used to increase the emissivity of the external surface of the chamber wall. In some cases, special coatings (e.g., Zr C with an emissivity of 0.86) have been considered (ref. 45). However, the oxidation-resistant silicide and aluminide coatings used internally

also provide high emissivities, usually about 0.75 to 0.85. Therefore, the common practice is to use these coatings externally as well as internally and thereby provide protection from atmospheric oxidation during testing at sea level and simulated low altitude. Atmospheric protection of other emissivity coatings or the emittance control surfaces discussed in section 2.2.1 require the use of inert-gas shrouds, the effectiveness of which is difficult to ensure (e.g., ref. 45).

Silicide coatings will sublime during operation in a vacuum, the rate of loss depending on the temperature of the wall. Chambers that operate at temperatures below 2400°F have a virtually unlimited life (ref. 41). Sublimation rates measured at 10^{-5} mm Hg are 0.8% per hour by weight at 2600°F and 4.0% per hour at 3000°F. Sublimation appears to pose no problem internally, where low pressures and high temperatures are combined only for short periods after shutdown.

Operation at temperatures above 3000°F is not possible with the presently available coatings; in fact, 2800°F is considered the upper limit except for short-duration duty cycles. New systems with higher temperature capabilities have been evaluated. The most promising so far is 80Hf-20Ta cladding on a 90Ta-10W substrate, a combination that has potential for operation up to 3800°F in engines with earth-storable oxidizing propellants.

2.2.1.3 WALL CONFIGURATION

The use of relatively thick walls to promote axial conduction and increase external radiation surface area in small chambers can reduce gas-side throat temperature several hundred degrees (refs. 45 and 46). However, the wall thickness cannot be increased advantageously without limit, since the increased radial thermal resistance eventually offsets these factors and causes the gas-side surface temperature to increase. Wall thicknesses in excess of structural requirements are used to provide greater conduction from local hot spots.

Refractory metal surfaces normally have relatively low emissivities (0.2 to 0.4). Use of fins, knurling, V-grooving, and sandblasting have been evaluated as a means to increase the effective emittance of the outer surface of the chamber wall. An emittance as high as 0.8 was obtained with V-grooves in a SCb-291 chamber (ref. 45); usually, though, an emissivity coating is applied.

2.2.2 Structural Design

2.2.2.1 CHAMBER

The development history of radiation-cooled chambers has been one of finding materials with suitable high-temperature properties and of understanding the limitations of these materials. Table V presents pertinent mechanical and physical properties of the most often

Table V. – Properties of Refractory Metals Used in Radiation-Cooled Chambers

Property	Metal*					
	Columbium		Molybdenum		Tungsten	
	C-103	SCb-291	Unalloyed	TZM	Unalloyed	90Ta-10W
Density, lbm/in.^{3}	0.32	0.347	0.369	0.369	0.69	0.61
Melting point, °F	4260	4710	4730	4730	6170	5516
Ultimate tensile strength, psi						
70°F	60 000	75 000	90 000	120 000	130 000	105 000
3000°F	8000[d]	10 000	9000	14 000	25 000	16 000
Tensile modulus, 10^6 psi						
70°F	13.1	15.0	43	47	55	26.5
3000°F	3.6**	7.0	9	26	47	9.0
Thermal expansion coefficient, 10^{-3} in./(in.-°F)						
3000°F	15.0	12.0	10.5	11.5	8.5	11.0
Thermal conductivity, Btu/(ft-hr-°F)						
70°F	26	22	78	81	95	—
3000°F	40	29	46	45	75	31
Ductile-to-brittle transition temperature, °F						
Initial	– 320	– 30	– 60	– 50	200	– 320
After cycling	– 320	--------	+ 70	+ 60	600	– 320

*Alloys are identified in Appendix D

**At 2700°F

used materials and also of unalloyed tungsten for comparison purposes. Tungsten is not a suitable wall material, in spite of its high-temperature strength and high thermal conductivity. Its high elastic modulus and especially its high ductile-to-brittle transition temperature cause brittle fractures in any but single-burn duty cycles.

All refractory metals and alloys recrystallize at temperatures below 2500°F, the result being grain growth and usually an increase in the brittle-to-ductile transition temperature. In the case of molybdenum, the transition temperature is raised to approximately 70°F, so that the chamber operating temperature range normally would span the transition zone. As a result, cyclic loading can result in brittle fracture initiated at flaws, inclusions, and stress concentrations. Molybdenum chambers that appeared to be suitable for steady-state operation have failed in this mode during pulsed operation because of start-transient pressure spikes, which can exceed the nominal chamber pressure by more than an order of magnitude. Molybdenum (the unalloyed form and the TZM alloy) is used successfully in radiation-cooled chambers only when it has been subject to stringent quality control during processing and fabrication.

Machining the chamber from forgings, rather than fabricating it by welding, minimizes the possibility of introducing flaws or areas at which failures might originate (ref. 44). Care is also taken in designing the chambers to avoid stress concentration areas (e.g., sharp corners, transitions from thick to thin sections). Screw threads and usually also bolt holes are avoided.

The two materials that have the lowest brittle-to-ductile transition temperature are 90Ta-10W and columbium. Both of these materials are ductile enough to repeatedly absorb and attenuate the energy associated with altitude ignition pressure spikes; they also have good resistance to thermal shock.

2.2.2.2 ATTACHMENTS

The high wall temperatures associated with radiation-cooled chambers require special designs for high-temperature injectors or thermal insulation of the injector interface. Three different approaches to the design of the injector and chamber have been tried: (1) use injected film or barrier cooling to maintain the temperature of the forward end of the chamber at a minimum; (2) operate a refractory-metal injector at very high temperatures with the propellant manifolds thermally isolated; and (3) use a thermal barrier between injector and chamber.

The first concept is typified by the R-4D series of engines. Film cooling maintains the chamber forward flange below 350°F during operation. Although the throat wall temperature is about 2200°F, the combined effects of film cooling, thin chamber walls, and

injector mass limit the injector soak temperature to less than 350°F (the chamber forward flange does not exceed 500°F after shutdown). In general, this concept permits the injector and chamber to be bolted or clamped directly without the use of insulating gaskets. The forward end of the chamber is lapped to the injector, or a metal seal ring is used. In the Apollo LEM reaction control engine, an A-286 seal ring was used (fig. 6(a)). The seal ring was later modified as shown in figure 6(b) to minimize the gap between the injector face edge and the chamber and thereby reduce the possibility of combustible propellants and combustion product residues being trapped in confined spaces where detonations might have detrimental effects.

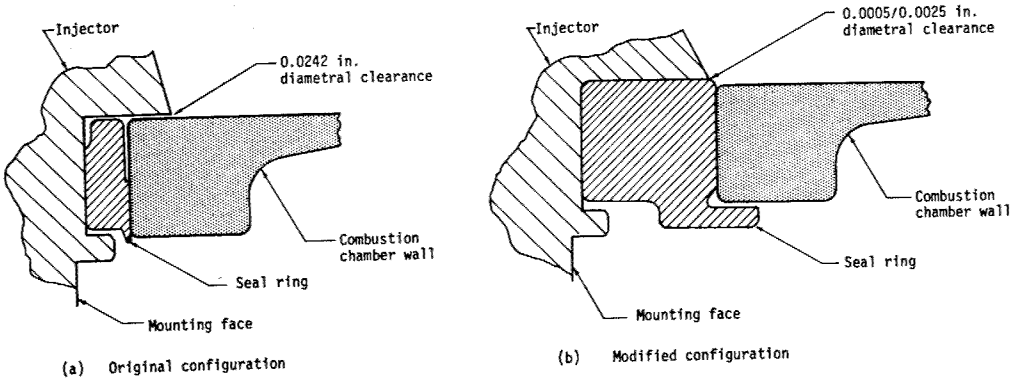

Figure 6. – Evolution of design for injector/chamber seal used on Apollo LEM RCS engine.

The second concept, the hot injector with thermally isolated bipropellant valve, is illustrated in figure 7, which shows a columbium injector electron-beam welded to a columbium chamber. Injector and chamber operate at high temperatures, and propellant tubes feed from the isolated valve to individual injector orifices. This unit is typical of an entire family of radiation-cooled engines (refs. 47 and 48).

The third concept, a thermal barrier between injector and chamber, is shown in figure 8. The pressure-sealing strip at the forward end of the chamber provides a minimum conduction path, permitting use of an elastomeric (rubber) O-ring seal. The conduction path through the bolts is minimized by the use of insulating ceramic cups that also shield the bolt heads from radiated heat from the chamber wall. This design concept was used on a throttleable engine for the Lunar Manned Flying System (ref. 42).

The thrust chamber can be attached to the injector or divergent nozzle by either metallic (welded or brazed) or mechanical joints. Although brazed interfaces have been used at the forward end of interegen cooled thrust chambers, there is no record of their use with hotter walled passively cooled units. Welded joints are used on a variety of engines, including the engine developed for the Lunar Manned Flying System (ref. 43). In this engine, a columbium chamber was electron-beam welded to a columbium injector and nozzle extension.

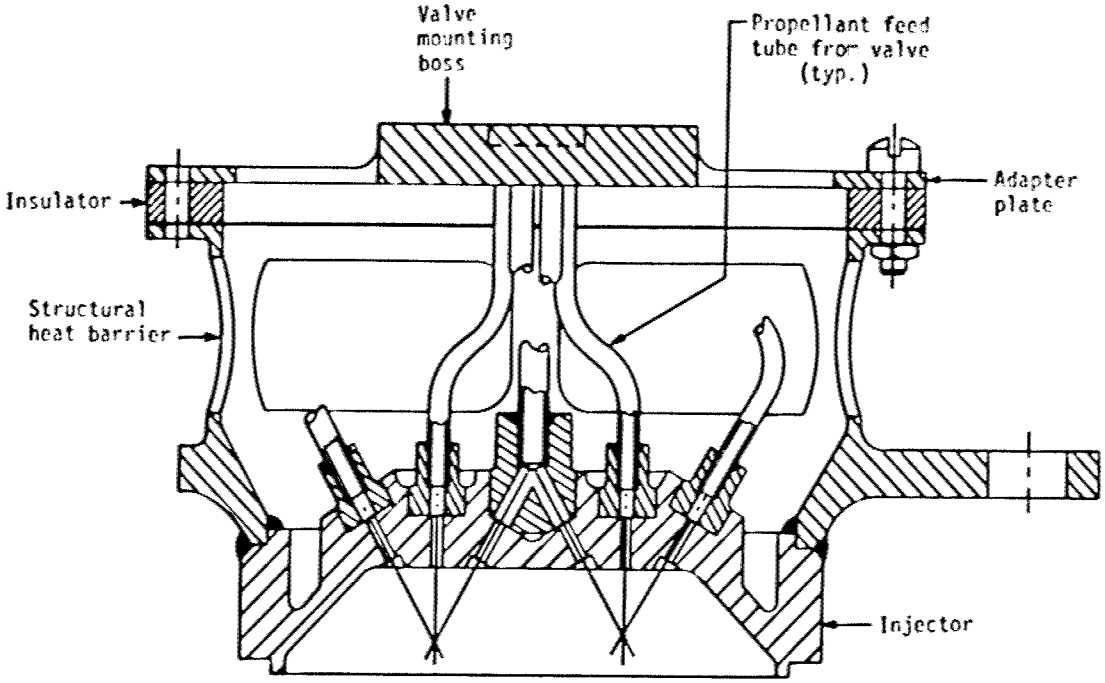

Figure 7. — Injector/chamber attachment design providing thermal isolation of bipropellant valve.

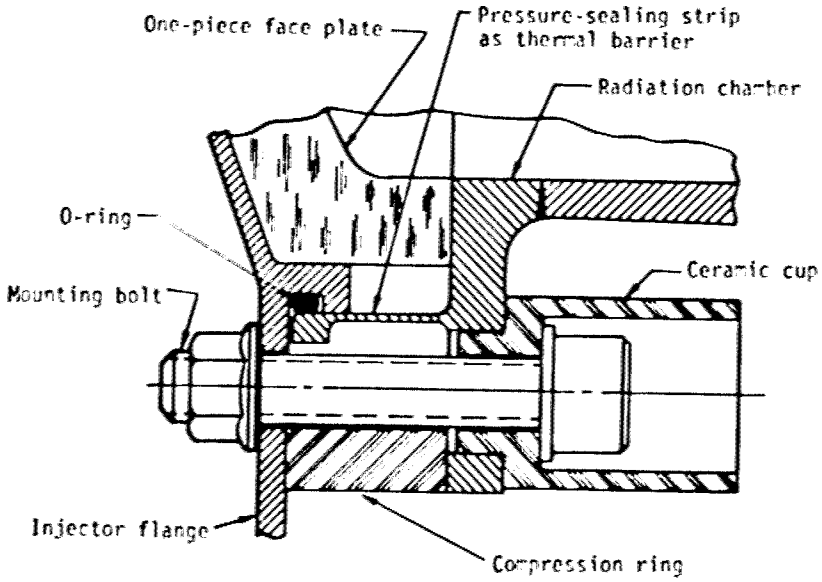

Figure 8. — Injector/chamber attachment design providing thermal isolation of injector.

The wall thickness at the welded interface is increased locally to compensate for reduced mechanical properties in the weld-affected zone. The refractory metals (e.g., columbium) require an oxidation-resistant coating. This coating must be removed from the welded area to preclude contamination of the weld joint; if any coating is allowed to migrate into a weld region, extreme embrittlement of the weld may result. The surfaces to be welded are machined free of coatings or the coating is applied after welding. Stripped areas can be recoated by spraying or the brush application of a slurry coating, which then is vacuum-furnace cured. An alternative method that has not been attempted on any production units is to apply a slurry coating but not to process it through diffusion. During the first engine burn, the slurry coating will then (probably) diffuse into the substrate.

Since uncoated columbium can operate safely at low temperatures ($< 1000°F$), the usual practice with small engines, where access through the throat is limited, is to locate the injector/chamber weld in a cooler area so that coating or recoating of the wall area on the chamber inner surface is unnecessary.

A divergent nozzle section usually is welded to a chamber prior to the application of a coating. On larger engines, there is a weight advantage in the use of titanium for the nozzle extension. The titanium extension is joined to a columbium thrust chamber by resistance welding or brazing to avoid formation of brittle alloys at the weld zone; in this instance, coatings are applied prior to the joining operation.

The use of a mechanical interface to attach the injector is quite common. The injector interface requires a seal to preclude leakage and usually incorporates some manner of split ring (ref. 35), because the diameter of the nozzle prevents slipping a continuous clamping ring over the aft end.

The mechanical attachment of a nozzle extension facilitates the use of dissimilar materials in the chamber and nozzle. On the reaction-control engine on the Apollo Service Module, a threaded one-piece clamping ring was installed from the chamber's forward end to engage a matching thread on the nozzle extension so that the clamp pressed against a shoulder on the chamber's aft end. The advantages of a clamp over a bolted connection are that stress raisers (e.g., bolt holes) are avoided, the bearing load is more uniformly distributed, and weight is reduced. A separate seal is not required at the nozzle extension joint because of the low pressures involved; however, the mating surfaces preferably are lapped. The clamped joint is preferred over a welded joint when the chamber material is molybdenum.

2.3 INTEREGEN AND HEAT-SINK CHAMBERS

Interegen (internal regenerative) and heat-sink chambers are discussed jointly herein since the former is essentially a special type of film-cooled heat sink. Heat-sink chambers utilize the transient-energy-storage capability of the chamber wall to limit surface temperatures;

typically these chambers are characterized by relatively massive walls of a high-conductivity metal. Although interegen designs physically are similar to film-cooled heat sinks and can be operated as such, they are distinguished by their ability to operate in thermal equilibrium at low thrusts and chamber pressures. The interegen cooling concept was first demonstrated in 1965 (ref. 49). In this type of chamber, heat is conducted away from the throat region and part of the expansion section and is absorbed by liquid film coolant at the forward end of the chamber, as shown schematically in figure 9. Thus, the interegen concept is analogous to

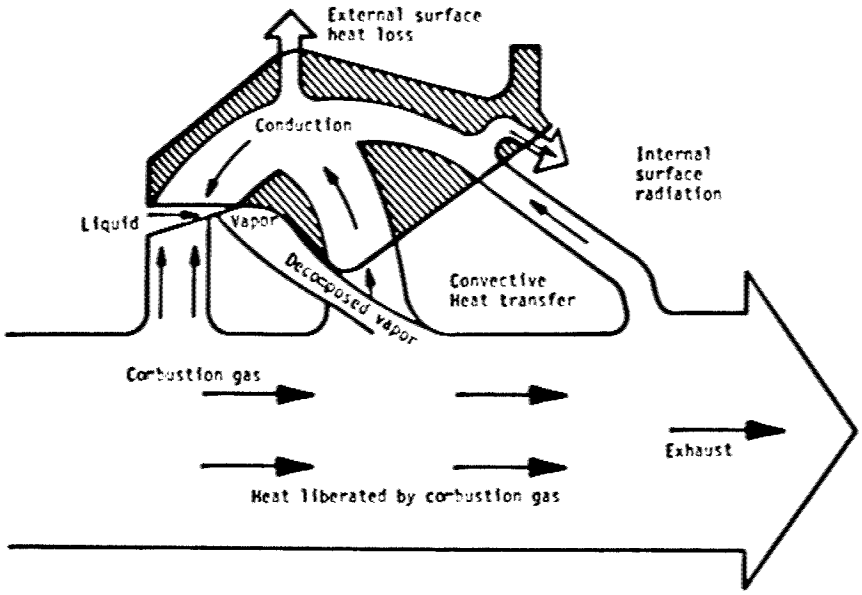

Figure 9. – Schematic of heat flow in an interegen chamber.

conventional regenerative cooling but with the coolant supplied by the injector to the inner surface of the wall and with axial rather than radial conduction through the wall. Both the sensible and latent heats of the coolant are utilized in the liquid film, and downstream of the liquid region the film coolant serves its normal function of reducing the heat flux to the wall.

Heat-sink thrust chambers are of two types: workhorse units, which are operated for short durations in order to characterize the injector and to acquire data on heat-transfer capability of the chamber wall; and flight configurations, which use the heat sink in conjunction with film cooling as a suitable thermal-management technique. Workhorse heat sinks are not treated in this monograph. Table VI gives basic features of the flight applications of interegen and heat sink chambers to date.

Table VI. – Basic Features of Operational Engines with Interegen and Heat-Sink Combustion Chambers

Engine designation	Thrust, lbf	Chamber pressure, psi	Propellants*	Chamber type; material*
RS-14 PBPS	300	125	N_2O_4/MMH	Interegen; beryllium
Mariner '71	300	117	N_2O_4/MMH	Interegen; beryllium
Viking Orbiter '75	300	125	N_2O_4/MMH	Interegen; beryllium
Model 8250, unit II**	200	96	N_2O_4/A-50	Radiative/heat-sink; Haynes 25

*Identified in Appendix D. **See table IV

Because of its favorable density, thermal conductivity, melting point, and combustion-product compatibility, beryllium has been used in the bulk of the development work on interegen chambers employing monolithic walls; references 50 through 53 describe this development. Successful equilibrium operation with N_2O_4/MMH has been demonstrated at 100 psi pressure for thrust levels from 25 to 1000 lbf and at 150 psi for 100 lbf thrust. Beryllium chambers also have been used for limited durations (80 sec) with CTF/MMH at 300 psi and 1000 lbf thrust. Tests of a copper chamber indicate that a copper wall can extend the thrust and chamber pressure capability of the monolithic interegen concept beyond that demonstrated with beryllium (ref. 51). Reference 54 reports on an investigation of copper chambers for FLOX/LPG at 100 psi.

Bimetallic chambers combining a flame liner of Inconel 600 with axial conductors of copper have also been demonstrated. Operation in thermal equilibrium has been demonstrated with N_2O_4/A-50 at a chamber pressure of 200 psi with 75 lbf thrust and at 125 psi with 100 lbf thrust (refs. 55 and 56).

2.3.1 Thermal Design

2.3.1.1 WALL THICKNESS AND FILM COOLING

The amount of film cooling required for an interegen design is not unique, since the wall thickness usually can be adjusted to accommodate a range of film-cooling flowrates (sec.

3.5.2). Most designs to date have used relatively large amounts of film cooling, typically 30 to 40 percent of the fuel flow or about 15 percent of the total flow. The use of large film-cooling flows is justified at low chamber pressures, for which it is not necessary to maintain a vapor or decomposition-product cooling effectiveness to the throat. In this case, the injector core flow can be designed to burn the film coolant and provide good performance without destroying the liquid region that provides the primary interegen heat sink. Reference 51 indicates a 94-percent c* efficiency for this concept with about 38 percent of the fuel being used as film coolant. The minimum allowable film coolant flow is established by the need to (1) prevent film boiling and monopropellant detonation with practical wall thicknesses in the liquid region and (2) allow the nozzle throat and nozzle to reach allowable structural temperatures.

Determination of the wall-thickness profile for existing interegen chambers appears to have been accomplished largely by trial and error. In the liquid region the wall must be thick enough to conduct heat efficiently as a fin. Coolant boiling curves for this region may be obtained from laboratory tests. A good curve for B_2H_6 is given in reference 57 and clearly illustrates the high wall temperatures associated with film boiling in comparision with those for nucleate boiling; incomplete boiling curves for MHF-3 and MMH are given in reference 58. Use of a constant wall thickness in the liquid region appears to be the most common practice, although a tapered wall was used in the work reported in reference 52 and was studied analytically in reference 54.

An optimum axial temperature distribution (and thus wall thickness variation), constrained by liquid-region temperature requirements at one end and by structural temperature limits at the other, has not been defined. A parabolic distribution is proposed in reference 54, and an almost linear distribution has been used for the copper conductor in some bimetallic designs. However, any advantages of these particular distributions have not been clearly identified. It is important to provide as much thermal resistance between the throat and the liquid region as the above constraints will allow in order to minimize the heat transfer to the liquid region and thus the film coolant required. Reference 54 proposed use of an isolation slot for this purpose instead of a contoured wall thickness. However, the additional weight and energy storage of such a design must be balanced against the claimed advantage of the 5-percent reduction in heat load. Two-dimensional heat conduction is significant in beryllium chambers; a local maximum in internal surface temperature in the throat region can occur even though the external temperature increases monotonically along the length of the interegen section. In designs to date, this throat peak has been both less than and greater that the aft-end temperature.

The use of composite chamber walls offers improved combustion-product compatibility and reduced heat loads (due to higher surface temperatures). Such chambers to date have been bimetallic, with liners of Inconel 600 and axial conductors of copper. In addition to their desirable individual characteristics, this combination provides matching thermal expansion coefficients. The flame liner usually is not operated at its maximum temperature capability, since this requires too great a thickness; the reduction in heat flux to the copper would be

relatively small, and the corresponding reduction in copper thickness cannot compensate for the added weight of the liner. Maximum liner thicknesses have been limited to about 0.25 in. Away from the throat region, the liner is tapered to about 0.05 in. in the liquid region and also at the aft end of the conductor, where the liner continues as a radiation-cooled nozzle extension.

The film cooling associated with the chamber must also cool the nozzle extension, part of which is essentially adiabatic in a buried installation. Fortunately, high-speed recovery effects and reduced mixing rates between the film coolant and core flows usually limit adiabatic wall temperatures in the nozzle to values a few hundred degrees higher than those at the throat. However, the higher temperatures may require use of a high-temperature alloy (e.g., Haynes 188 or L-605) or of a refractory metal such as columbium for the nozzle. Alternatively, the film coolant flow may be dictated by the material selection.

Determination of film-cooling requirements and wall-thickness profiles for heat-sink chambers is a straight-forward procedure using two-dimensional transient-conduction networks, the boundary conditions discussed in sections 2.5 and 3.5, and the film-cooling models presented in Appendices A and B.

2.3.1.2 WALL CONTOUR

The internal contour of the chamber has a significant effect on both interegen and heat-sink designs through its effect on the length of the conduction path from the source region to the film-coolant sink and on the surface area for heat input in the source region. The monolithic beryllium designs of references 50, 51, and 52 employed contraction ratios of 4.0 to 6.5, a convergence angle of 45°, and initial expansion angles of 31° to 40° in order to minimize the conduction path and surface area. Design analyses in reference 45 revealed the following contour effects: (1) perturbation of the contraction ratio about a value of 4.0 with a fixed L* had a small effect on the equilibrium temperature distribution; (2) increasing the convergence angle to 60° reduced the maximum temperature by about 200°F; and (3) a standard 80-percent bell nozzle could be modified to provide an initial expansion angle of 40° with only minor performance degradation. Equilibrium operation to date has been limited to injector-to-throat contour lengths of 4.5 in. or less. Large contraction ratios provide low gas velocities over the liquid film in addition to reducing the conduction-path length for a given L*. Use of large convergence angles to reduce the conduction length may be limited by undesirable injector impingement effects. The types of contours used for interegen chambers along with the low thrusts and chamber pressures at which they operate in thermal equilibrium act to promote reverse transition in the convergent-section boundary layer (sec. 2.5.1). However, the effects of the film coolant on reverse transition and laminarization are not known.

An interegen chamber normally is terminated at as low an expansion ratio as possible in order to minimize the heat load carried by the wall and the length of the conduction path to

the film coolant heat sink. Previous designs (e.g., ref. 50) have demonstrated the feasibility of thin, integral, radiation-cooled continuations of the wall or chamber liner to form the remainder of the expansion region for some applications. Mechanical attachment of thin high-temperature nozzle extensions also has been common (sec. 2.3.2.2). For the range of operating conditions appropriate for interegen designs, the radiation-cooled extensions start at area ratios of 3 to 10.

2.3.1.3 HOT RESTART

The problems of film boiling and monopropellant detonation are of concern for hot restarts with interegen and film-cooled heat-sink chambers. Heat soaks to the forward end of the chamber after shutdown, so that potential restart temperatures in the liquid region can be substantially higher than firing values. Although some film boiling is to be expected and can be tolerated during the restart transient, excessive restart temperatures may trap the liquid region surface in the film boiling regime and result in catastrophic throat temperatures. Heated-strip laboratory tests indicate no detonation problems with B_2H_6 for initial temperatures as high as 1000°F or with MHF-3 and MMH for initial temperatures of 800 to 900°F (refs. 57 and 58). However, these tests are not necessarily representative of chamber walls because the strip cools rapidly. Hot restart firings of interegen chambers have been demonstrated for initial temperatures as high as 900°F with MMH and 700°F with A-50 (ref. 50). Additional data are needed to define the ultimate limiting temperatures for successful restart.

2.3.2 Structural Design

2.3.2.1 MATERIAL PROPERTIES

The most suitable materials for monolithic designs are beryllium, copper, and graphite. Beryllium has been used in all applications to date. It combines low density with very high heat capacity, high conductivity, good strength at elevated temperatures, and compatibility with most combustion products. The low room-temperature elongation of beryllium results in its being very sensitive to low-cycle fatigue resulting from thermally induced strain; data on allowable strain vs cycle life are not available. In work reported in reference 58, induction-heated laboratory specimens simulating chamber thickness/radius ratios were cycled between 1000°F and −320°F; cracking occurred in 7 or 8 cycles. The history of cracking during beryllium heat sink and interegen chamber development is reviewed in section 2.3.2.2. On the other hand, the ultimate strength of beryllium is very good; reference 58 reports a room-temperature endurance limit of 44 000 psi for hot-pressed beryllium in the transverse direction. Therefore, beryllium is well suited to pulsed or restart applications in which thermal strains are low or in which restart does not result in complete strain reversal. In work reported in reference 50, two chambers were successfully subjected to large numbers of restarts.

Beryllium properties can vary significantly, the extent depending on the alloy, metallic impurities, and processing methods. Selected mechanical and physical properties of a hot-pressed 2-percent-BeO alloy are reported in references 58 and 50. It was found that control of the ratio of Fe to (Al + Si) impurities can lead to significant improvements in mechanical properties at elevated temperature. Tensile data at 1000°F for material with a ratio of 0.53 indicated strength about half that given in the literature, whereas significantly higher tensile strengths were obtained at a Fe/(Al + Si) value of 1.44.

Room-temperature elongation, and thus thermal-cycle capabilities, can be controlled to some extent by alloy selection and processing methods. Work reported in reference 60 evaluated three different alloys and attempted to match the elongation to the severity of the duty cycle; three chambers with square cross-sections were tested at 500 psi and 1600 lbf thrust. An aircraft-brake-grade beryllium alloy, modified to improve high-temperature ductility and having a transverse elongation of 3.0 percent at room temperature, was used for a duty cycle that resulted in four thermal stress reversals and the highest expected bulk temperature. A 2-percent-BeO alloy with 3.2-percent elongation was used for a 10-sec continous firing that was predicted to give the highest radial temperature gradient. A 3-percent-BeO alloy with 1.7-percent elongation was used for a nearly even pulse-distribution duty cycle that resulted in a lower temperature gradient and a lower final bulk temperature than the other duty cycles. All tests were completed successfully without incident. However, subsequent to hardware cooldown, hairline cracks were observed in the corners of the 2-percent- and 3-percent-BeO chambers. The brake-grade alloy showed no evidence of cracking and later was used for a series of vacuum start tests. A specially processed alloy with a 4.5-percent elongation was also obtained but not tested. Note that elongations can vary within a given grade specification; references 51 and 58 indicate a 2.5-percent transverse elongation for the 2-percent-BeO alloy at room temperature compared with the 3.2-percent elongation noted above.

2.3.2.2 CHAMBER WALL

Beryllium Chambers. – Beryllium chambers have failed primarily as a result of

(1) Low-cycle fatigue failure of the inside surface as a result of steep temperature gradients through the wall, and

(2) Excessive yielding due to a combination of pressure and thermal loading. For non-axisymmetric chambers, this failure mode is especially important, since the required thickness is more sensitive to pressure loads.

The design of thermally cycled beryllium chamber walls must limit the compressive strain on the inner surface during operation; strain reversal during cooldown can easily produce a

tensile strain in excess of the low-temperature elongation of the material. In any case, the throat region normally will undergo some plastic yielding when initially cycled to high temperature, the result being a minor decrease in the throat diameter, that is maintained without change during further cycling. In one test (ref. 57), a crack on the chamber wall was noticed after a film-coolant-ring failure "quenched" the hot inner surface of the beryllium, causing a reversal of the thermal stress from compression (at an elevated temperature probably in a range of relatively high strain) to tension in a range of lower allowable elongation. This crack was initiated at a tapped bolt hole that acted as a stress raiser. Other chambers in this program, including precontract development hardware, functioned without failure.

In the program reported in references 51 and 52, two thick-walled beryllium chambers cracked in the throat region during cooldown. A fractographic analysis of one chamber indicated that the fractures were brittle, a condition that is typical of low-temperature fractures, and that the fracture had originated internally just aft of the throat. It was theorized that the failure occurred on cooldown at a temperature between 200 and 800°F. It was further concluded that it was a thermal-stress-induced fracture with no evidence of material or manufacturing flaws. Consequently, an objective of a later phase of the program was to reduce the thermal stress level by recontouring the outside of the wall to remove extra material.

Cracking has occurred in other beryllium heat-sink chambers. For example, in one instance, a hairline crack was observed after cooldown following a 90-sec., 100-psi test without film cooling; this crack extended nearly the full length of the chamber and was approximately 1/4 in. deep at the injector. An additional test was then conducted for 60 seconds; during hardware cooldown, the crack progressed through the chamber wall. The pretest crack depth was distinguished by an oxide-like discoloration, whereas the post-test crack was observed to be clean and free of evidence of heating. In another example, the chamber used had previously been tested for 10 times before remachining to a larger internal diameter. This unit failed during firing at 500 psi, presumably because of residual stresses from its previous use. During cooldown, the fracture continued separating the chamber into halves. Post-test examination showed no anomalies in the metal. A structural analysis concluded that the wall thickness should be decreased to reduce the level of thermal stress. Two units incorporating the stress-analysis recommendation were fabricated and successfully tested.

Graphite chambers. – The tensile strength of graphites is quite low (table VII). Thus, bulk graphite chambers require rigid external support to prevent excessive tensile stresses from developing in the graphite; this support usually is provided by a steel housing. It is necessary either to insulate the structural case or to balance the mass of the case and graphite to ensure that the metal shell is not damaged by heat soakout from the graphite liner. Asbestos/ or silica/phenolic commonly is used as insulation. Crushable gaskets normally are used to prevent excessive loads from being imposed on either the liner or the structure by

Table VII. – Properties of Various Kinds of Bulk Graphite

Material*	Tensile strength, psi		Young's modulus, 10^6 psi		α, 10^{-6} in./in.-°F	
	W.G.	A.G.	W.G.	A.G.	W.G.	A.G.
ATJ	3300	2900	1.45	1.15	1.22	1.90
CHY	2750	2850	1.4	1.4	2.5	2.55
H-205-85	3500	3000	1.7	1.5	2.3	2.8
P-2239	3200		1.4		2.2	
AXF-5Q	10 000		1.7		4.8	

*Identified in Appendix D. W.G. = with grain A.G. = against grain

axial thermal expansion of the graphite. Gaskets of porous fibrous-graphite composites and of Grafoil have been used successfully.

2.3.2.3 ATTACHMENTS

The relatively high average temperatures and large mass associated with interegen and heat-sink chambers result in a large quantity of stored energy, so that insulation between the injector and chamber is needed to prevent injector overheating after shutdown. The kinds of insulation used range from low-cost rubber-impregnated asbestos to relatively costly mica. The selection of insulation is based on the operating temperature of the chamber, the duty cycle, and the temperature limits of the injector.

Failures in tests have occurred when the injector-to-chamber seal was lost. On metal heat sinks, this kind of failure has occurred during firing as the chamber overheated. On graphite units, the cause has been heat flow from the graphite to the metal case during post-test soakout. Aluminum crush gaskets are especially sensitive to the soak phenomenon. Heat input causes the seal to yield and become unloaded; leakage on the subsequent test results in a localized burnout. Copper chambers with bird-cage attachments have required retorquing of bolts to maintain seal loads on multiple restart test series; in a bird-cage attachment, bolts extend the length of the chamber to a separate retaining ring at the aft end. During high-pressure testing of copper chambers with a through-bolt forward flange, there have

been instances of flange distortion and loss of seal resulting from compressive yielding induced by chamber axial thermal expansion.

Loss of the injector-to-chamber seal can also be caused by metal diffusion at high temperature, which results in a brittle interstitial phase that can fracture on subsequent thermal cycling. Leakage past a gold-plated (0.0007 in.) primary seal in a beryllium chamber occurred as a result of fracture of a hard, brittle intermetallic beryllium-gold phase formed at the interface joint (ref. 61). Subsequent laboratory tests revealed that beryllium diffusion into gold starts at 500°F and that complete penetration of a 0.0007 in. gold plating occurs after 30 minutes at 800°F.

The techniques used to attach beryllium thrust chambers to injectors and to steel high-temperature nozzle skirts have progressed from conventional tapped-hole and through-bolt flange arrangements to more sophisticated concepts that minimize loads and discontinuities. Reference 52 describes a program in which drilled and tapped holes were used in the attachment of the injector to a beryllium chamber; the nozzle skirt of Haynes alloy L-605 was attached to the chamber by through-bolts and flanges on the chamber and nozzle skirt. Reference 50 reports a failure attributed to this type of attachment design: a crack that subsequently propagated through the chamber wall was initiated at the end of a thread in one of the tapped holes at the forward end of the chamber (sec. 2.4.2). However, tapped holes were used successfully for other beryllium chambers in that program as well as in the one in reference 52. Heli-coil* inserts normally are used with tapped holes. Flanges with through-bolts were used successfully in the program that preceded the work in reference 50.

In one development concept, a short rectangular beryllium chamber was retained between the injector and a graphitic nozzle by a metallic external shell that was part of the nozzle. A series-parallel spring-washer arrangement was used to accommodate chamber expansion, thereby limiting thermally induced loads on the graphitic nozzle.

Reference 51 describes a method by which the chamber was attached to the injector with a slip ring and segmented retaining ring that allowed secure retention of the chamber with a very small flange or lip on the beryllium chamber (fig. 10). Care was exercised to provide a smooth blend radius at the flange-to-chamber transition. Uniform load distribution was ensured by soft copper shims that provided compliance to eliminate load concentration due to point contact. Lamp-base threads were used on the nozzle skirt attachment flange and on the chamber as shown in figure 10; the beryllium had a nickel-copper-rhodium plating in this region. Both of these attachments introduced small discontinuities in the chamber wall section; also, both were thin and radially compliant and thus minimized the constraint of the beryllium by the attached members.

*Trademark of Mite Corporation, Danbury, CT.

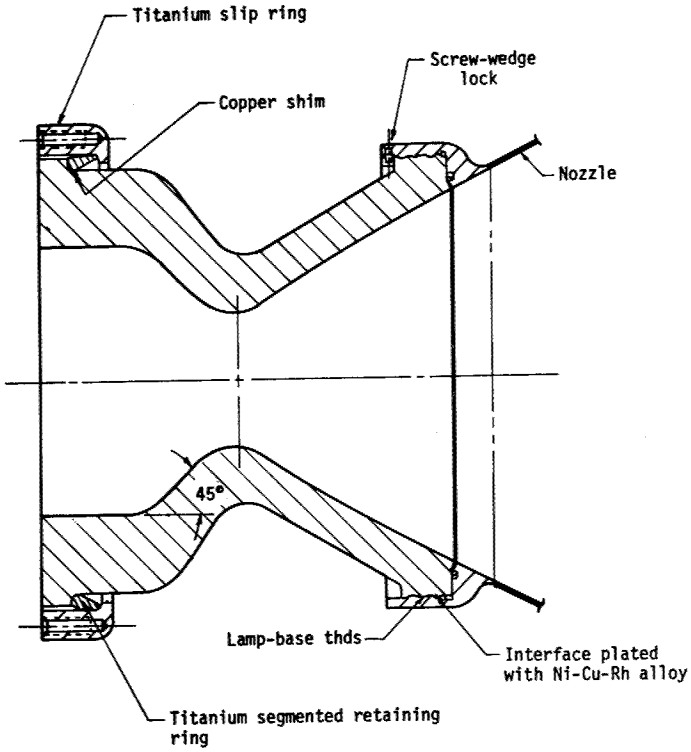

Figure 10. – Designs for attachment of beryllium chamber to injector and to nozzle.

Separate retaining rings have also been used for attachment of injectors to beryllium chambers. In a design with low expansion area ratio, the ring passed over the nozzle and engaged a lip at the injector end of the chamber. In the program of reference 60, chambers with a square cross section were attached to the injector by a rectangular slip ring and four-segment retaining ring that engaged a lip on the beryllium chamber. More recently a stainless steel injector was electron-beam welded to a Haynes L-605 transition ring that was brazed to the beryllium chamber (ref. 62). This joint was subjected successfully to vibration tests simulating 100 missions for the Space Shuttle RCS engines.

2.4 ADIABATIC-WALL CHAMBERS

As noted earlier, an adiabatic-wall chamber is one in which wall temperature control is provided by film cooling or peripheral mixture-ratio control or both; radiation losses are not

important, and the chamber wall operates close to the local adiabatic wall temperature. The actual components of adiabatic-wall and radiation-cooled chambers often are similar, and the discussion about design of radiation-cooled chambers (sec. 2.2) therefore is largely applicable here. References 63, 64, and 65 describe recent developments in film-cooled columbium chambers designed for essentially adiabatic operation. In engines where high combustion temperatures and often high chamber pressures are required, however, the conventional chambers made of coated refractory alloy are no longer adequate, even with use of film or barrier cooling. Typical examples are engines using fluorinated oxidizers. The technology in this area has not developed sufficiently to have yielded any flight-proved designs; however, it is an area where considerable R&D effort has been expended and where future development appears promising. The following discussion is limited to adiabatic-wall chambers for engines using fluorinated oxidizers. Table VIII lists the major programs conducted with adiabatic-wall chambers and fluorinated oxidizers. It should be noted that all are R&D programs.

2.4.1 Thermal Design

The thermal design of adiabatic-wall chambers consists of matching material compatibility and temperature limitations with the gas composition and maximum adiabatic wall temperature associated with the film cooling. Since there is no heat transfer within the wall, other thermal design considerations do not arise. Therefore, the following discussion is limited to materials considerations; film-cooling characteristics are treated in section 2.5.2.

2.4.1.1 MATERIALS

The very high combustion-gas temperatures (> 7000°F) typical of operation with fluorinated oxidizers limits the choice of chamber wall materials to graphite. Fortunately many propellant combinations are chemically compatible with graphite (e.g., all the propellants shown in table VIII). Some fuels, notably MMH, produce excess free carbon in the combustion gases, and this carbon is deposited on the chamber walls. Other fuels range from those that are slightly corrosive to carbon (e.g., straight N_2H_4 and BA-1014) to those that are essentially neutral (e.g., M-20). Figure 11 illustrates the corrosive effect of various fuels, as a function of mixture ratio, at 6000°F.

Of the fuels used with OF_2 as oxidizer, methane produces combustion gases compatible with carbon; diborane (B_2H_6) on the other hand, does not. The corrosive attack on graphite by OF_2/B_2H_6 combustion products currently is one of the stumbling blocks preventing further development with this propellant combination. Excessive carbon buildup, on the other hand, as experienced with MMH fuel, can also be a problem. Reference 69 reports that with this fuel nozzle throat area decreased by 20% after a test duration of 150 sec. Satisfactory methods for removing the carbon buildup have not yet been found.

Table VIII. – Basic Features of R&D Engines with Adiabatic-Wall Combustion Chambers

Engine Program	Thrust, lbf	Chamber pressure, psi	Propellants*	Firing duration, sec	Chamber material*
Fluorinated Oxidizer Thrust Chamber Materials Evaluation Program (ref. 66)	100 5000	200 100	LF_2/BA-1014 LF_2/BA-1014	10 270	Carb-I-Tex AG Carb 101
Development and Demonstration of Ablative Thrust Chamber Assemblies Using LF_2/N_2H_4-Blend Propellants (refs. 67 and 68)	5000	100	LF_2/BA-1014	600	AG Carb 101
Development and Demonstration of Passively Cooled Thrust Chamber Assemblies for Fluorinated Propellants (ref. 69)	3000 3000 3000	300 500 300	CTF/BA-1014-MMH CTF/M-20 CTF/BA-1014	450 8 300	AG Carb 101 AG Carb 101 PG/Carb-I-Tex
Space Storable Thrustor Investigation (ref. 70)	100	100	FLOX/Methane	320	PG/Carb-I-Tex
Free-Standing Pyrolytic Graphite Thrust Chambers for Space Operation and Attitude Control (ref. 71)	1000	100	LF_2/MMH	1000	PG

*Identified in Appendix D.

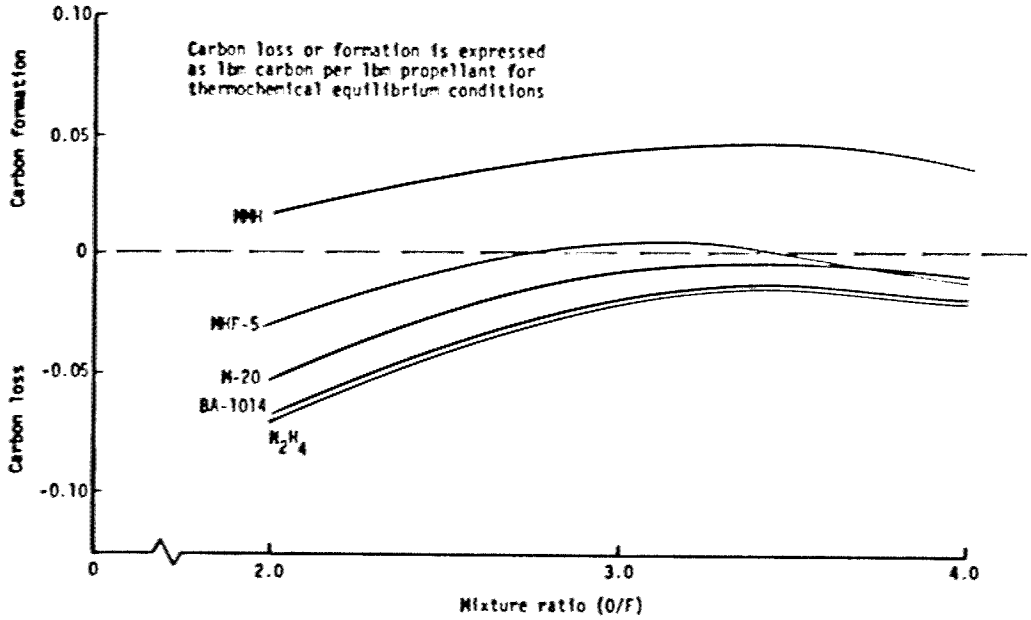

Figure 11. – Corrosion characteristics of carbon with CTF oxidizer and various fuels at 6000°F and 500 psi.

In chambers where graphite corrosion occurs, the type of wall material has marked effects on the amount of material removed. Pyrolytic graphite (PG) has consistently exhibited surface regression about one order of magnitude less than conventional bulk graphites and fiber-reinforced graphite composites; PG coatings on the inside chamber walls therefore are very effective in minimizing surface regression. To achieve satisfactory coatings, the substrate is provided with a surface finish as smooth as possible, because any irregularities in the surface are propagated through the coating as the PG layers are being generated and may become points of potential spalling of the coating.

The thermal and structural loads imposed on adiabatic-wall chambers preclude the use of most bulk graphites. The conventional types such as ATJ, G-90, and HLM-85 have too low a tensile strength to operate without external hoop and meridional support. Special high-strength grades of bulk graphite such as AXF-5Q are size limited. Practical engineering materials, therefore, are limited to PG and fiber-reinforced graphite composites.

Pyrolytic graphite is produced by chemical vapor deposition of a hydrocarbon gas (e.g., methane) on a graphite substrate, the result being deposited layers of uniform thickness. A free-standing PG combustion chamber (obtained by removing the graphite substrate

mandrel) therefore exhibits a constant wall thickness whether desired or not. The "c" direction of PG (normal to the deposited layers) has the lowest thermal conductivity and the highest thermal expansion. This condition often leads to delamination or spalling during fabrication. The suppliers of PG have found by experience that certain thicknesses should not be exceeded and curvatures should not be made too small if consistently satisfactory components are to be produced.

The graphite form that has seen the widest use in development of adiabatic-wall chambers for use with fluorinated propellants is the fiber-reinforced graphite composite, frequently called carbon/carbon even when it has the more ordered crystal structure typical of graphite. The reinforcement or fibrous component of this composite material consists of one of many forms: graphite or carbon felt; chopped, randomly oriented fibers; unidirectional fiber tape of yarn or roving; filament-wound fibers; fibers woven into cloth; even 3-D (three-dimensional) woven fabric and yarn assembled in a 3-D orthogonal arrangement. The binder phase or matrix is graphite or carbon produced by carbonization of an organic resin, by pitch impregnation, or by chemical vapor deposition of pyrolytic graphite or carbon. There are several fiber-reinforced graphite composites on the market. They include AG Carb, Carb-I-Tex, and Pyrocarb. Typical material properties are listed in table IX; actual properties vary greatly as a result of fiber reinforcement, form of reinforcement, method of fabrication, degree of graphitization, and method of reimpregnation.

Table IX. – Typical Room-Temperature Properties of Fiber-Reinforced Graphite Composites

Property	Value
Density, gm/cm^3	1.35 to 1.50
Tensile strength, with lamina, psi	5000 to 11 000
Tensile strength, across lamina, psi	350 to 650
Shear strength, interlaminar, psi	600 to 1800
Compressive strength, with lamina, psi	6000 to 9500
Compressive strength, across lamina, psi	13 000 to 15 000
Young's modulus (sonic method), 10^6 psi	2.3 to 2.9
Thermal exp. coeff., across lamina, 10^{-6} in./in.-°F	1.6 to 2.6
Thermal conductivity, across lamina, Btu-ft/hr-sq ft-°F	15 to 20

2.4.2 Structural Design

2.4.2.1 CHAMBER WALL

Several programs evaluating free-standing PG combustion chambers in the 100-psi, 100-lbf-thrust size have been conducted (ref. 72). The chambers performed well in a sea-level test configuration, but the altitude chambers failed at the juncture of the throat and the expansion cone. This failure was attributed to residual stresses superimposed on thermal stresses that are induced by the anisotropic nature of this material. To overcome this problem, external reinforcement of graphite filaments on free-standing PG chamber liners, internal PG coatings on filament-wound graphite-yarn chambers, and a high-modulus graphite yarn in a PG matrix were evaluated (refs. 70 and 73 through 75). The results were encouraging in that a test duration of 322 sec was achieved with a 100-psi, 100-lbf-thrust chamber operating with FLOX/methane. A larger chamber (300 psi, 3000 lbf) was tested successfully for 300 sec with CTF/BA-1014.

The fiber-reinforced graphite composites are characterized by relatively high tensile and compressive strengths and thermal shock resistance. The chief weakness is relatively low interlaminar shear strength, which generally ranges from about 600 to 1800 psi, and low so-called block-tensile strength (normal to the plane of reinforcement fibers), which is generally about half of the interlaminar shear strength (table IX). As a consequence, delaminations (separations between plies) can occur during fabrication as well as during operation. Minor delaminations, appearing as hairline cracks of short length, would in most cases have no deleterious effects on the performance of a combustion chamber. Even large internal delaminations, discernible by radiographic examination, would not be detrimental unless exposed to a pressure drop along the separated surfaces with an attendant gas flow or loaded in a manner that would tend to propagate the delamination (e.g., loaded in block tension or interlaminar shear).

In one program, a combustion chamber failed in a test firing because of a leak path leading from the injector interface to an internal delamination (ref. 69). The mode of failure was postulated to be detonation of propellant that had been trapped in the delamination after a previous test. Besides the obvious corrective action to provide a gas-tight seal between the injector and chamber, the elimination or reduction of delaminations was also desired; marked improvement was attained by controlling fabrication processes and by designing to prevent loading in interlaminar shear. Work has also been done to increase the interlaminar shear strength of the laminate composites. Increased strength has been obtained by pulling barbed needles through the laminates to achieve a fiber interlock between laminates or by incorporating fibers in the transverse direction by special fabric weaving techniques. In most cases, a two-dimensional reinforcement will suffice, provided the laminate orientation is at an angle with the load path and the material is loaded in compression, with-ply tension, or cross-laminate shear.

2.4.2.2 ATTACHMENTS

The attachment of an adiabatic-wall chamber to the injector presents two potential problem areas: heat soakback to the interface during coast periods, and differential thermal expansion of the hot chamber relative to attachment components. The heat flux to the bolts and gas seal usually is minimized by recessing the injector into the chamber, with the attachment flange located upstream of the injector face, and by providing a barrier for axial heat flow by making the chamber wall as thin as possible.

Thermal expansion of the fibrous-graphite composite is accommodated in the design of a combustion chamber by allowing the graphite to expand without imposing bending loads. Figure 12(a) shows a design incorporating a sliding joint to allow such expansion; figure 12(b) illustrates a design that allows thermal expansion in the hoop direction. Fibrous-graphite composites have an elongation of about 0.5% or less, and excessive bending moments have led to structural failures; e.g., a combustion-chamber fracture near the injector end (ref. 67). This condition was brought about by an attachment design that mechanically restrained the forward end of the chamber liner in hoop while it was free to expand directly downstream of the supported area. The imposed bending moment was sufficient to fracture the chamber. The design that led to failure is illustrated in figure 12(c); the graphite/phenolic insulation kept the steel collar flange cool and the high-modulus steel provided a rigid restraint. This design was an outgrowth of an earlier successfully tested chamber, shown in figure 12(d), that provided less rigid attachment.

2.4.3 Fabrication

Certain characteristics of the fabrication processes associated with fiber-reinforced graphite composites impact the design of combustion chambers. Most of the graphite composites are fabricated from fabric impregnated with an organic resin. The initial fabrication process, therefore, is the same as for an ablative chamber. In subsequent processing, the resin matrix is pyrolyzed, the volatiles being driven off; the volatiles thus lost amount to about 20 percent of the total composite weight. High pressure buildup due to volatile escape and stresses caused by shrinkage of the resin (about 2%) with a dimensionally stable reinforcement usually cause delaminations, especially in weakened places such as areas of wrinkles. Delaminations can also occur in components without wrinkles, but normally are not detrimental. Frequently, delaminations can be repaired (filled) by reimpregnation; however, the interlaminar and block tensile strengths are reduced. Wrinkles are of greater consequence to the performance of the end product since they can drastically reduce the strength. Measurements of the hoop tensile strength of AGCarb-101 revealed a strength reduction of more then 50 percent in rings with wrinkles in comparison with non-wrinkled rings. A liner for a combustion chamber of 5000 lbf thrust failed during a test firing; according to reference 68, the failure was postulated to have initiated in an area of excessive wrinkles.

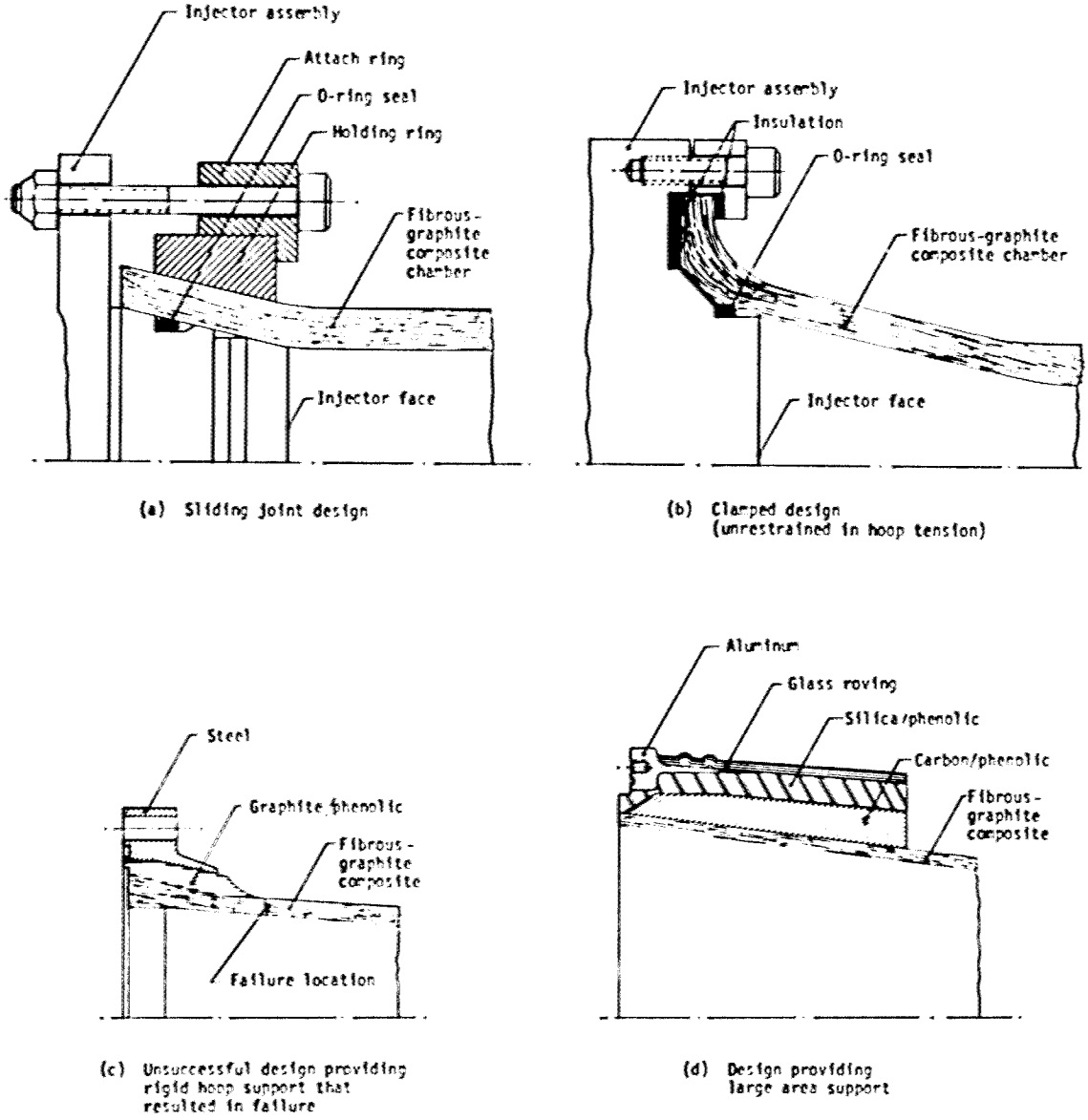

Figure 12. – Four injector/chamber attachment designs for an adiabatic-wall chamber.

No comprehensive programs have been undertaken to establish acceptable limits for wrinkles. What may be considered acceptable is essentially the same as for ablative chambers, as is the problem of how to design to avoid or minimize wrinkles (sec. 2.1). The fibrous-graphite composite is, however, more critical than the standard ablative component in regard to wrinkling.

Fabrication in female molds or in matched metal dies eliminates or greatly reduces wrinkles. In female molds the compaction of the material by the applied pressure will stretch the innermost fabric layers by pushing them outward toward the mold. In matched metal dies, the individual layers of precut fabric will be pressed closer together without either stretching or wrinkling the fabric.

Shingle or rosette layups are most suitable for use in female molds. A carefully controlled post-cure and carbonization cycle is required to prevent delamination during this process. Delaminations, when they occur, have been filled by reimpregnation with phenolic or furfuryl-alcohol resins. Precut patterns of fabric are the preferred reinforcement for use with matched metal die molding. This method of fabrication is most suitable for small (< 200 lbf thrust) chambers.

2.5 HEAT TRANSFER TO THE CHAMBER WALL

Convection is the primary mode of heat transfer to combustion chamber walls; the amount transferred by radiation from the combustion products usually is small. The convective heat flux usually has been based on the adiabatic wall or recovery temperature, i.e.,

$$\dot{q}_c = h_g (T_{aw} - T_w) \tag{3a}$$

$$= \rho\, u_e\, St\, C_p\, (T_{aw} - T_w) \tag{3b}$$

where

$\dot{q}_c$ = convective heat flux

h_g = convective heat-transfer coefficient

T_{aw} = adiabatic wall temperature

ρ = density of combustion gas

u_e = velocity of free-stream gas

St = Stanton number for temperature difference

$= h_g/(\rho\ u_c\ C_p)$

C_p = specific heat at constant pressure

with the Stanton number based on pipe-flow correlations or integral boundary-layer analyses and ρ and C_p based on reference conditions. References 76 and 77 confirm the adiabatic wall temperature as the appropriate driving temperature with film cooling as well, implying that the thermal boundary layer at the wall is much thinner than the coolant/core-stream mixing layer. In order to account for chemical reactions in the boundary layer, the product of specific heat and temperature difference [i.e., the C_p $(T_{aw} - T_w)$ term] must be replaced with the corresponding enthalpy difference. Use of enthalpies has been found to be important for O_2/H_2, F_2/H_2, FLOX/methane, and other propellant combinations with combustion temperatures over about 5500°R. Ammonia reactions in N_2O_4/hydrazine-type propellant systems can be important with film cooling. The predicted convective heat flux for reacting systems should also be corrected when energy and mass diffusion rates are unequal, i.e., when the molecular Lewis number is not near unity (ref. 78). However, this correction apparently is ignored or assumed to be small in present design practice.

Three reference temperatures are used frequently in property evaluation: (1) the adiabatic wall temperature, recommended in reference 79; (2) the Eckert reference temperature (ref. 80); and (3) the arithmetic mean of the wall and adiabatic wall temperatures. References 76, 81, and 82 indicate that with film cooling it is essential to evaluate properties at the local gas mixture composition. Reference 76 found that the use of local gas compositions and the arithmetic-mean reference temperature allowed the same pipe-flow coefficients to correlate Stanton number data with and without film cooling, except for effects of injection velocity near the coolant injection point. The following sections consider the evaluation of the Stanton number and of the adiabatic wall conditions with film cooling.

2.5.1 Evaluation of Stanton Number

Most predictions of combustion-chamber wall temperature are based on the *a priori* assumption of turbulent flow with the Stanton number predicted from some form of the "simplified Bartz" pipe-flow correlation (ref. 12), or from a boundary-layer analysis of the integral type, or from a combination of these methods. The use of a constant correlating coefficient in the pipe-flow approach is unacceptable; the value of 0.026 recommended in reference 12 typically underpredicts the Stanton number in the cylindrical section and in the first part of the convergent section, where the boundary layer is in its initial stages of development, but overpredicts in the throat region where the pressure gradient is large. Therefore, it is necessary to use empirically determined local correlation coefficients that

are functions of the chamber contour and injector design. References 79 and 83 review much of the nozzle heat-transfer data.

Use of a boundary-layer expression is consistent with the physical flow phenomena in a combustion chamber and can partially eliminate some of the shortcomings of the pipe-flow approach. The expressions most widely used in combustion chamber work are those of Mayer (ref. 84), which is based on the method of Ambrok (ref. 85), and of Elliott, Bartz, and Silver (ref. 86); the latter represents a sophistication of the basic Ambrok method that cannot be justified by better agreement with reality. Two problems remain with the boundary-layer approach: where and/or with what initial conditions to start the boundary-layer analysis, and how to accommodate the pressure gradients of interest for combustion chamber application. One approach to the former problem is to start the boundary-layer analysis at the beginning of convergence or at the point where an axial line from the outermost injector elements intersects the convergent section, with the initial thickness such that the Stanton number matches that obtained from pipe-flow correlations used upstream. An alternate method starts the boundary-layer analysis at the location of the maximum empirical Stanton number, with the initial thickness based on that Stanton number. The second problem, that of accommodating the pressure gradient, is inherent in the use of empirical generalizations derived from data for zero pressure gradient. This limitation is not restricted to the simple methods that assume velocity and temperature distributions across the boundary layer; finite-difference solutions of the boundary-layer equations (refs. 87, 88, and 89) exhibit the same inability to treat significant favorable pressure gradients and for the same reason, even though the empirical input is of a much more fundamental nature. The BLIMP-J computer program of reference 89 was developed specifically for prediction of performance of liquid rocket engines and includes the effects of chemical reactions; however, this program has not been used extensively for thermal design of rocket chambers.

Combustion-chamber boundary layers are not always characterized by turbulent flow. The phenomena of reverse transition and laminarization, which are associated with large favorable pressure gradients, have been clearly demonstrated (refs. 90 through 97) and are illustrated in figure 13. This figure, along with the data of references 90 through 97, indicates that laminarization can reduce the local Stanton number by a factor of two to three below that which would be obtained for turbulent flow at the same Reynolds number. Laminarization typically occurs for values of chamber pressure times thrust ($P_{ch} \times F$) less than about 10^5 $lbf^2/in.^2$, which is the range of application for many self-cooled chambers.

A theoretical laminarization criterion (ref. 98), which is in agreement with the data of reference 93, requires that, over a certain distance upstream of any point,

$$K = \frac{\mu_e}{\rho_e u_e}\left[\frac{1}{u_e}\frac{du_e}{dx} + 0.4\frac{1}{r}\frac{dr}{dx}\right] \geqslant 3.3 \times 10^{-6} \tag{4}$$

where

K = flow acceleration parameter

μ_c = dynamic viscosity of freestream gas

r = local chamber radius

x = distance along chamber contour

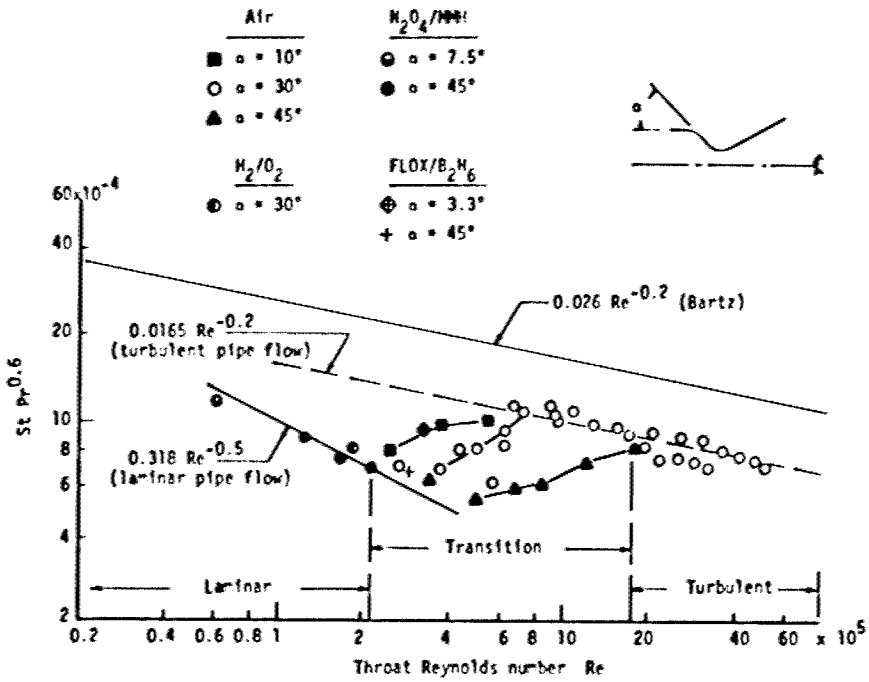

Figure 13. – Graph of heat-transfer data illustrating regions of reverse transition and laminarization.

It has been demonstrated that there is a considerable delay or lag in the influence of flow acceleration on the Stanton number. Reference 93 indicates that the above condition may have to persist for 100 to 200 momentum thicknesses in the case of essentially constant K at the threshold level. When K varies, as it does in combustion chambers, the criterion may have to be modified. The laminarization criterion in equation (4) is limited to relatively smooth walls; additional work is required to clarify the influence of roughness, wall cooling, film cooling, and freestream turbulence on laminarization.

The laminarization criterion $K \geqslant 3.3 \times 10^{-6}$ is in reasonable agreement also with the axisymmetric-nozzle data of references 90, 91, and 97, although there is some indication that the criterion may be conservative near the throat. Since K decreases rapidly near the throat (ref. 97), a lower laminarization limit in this region could result from the influence of the higher K values upstream. It should also be noted that references 94 and 95 give lower values of K for laminarization, with reference 95 indicating a reduction as the momentum-thickness Reynolds number decreases. References 90 and 97 confirm that the reduction in K near the throat can result in laminarization upstream of the throat when the throat is in the reverse-transition regime.

The parameter K is essentially the ratio of a geometric acceleration parameter to the local Reynolds number based on chamber diameter; e.g., for one-dimensional isentropic flow

$$K\,Re = 2\left[\frac{2}{1 - M^2} - 0.4\right]\sqrt{\epsilon}\,\sin\beta \tag{5a}$$

$$= 2\left[\frac{2r_t}{R_u\,(\gamma + 1)}\right]^{0.5} \text{ at the throat} \tag{5b}$$

where

Re = Reynolds number

M = Mach number

ϵ = local area ratio = $\dfrac{\text{local geometric flow area}}{\text{geometric flow area at nozzle throat}}$

β = angle between chamber centerline and wall tangent

R_u = radius of curvature of chamber wall upstream of throat

r_t = radius of nozzle throat

γ = isentropic flow coefficient

Therefore, laminarization is controlled by the chamber contour and by the product $P_{ch} \times F$, since the latter determines the throat Reynolds number. It is apparent that large convergence angles, large contraction ratios, and small throat radii of curvature promote laminarization; figure 13 demonstrates the effect of convergence angle. For typical contours, the product (K Re) will be 1.5 or greater just upstream of the throat, so that the

criterion of equation (3) indicates laminarization for throat Reynolds numbers as high as 450 000; the laminarization limits in references 90 and 91 occur in the range 500 000 to 600 000. For a specific impulse of 300 sec, thrust coefficient of 1.8, and typical combustion product viscosity, a Reynolds number limit of 450 000 corresponds to P_{ch} F $\leq$ 140 000 $lbf^2/in.^2$; this result is indicative of the design conditions for which the possibility of boundary-layer laminarization must be considered. Note that this phenomenon may preclude the extrapolation of subscale test results to large turbulent chambers.

Stanton numbers in the laminarized regime can be predicted from laminar boundary-layer theory, with the development starting where the pressure gradient or flow acceleration first becomes significant (refs. 93 and 96). Reference 96 suggests a procedure for determining such a starting point that is in good agreement with the Stanton-number data of reference 90. Figure 13 also indicates agreement between laminarized data and a laminar pipe-flow correlation. Stanton-number correlations for all regimes, based on a modified pipe-flow approach, are given in reference 80.

2.5.2 Film Cooling Analysis

When the injector provides film cooling or a special mixture-ratio zone at the periphery that supplies combustion products that act as film coolant, a prediction of the adiabatic wall conditions as a function of axial position is required in order to determine the film coolant flow required. Such design predictions have been based primarily on correlations of laboratory data, usually for flat-plate configurations. Future analytical film-cooling models undoubtedly will continue to be founded on laboratory test data. Therefore, the overriding problem in the film cooling area is one of utilizing firing data to adapt laboratory models to actual rocket applications. Recent work, described below, confirms that mixing rates in combustion chambers differ significantly from those in analytical models based on laboratory data. In addition, adequate laboratory investigation of coolant effectiveness downstream of a liquid film is lacking, particularly for the monopropellant coolants typically used in self-cooled chambers.

Gas Film Cooling. – Adiabatic wall temperatures with gas film cooling have most frequently been predicted by means of the semi-empirical flat-plate model of Hatch and Papell (ref. 99) with various modifications to account for the axial variation of freestream mass velocity in a combustion chamber. However, this approach is based on a physically unrealistic heat-exchanger model with no explicit representation of the entrainment of freestream or core flow into a mixing layer containing all the film coolant, and it correlates only the data for locations that are relatively close to the coolant injection point. Reference 100 provides a method of correlating the data far downstream of the injection point by use of an entrainment model based on conventional incompressible-boundary-layer theory. Reference 101 extended the latter approach to compressible, accelerating flows and used it to present data for various freestream turbulence levels and convergence angles with two-dimensional flow.

Reference 76 developed an entrainment model based on five sets of flat-plate laboratory data; these data ranged from the isothermal region near the injection point to an effectiveness of 0.1 and were obtained with helium (ref. 99), air (refs. 77 and 102), argon (ref. 102), and Arcton (ref. 102) as the film coolant with air as the freestream flow, combinations that provided a wide range (0.26 to 4.2) of coolant/freestream density ratio. References 76 and 103 demonstrated the applicability of this model with hydrogen film coolant (N_2 freestream) and indicated that the model is valid for coolant effectiveness as low as 0.02. In this model the coolant effectiveness is based on total enthalpy and by the usual mass-transfer/energy-transfer analogy for a turbulent Lewis number of unity (ref. 103) is also equal to the effectiveness based on element rather than species mass fractions. This approach allows data based on gas compositions at the wall (ref. 102) to be compared with those based on adiabatic wall temperature, provides a basis for introducing the effects of chemical reactions and high-speed flow (which are missing in most laboratory tests), and defines the local gas composition on which to base the properties required to determine the heat flux to non-adiabatic walls. The entrainment model used in references 76 and 103 also provides for generalization to axisymmetric accelerating flows. Details of this model are presented in Appendix A.

For normalized mixing rates of flat-plate and nozzle configurations, reference 76 identifies significant differences that result from flow turning and acceleration in the nozzle. These turning effects, observed also in the data of reference 104, are attributed to the imbalance in fluid centrifugal stresses caused by density differences between the coolant and freestream flows. References 81 and 105 provide direct measurement of adiabatic wall temperatures with hydrogen film cooling during H_2/O_2 firings. Comparison of these data with the model of reference 76 revealed initial mixing rates 2 to 4 times those predicted, presumably because of the effects of injector core flow, higher freestream turbulence intensities, and different coolant injection configurations; mixing rates at the throat were 1.5 to 2.0 times those predicted. Both references 76 and 81 indicated mixing rates downstream of the throat significantly lower than those predicted on the basis of flat-plate data; in some cases the mixing rate was low enough that the imperfect recovery of kinetic energy more than offset the mixing, thereby causing adiabatic wall temperatures to decrease. Therefore, while the film-cooling model of reference 76 provides a sound framework for treating real nozzle flows and is in good agreement with flat-plate laboratory data, considerable effort will be necessary to characterize the effects of flow turning and acceleration, coolant injection from configurations other than continuous slots, and core injection and combustion.

Liquid Film Cooling. – The most common type of film cooling used in combustion chambers involves injection of the fuel as a liquid. In this case, two regions are of interest: the region in which the wall is covered by a liquid film (liquid length), and the downstream region in which the wall is covered by a mixing layer composed of coolant vapor, decomposition products, and combustion products. In rockets, the surface of the liquid film is unstable, and it is essential to include instability effects in the prediction of liquid lengths.

Liquid-region lengths usually are determined by a simple energy balance that accounts for the sensible and latent heat absorption required to reach the saturated vapor state and for mass-transfer effects at the liquid/gas interface. However, this energy balance must include empirical factors to account for augmentation of heat-transfer coefficient and liquid entrainment due to liquid surface instability; references 106 and 107 review these phenomena. Most data are for adiabatic walls, in which case these factors can be combined into a single flow-effectiveness factor that frequently has been correlated with a film-coolant Reynolds number, as in reference 106. Reference 53 presents such a correlation based on wall-temperature data acquired during chamber firings. For interegen-chamber designs and hot-restart analyses in which the heat transfer from the wall to the liquid film is significant, it is necessary to separate entrainment and heat-transfer effects. Reference 107 has separated these effects, using laboratory data on adiabatic walls, and found that both effects depend on the core-flow momentum rather than the coolant Reynolds number. Reference 107 represents the best available laboratory data, but comparison of this model with liquid lengths in rocket engines indicates modification of the laboratory model is required for the typical rocket environment. In addition, considerable extrapolation is required to cover the range of core-flow momentum of interest for rocket application.

It has been common practice to analyze the region downstream of the liquid film with a model for gas film cooling. However, the effective coolant velocity required for such an analysis is unknown; laboratory data required to define such a velocity or establish a separate model for the liquid case are lacking. In addition, there is a lack of agreement on the analysis of the vapor/decomposition-product region downstream of the liquid film in the case of a monopropellant coolant. A heat-exchanger model used in references 51 and 52 assumes that the coolant vapor is superheated until either a critical wall temperature or degree of superheat causes decomposition, which is considered to disrupt the coolant flow and cause complete mixing with the core flow. Another approach (ref. 82), which has been confirmed experimentally for MMH, assumes that the vapor decomposes near the liquid surface and includes a region above the liquid in which the decomposition products begin mixing with the core flow; the latter region continues downstream of the liquid film in a manner similar to a gas film-cooling mixing layer. Details of this analytical model are presented in Appendix B.

2.5.3 Film Coolant Injection

Efficient methods of injecting liquid film coolant are required to provide uniform coverage and to minimize liquid entrainment by the combustion products. The combination of film-coolant orifice diameter and spacing affects circumferential distribution of heat flux. A small orifice spacing is desirable but sometimes is difficult to achieve with reasonably sized orifices. Orifices less than about 0.015 in. in diameter are difficult to machine accurately and are susceptible to plugging problems, although orifices 0.010 in. in diameter have been used. Experience has shown that a maximum center-to-center orifice spacing of 0.25 to 0.30 in. will provide a sufficiently uniform film-coolant coverage.

Alternate injection schemes have been used in systems where prohibitively small orifices are required to give the desired spacing. Larger spacings with improved circumferential distribution can be accommodated by swirling the film coolant; however, swirling cannot be used in the presence of injector baffles. Impingement of pairs of film cooling streams to provide tangential fan patterns has also been used.

The angle at which liquid film coolant impinges on the chamber wall is important in providing good coverage and in minimizing droplet formation and entrainment from the liquid film. Visual observations with a transparent chamber indicated significant uncooled areas next to the injector for impingement angles less than 28°, while angles greater than 35° resulted in instabilities in the impingement area and loss of coolant due to droplet formation (ref. 51). Reference 58 noted much greater loss of coolant for an angle of 45° than for an angle of 30° in single-jet laboratory tests. Reference 53 notes little difference between 20° and 30° impingement angles, on the basis of heat-flux measurements in hot firings. Reference 51 also indicates less coolant entrainment with a circumferential velocity component or swirl, presumably because the centrifugal forces tend to hold the coolant on the wall.

Laboratory data on gas film cooling with continuous slot injection indicate a maximum coolant effectiveness when the ratio of coolant injection velocity to core-stream velocity ranges from 1.2 to 1.4; thus, increasing coolant flow with a fixed slot height can increase adiabatic wall temperatures if the velocity ratio is too large. For example, the model of reference 76 gives a broad maximum between velocity ratios of 1.15 and 1.5. The cylindrical chamber data of reference 76 peak at a velocity ratio of 1.2, while the conical chamber effectiveness values continue to increase slightly between velocity ratios of 1.2 and 1.4. Application of the model of reference 76 to a design situation, in which the coolant effectiveness is held constant while the slot height is allowed to vary, indicates that the minimum coolant flow is obtained at a velocity ratio of 1.0 to 1.05. The increase in coolant flow required for deviations from this range is shown in figure 14.

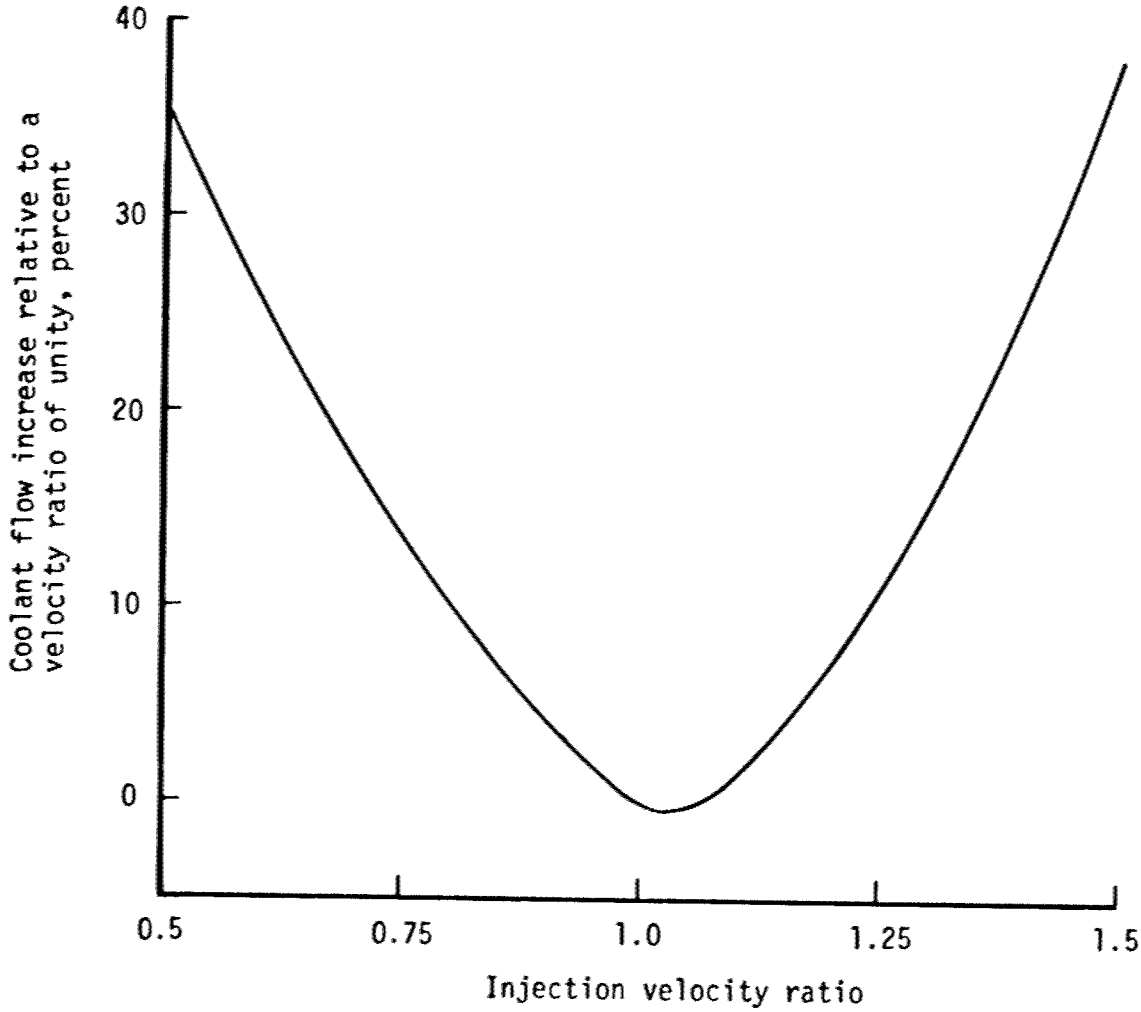

Figure 14. – Effect of coolant/core-stream velocity ratio on coolant flow requirements.

3. DESIGN CRITERIA and Recommended Practices

3.1 ABLATIVE CHAMBERS

3.1.1 Thermochemical Design

3.1.1.1 LINER

3.1.1.1.1 Surface Regression

Surface regression of the ablative chamber liner shall remain within acceptable limits.

Normally the engine performance requirements dictate the maximum allowable increase in throat area. This limit together with the firing duration establishes the permissible regression rate. In ablative chambers without throat inserts, the liner material selected must be adequate for the regression requirements and compatible with the thermochemical environment.

Silica or quartz reinforcement should be used in all engines operating with propellants producing combustion products with high concentrations of water vapor (> 33%). Carbon or graphite reinforcement should not be used unless an effective non-oxidizing boundary layer can be provided (by fuel-film or barrier cooling).

In general, surface temperatures should be limited to about 3000°F for silica and quartz chamber liners. This limit can be maintained by film or barrier cooling. Under special circumstances (e.g., chamber pressure less than 125 psi, short firing durations, and nonstreaking injectors), allowable surface temperatures may be as high as about 3400°F, subject to experimental verification. At high chamber pressures (> 300 psi), surface temperature is no longer the limiting condition in regions of high gas shear forces, and throat inserts may be required to prevent excessive surface regression. See section 3.1.1.2 for selection of throat insert material and section 3.1.2.1 on insert design.

Although analytical models with explicit surface thermochemistry (e.g., those in refs. 5 through 7) cannot be used for prediction of absolute surface recession rates without empirical adjustment of key parameters, they are recommended as the best available method for predicting the relative effects of the various design parameters that influence recession, for interpreting test results, and for extrapolating from experimentally confirmed base points.

3.1.1.1.2 Erosion Characteristics

Ablative chamber liners shall not exhibit gross, non-uniform erosion characteristics.

Material loss due to spalling or chunking of larger pieces in a sporadic or random fashion must be avoided. Materials selected must develop a char sufficiently strong to remain in place during engine firings. Magnesium hydroxide and asbestos reinforcements should not be used in high-pressure, high-gas-shear environments. Asbestos can be used in nozzle extensions at low pressures; however, cracks in addition to delaminations should be expected. Silica and quartz reinforcements generate stable chars provided the resin system is relatively stable, i.e., has low thermal expansion and contraction. The prepreg should have a resin content between 20 and 35 percent, with either silica or quartz reinforcement. The lower resin content generally will provide a greater thermal stability but also a higher density and higher thermal conductivity, and the material is a little harder to fabricate. A post-cure usually is helpful in improving the thermal stability of the composite.

When design requirements necessitate selecting a material with a low modulus or low density and low thermal conductivity, a higher resin content (up to about 50 percent by addition of a rubber filler) may be used; however, such a material is subject to large thermal expansion and subsequent shrinkage and has a tendency to chunk. Caution should be exercised in its use. An overwrap of a standard silica- or asbestos-reinforced phenolic must be incorporated to prevent excessive liner shrinkage as well as to prevent combustion gas flow to the structural shell in any delaminated areas of the liner. Overwrap is not recommended for chamber liners operating at pressures above about 125 psi.

3.1.1.1.3 Thermostructural Integrity

Over the chamber operational life, the ablative chamber liner shall not degrade to the extent that the chamber cannot perform as required.

The liners must be made thick enough and the reinforcement must be oriented such that the outermost part of the liner is not charred at the end of the duty cycle. Determine the char depth by methods given in reference 6, using char thermal conductivities that have been shown to correlate firing data. Direct use of laboratory data on char properties is not recommended.

A safety factor of 1.25 should be applied to the predicted char depth to account for uncertainties in local injector characteristics and material properties, unless these factors have been accounted for explicitly in the boundary conditions and properties used in the analytical model.

Additional virgin liner material or insulation overwrap consistent with the structural-shell temperature limits of section 3.1.1.3.1 should be provided.

3.1.1.1.4 Fiber Orientation

In ablative chamber liners made of fabric or tape, the fiber orientation shall be optimum for each specific area of use within the chamber.

The factors to be considered in the optimization include structural integrity, erosion resistance, thermal conductivity, thermal expansion, fabricability, and cost. General guidelines are given below for the three major regions of the combustion chamber.

Chamber. – Orient the fibers to the chamber wall at an angle of 6° to 60°. Recommended angles are 30° and 45°. Low angles should be used for low thermal conductivity in the radial direction and low thermal expansion in the axial direction. Delaminations usually are also minimized with low-angle orientations. Higher angles may result in somewhat improved erosion resistance and allow easier fabrication of thick-walled chambers. The front end (nose) of the chamber will, of necessity, have some short plies on the inside. To prevent losing these plies during firings, the nose should be brought forward of the injector face, or coolant should be provided to prevent charring the nose.

Throat. – Orient the fibers to the chamber/nozzle axis at an angle of 30° to 60°. Angle selection is influenced by the fabrication method. A 45° angle generally is optimum when this material portion extends into the divergent nozzle.

Divergent Nozzle. – Orient the fibers to the gas-side wall at an angle of 15° to 45°. Caution should be exercised that the configuration of the aft end of the part does not result in charred areas where the reinforcement fibers are not anchored in virgin material or held in place by hoop reinforcements and a mechanical retaining shoulder or taper.

3.1.1.2 THROAT INSERTS

Throat inserts shall restrict throat area changes to acceptable limits.

The throat insert material must be compatible with the combustion gases. In chambers with combustion gases containing 1/3 or more water vapor, either KT silicon carbide or JTA graphite composite throat inserts should be used if wall temperatures can be controlled to 3600°F or less. Silicon carbide has a somewhat greater propensity for cracking; JTA, on the other hand, will erode slightly more. These materials should be used only in smaller engines (< 1000 lbf thrust). In larger engines, molybdenum throat inserts may be considered provided that they have oxidation resistant coatings (e.g., silicides).

For higher temperatures (> 3600°F), pyrolytic graphite (PG) washers should be used, provided that a fuel-rich boundary zone can be generated.

3.1.1.3 INSULATION AND STRUCTURAL SHELL

3.1.1.3.1 Thermostructural Adequacy

The insulation and structural-shell combination shall ensure structural adequacy of the chamber at the highest temperature to which it is exposed.

Since the strength of structural materials is a function of temperature, one of two conditions must be satisfied: (1) the structural-shell material must be able to withstand the maximum liner temperature, or (2) the liner and insulation overwrap thickness must be adjusted to limit the temperature to that which the shell material is capable of sustaining without its strength being reduced to a level approaching the highest imposed stress.

Materials that should be considered for use as structural shells on flight hardware include fiberglass/resin, aluminum, titanium, and stainless steel. The upper temperature limits of these materials for this application are as follows:

Fiberglass/epoxy	300°F
Fiberglass/phenolic	500°F
Fiberglass/polyimide	700°F
Aluminum	350°F
Titanium	800°F
Stainless steel	800°F

In addition to temperature capability, other factors to be considered in selecting the shell material include weight, cost, fabricability, reliability, and envelope restrictions.

3.1.1.3.2 Prevention of Gas Flow

The structural shell shall not be exposed to combustion gas flowing through the liner.

The ablative liner should be provided with a flatwise overwrap of either silica/phenolic or asbestos/phenolic. The latter preferably should not be used in sections thicker than 0.3 in. To minimize residual volatile matter in the overwrap, especially with asbestos/phenolic, use a highly B-stage material and orient the wrap to permit escape paths for volatiles between plies.

The overwrap can be made an effective, lightweight insulation by using a silica (or asbestos) reinforcement in a phenolic resin filled with micro-balloons. With this material, a weight reduction of nearly 50 percent in comparison with standard reinforced phenolics is possible.

If a flat overwrap is not used, the liner must be thick enough so that it will not char through (sec. 3.1.1.1.3).

3.1.2 Structural Design

3.1.2.1 THROAT INSERTS

3.1.2.1.1 Configuration

Throat-insert configuration shall ensure retention of the insert under all imposed loads.

The throat inserts should be provided with external support sleeves of graphite or tungsten as shown in figure 1. The graphite selected should have a thermal-expansion coefficient matching or slightly lower than that of the insert material. If tungsten is used, the interface between insert and sleeve should be filled with an elastomeric compound such as silicone rubber that acts as a cushion for expansion.

A design without an external support sleeve may be acceptable for engines with short firing duration and for engines where restarts after cooldown are not required or where the ablative backup would not appreciably degrade during firing.

The insert should have a conical outer contour (fig. 1), and it should be lapped into the supporting sleeve if one is used. Its smallest OD should be at the aft end so that, even if the insert cracks in a radial plane, it will not be ejected. To minimize the potential for cracking, the insert should be made with nearly uniform wall thickness. The thickness-to-ID ratio should be 0.2 to 0.3 and the length-to-thickness ratio should not exceed 6.

In all cases, thermal and stress analyses must be performed to verify design adequacy.

3.1.2.1.2 Thermal Expansion

The ablative chamber shall accommodate thermal expansion of the throat insert.

The throat inserts should be made short in the axial direction to minimize thermal expansion. No special provisions need be made for inserts of silicon carbide or JTA; however, PG inserts designed as a stack of washers require allowance for the high expansion

in the direction perpendicular to the washer face. In chambers that do not cool to ambient temperature between firings, a crushable gasket of porous carbon or exfoliated PG laminate should be installed upstream of the stack, which should not exceed 2 in. in length. Such gaskets will take a permanent set, and to avoid gaps between the PG stack and adjoining components it may be necessary to incorporate springs in chambers that are exposed to multiple firings and cool to ambient temperature between firings.

3.1.2.2 STRUCTURAL SHELL

3.1.2.2.1 Structural Adequacy

The structural shell shall be adequate for all loads and combinations of loads due to internal pressure, thermal environment, vehicle acceleration, start and shutdown dynamics, and gimbal actuation.

For fiberglass support structures, it is recommended that the glass fabric (type 143) be laid up outside the ablative liner (or insulation) with the high strength in the axial direction and that glass roving be wrapped over the fabric in the hoop direction. A bidirectional glass fabric (type 181) can also be used. This material will provide structural support in the hoop direction, reducing or deleting the requirement for glass roving. This approach should be used in nozzle regions where hoop stresses are low and in locations where the ablative liner outside surface has a large angle with the axis that makes application of roving difficult.

To prevent excessive strain-induced loads resulting from thermal expansion of the liner, a structural shell with comparable elastic modulus (fiberglass) should be used; otherwise, an adhesive- or sealer-filled gap between the liner and a metal shell must be incorporated to limit the maximum liner compressive stresses. The gap generally should not exceed 0.030 in. radially.

In calculating design stresses at allowable strain levels, apply a factor of safety to the predicted loads to account for uncertainties in loading, analytical methods, and material characterization. For metal shells, whose properties are normally well defined, a factor of safety of 1.25 to 1.50 is recommended. For fiberglass structures, whose properties are more dependent on fabrication quality and methods, a factor of safety of 1.5 to 1.8 is recommended.

3.1.2.2.2 Liner Retention

The structural shell shall provide positive retention of the ablative liner.

The structural shell must be configured with internal shoulders, flanges, or tapers that will retain the liner mechanically even if adhesively bonded joints fail because of adhesive deterioration.

Metal shells, when used, should be made conical with the small end aft or with an integral or bolted-on flange at the aft end. Fiberglass shells are wrapped in place on the liner, and since the liner usually is hourglass shaped, it will be locked in place by the fiberglass overwrap.

3.1.2.3 ATTACHMENTS

3.1.2.3.1 Method

The method for joining attachment flanges and structural shells of dissimilar materials shall ensure positive retention of the attachment.

Metal flanges should be joined to a fiberglass structure by incorporating circumferential ridges and grooves in the flange, laying up the glass fabric over the ridges and into the grooves, and then widening glass roving to fill the grooves and lock the fabric in place. The concepts shown in figure 3 illustrate this practice. The first two designs (figs. 3(a) and 3(b)) are satisfactory if the fiberglass temperature stays low enough to prevent degradation of the resin bond. The designs in figures 3(c) and 3(d) are improvements and provide better locking of the glass fabric to the metal flange, even at high temperatures.

Tapered surfaces and retaining rings or pins can also be used. However, adhesive bonding is not considered to constitute positive retention, since most adhesives degrade rapidly at temperatures to which the joints are exposed in flight designs.

3.1.2.3.2 Interface Characteristics

Interfaces of components in an ablative chamber attachment shall prevent gas flow within the interface. The design

The design of ablative combustion chambers must take into account the shrinkage of charred material and its possible consequence of creating gas flow. At the injector-to-chamber interface, gas flow can best be prevented by recessing the injector into the chamber a distance greater than the estimated shrinkage; see figures 1 and 3. This practice will also protect the forward end of the chamber liner and prevent loss of short fabric plies in that region. Redundant seals at the injector interface are also recommended.

To prevent separation of mating components in contact with combustion gases, the thermal expansion coefficients and elastic moduli should be matched as closely as possible. Provide

step joints at the interfaces (fig. 1) to reduce the possibility of gas flow in case of separation (opening of gaps).

3.1.2.3.3 Location

Attachment joints shall be remote from hot areas.

Recess the injector into the chamber and use the same chamber wall thickness in the attachment area as in the combustion chamber to provide adequate temperature control of the forward flange. An aft flange for a radiation-cooled nozzle extension should be located far enough forward, with respect to the aft end of the liner, to (1) be insulated by the full thickness of the ablative liner, (2) control the thermal conductance from the nozzle extension, and (3) allow the chamber wall to shield the flange from radiation from the nozzle. This concept is depicted in figure 4.

3.1.3 Fabrication

3.1.3.1 PROCESS CONTROLS

Fabrication process controls shall ensure the quality of the finished product.

Process controls should include, but not be limited to, "staging" of material prior to layup, temperature of material and mandrel, tension of tape and feed rate (if tape-wrapping), as-wrapped density (percent debulking), cure cycle times, and rates of temperature and pressure changes. Components tape wrapped on male mandrels should be made with a minimum debulking of 85% (85% of final cured component density). When warp-cut tape is used, a debulking of 90% should be achieved.

Components made of precut fabric and molded in matched metal dies should be debulked in steps, the material thickness in each step not exceeding two inches.

Specific cure-cycle parameters are functions of materials (primarily the resin) and of component size and configuration (primarily the wall thickness). The material suppliers and fabricators generally provide recommendations for each specific design.

Properties of prepreg and finished cured material should be specified. The values listed in table III are considered representative of various materials and constitute the minimum number of properties required.

It is recommended that additional length be added to a component during fabrication and that this "tag-end" material be used to evaluate properties.

3.1.3.2 PROCESSING DISCREPANCIES

Allowable processing discrepancies (i.e., wrinkles and delaminations) in the finished chamber shall not degrade ablative chamber performance.

Limits for wrinkles should be established in terms of wrinkle amplitude and radius of curvature. Such limits preferably should be based on results of a materials evaluation program. In the absence of such data, however, practical limits are as follows: no wrinkles should extend through the chamber wall, the amplitude of a wrinkle should not exceed one-quarter of the chamber wall thickness, and wrinkle radius of curvature should not be less than one-tenth of the chamber diameter.

Limits of delaminations should be based on results of a materials evaluation program in which the effects of various delaminations on material properties and performance have been determined. Since most engine programs, however, do not permit extensive materials evaluation, it is recommended that the following arbitrary limits be used:

- No delaminations should be permitted in the throat region or in areas where imposed loads would tend to open a crack.
- In noncritical areas, the maximum number of delaminations should be specified in relation to surface area (e.g., there should be no more than one (1) delamination in any 5 in. x 5 in. area).
- The width, depth, and length of a delamination should not exceed 0.005 in., half of the wall thickness, and 30° in arc of the chamber circumference, respectively.
- No delaminations should be permitted anywhere unless the chamber liner is provided with a structural overwrap.

A delamination or crack in a noncritical area of an ablative liner may be repaired by filling with an epoxy resin. This action will not, however, improve the liner's ablative performance, i.e., reduce regression or char depths.

3.2 RADIATION-COOLED CHAMBERS

3.2.1 Thermal Design

3.2.1.1 WALL MATERIALS

The wall material shall be capable of operating effectively by radiation cooling at the required chamber temperatures over the required duty cycle.

Only refractory metals and alloys have sufficient high-temperature strength to withstand the operating temperatures of most radiation-cooled applications. Columbium alloys such as C-103 are recommended. The 90Ta-10W alloy is not recommended, because it is much more dense and its strength at higher temperatures cannot be utilized because of present coating limitations. Molybdenum and its alloys are not recommended because of the structural problems discussed in section 2.2.2.1.

3.2.1.1.1 Embrittlement by Coating

Chamber wall material must not be subject to embrittlement by the coating(s) selected.

Determine if the wall material will be embrittled by the application of the oxidation-resistant coating or the emissivity coating. Prepare coupons and perform bend tests or other suitable tests to verify that the wall material is in fact not adversely affected. Silicide coatings tend to embrittle more than aluminide coatings. The C-103 columbium alloy is not embrittled by silicide coatings.

The same coatings used for internal oxidation resistance should be used externally to increase the surface emittance. If other than diffusion-bonded coatings are used, the surface may be sand- or grit-blasted prior to coating.

3.2.1.2 WALL COATINGS

3.2.1.2.1 Compatibility

Internal chamber wall coatings shall be compatible with the propellants and the combustion products at the maximum wall temperature for durations required by the duty cycle.

Oxidation-resistant coatings compatible with the earth-storable propellants and their combustion products are silicides and aluminides.

The silicides allow operation at higher temperatures, provide more reproducible application, and tend to be self-healing because new films of SiO_2 are formed during each firing. The recommended coating is R512E. Diffusion-bonded aluminide coatings are recommended for use with fluorine or halogen-fluoride oxidizers.

Do not exceed one-hour exposure to 2800°F for silicides and 2400°F for aluminides. Silicides can operate for up to 10 minutes at 3100°F, whereas 2800°F is the maximum temperature limit of aluminides. If heat-transfer losses by radiation cannot control the coating temperatures to these limits, film or barrier cooling should be used.

3.2.1.2.2 Adhesion

Chamber wall coatings shall form a metallic bond with the wall and shall not be subject to spalling resulting from thermal shock or differential thermal expansion.

It is recommended that the coatings be applied by slurry and vacuum diffusion or by pack cementation processes. Plasma spray coatings should not be used to coat the inside of small combustion chambers. The coatings must be inspected for complete coverage and uniform thickness. Coating thickness should be as thin as possible to withstand the duty cycle without exposing areas of the substrate to oxidation. The coating thickness should under no circumstances be more than 8 mils.

3.2.1.3 WALL CONFIGURATION

The chamber wall design shall provide minimum gas-side wall temperature.

The wall thickness in the throat region should be determined by a series of two-dimensional (radial-axial) thermal analyses in which the wall thickness is increased until the minimum gas-side temperature is identified on the basis of counteracting effects of axial conduction and radiation surface area vs radial thermal resistance. Upstream of the throat a wall thickness greater than that required structurally is recommended, so that internal conduction from hot spots or streaks is enhanced.

3.2.2 Structural Design

3.2.2.1 CHAMBER

3.2.2.1.1 Wall Materials

The wall material shall withstand thermal cycling between space coast temperatures and maximum operating temperature without loss of ability to withstand ignition overpressures on cold starts.

Refractory metals and alloys that are sufficiently ductile to withstand the operating temperatures and start-transient pressures of most radiation-cooled applications are required. Columbium alloys such as C-103 are recommended. Tungsten and tungsten alloys should not be used since they are too brittle. Molybdenum and TZM alloy should not be used for restarts at wall temperatures below 70°F after repeated operation at temperatures above 2400°F. The SCb-291 columbium alloy should not be used for pulsed operation with restart wall temperatures below –30°F.

3.2.2.1.2 Wall Configuration

The chamber wall configuration shall minimize the number of stress raisers in the wall.

The design should be free of threaded connections and bolt holes. Transitions from thick to thin sections should be gradual, and sharp corner radii should be avoided. Molybdenum should not be welded at all, and stringent quality control must be instituted to select molybdenum without any flaws. For columbium and tantalum alloys, EB welding is recommended. Use of fins, knurling, or V-grooves to increase the external surface emissivity is not recommended.

3.2.2.2 ATTACHMENTS

3.2.2.2.1 Manifold Protection

The chamber/injector attachment shall prevent overheating of the injector manifold.

Three basic design approaches or combinations thereof are recommended:

(1) Cool the chamber/injector interface (below 350°F during operation and below 500°F after shutdown) by film or barrier cooling.

(2) Make the injector of high-temperature material (same as the chamber). This design requires the injector propellant manifolds to be located remote from the injector face.

(3) Use a thermal barrier between the chamber and injector. Keep the seal cool by locating it far forward of the injector face and by providing a minimum heat conduction path to the seal area. Minimize the heat conduction path through the bolts and shield the bolt heads against heat radiation from the chamber wall.

3.2.2.2.2 Voids and Traps

The chamber-to-injector interface shall not include regions where combustion product residues can accumulate.

The clearances and tolerances of the mating components must be selected to avoid traps. It is especially important to minimize the clearance between that part of the injector recessed

into the chamber and the chamber itself. A separate seal ring may be used, and it should be selectively fitted to the injector-chamber assembly.

3.2.2.2.3 Attachment Method

The method for making an attachment shall be suitable for use with the chamber material.

Columbium and tantalum alloy chambers may be attached to the injector or to a nozzle extension by welding or by clamping. Columbium can be welded to columbium and its alloys and to tantalum and the 90Ta-10W alloy. EB welding is recommended. Columbium can be resistance welded or brazed to titanium (chamber-to-nozzle extension interface). The chamber-wall thickness should be increased 50 percent in the area of the weld, with the thickened portion extending over a distance equal to 2.5 times the greater wall thickness. Coated surfaces should be machined to bare substrate prior to welding. Uncoated areas can be repaired by spray coating.

Molybdenum should not be welded, nor should it be provided with through holes or threaded connections. A small flange or shoulder clamped by a separate split ring or ring flange is recommended.

3.2.2.2.4 Flange Design

Flanges for injector attachment shall not constrain the structure or create discontinuities in wall temperature or stiffness.

A transition section should be included between an injector attachment flange and the relatively thin chamber wall to provide both a mechanical transition and a more uniform axial variation of transient temperatures. The latter may also be provided by the use of film or barrier cooling.

3.3 INTEREGEN AND HEAT-SINK CHAMBERS

3.3.1 Thermal Design

3.3.1.1 WALL THICKNESS AND FILM COOLING

3.3.1.1.1 Interegen Chamber

The interegen chamber wall thickness profile and film coolant flow shall limit heat conduction to the liquid film region to prevent film boiling and detonation while allowing throat and nozzle temperatures to reach their acceptable limits.

The wall thickness in the liquid region should be determined from a fin-type thermal analysis (i.e., one neglecting radial temperature gradients) to ensure that the wall distributes the heat load efficiently over the length of the liquid film. When the wall surface temperature is less than the coolant saturation temperature, a forced-convection heat transfer coefficient is appropriate. References 52 and 108 indicate a method for determining the liquid velocity and such a coefficient. When the wall temperature exceeds the coolant saturation temperature, the coolant boiling curve provides the wall boundary condition. Laboratory tests should be run to establish the coolant boiling curve and detonation characteristics; the boiling curve may be obtained by the method of references 57 and 58. Tapering the wall thickness from the downstream end of the liquid region to a thinner section at the forward end provides more efficient use of the liquid film, but this design is not recommended for general use, since it aggravates the heat soak and restart problems (sec. 3.3.1.3).

Downstream of the liquid region, the wall thickness should be contoured to provide the axial thermal resistance that yields the minimum required film coolant flow. This thickness must be determined parametrically, as illustrated in figure 15, on the basis of the film boiling or detonation limit in the liquid film and the structural limit in the heat-source region (usually the thermal-strain limitation of sec. 3.3.2.2.1).

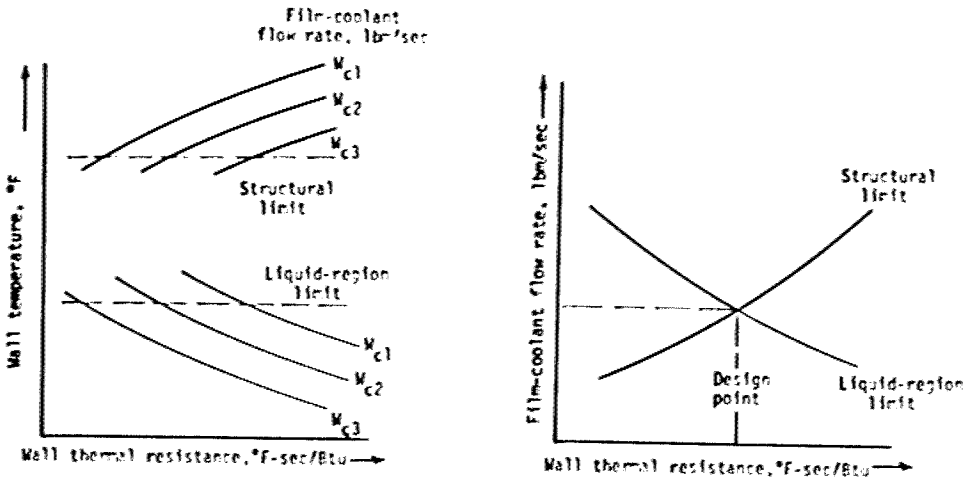

Figure 15. – Parametric curves for determining wall thickness and coolant flowrate.

Optimum axial temperature or thermal resistance distributions for the contoured wall are not known; use of a thermal isolation slot is not recommended. In a copper chamber, the radial wall-temperature variation will be negligible and the maximum temperature will occur at the downstream end of the interegen section; two-dimensional effects are important in beryllium chambers. The interegen section should terminate where internal and external radiation losses can provide temperature control of a thin chamber wall.

After the wall thickness of the forward end has been established with the fin analysis recommended above, an initial design for use in more detailed two-dimensional wall analyses should be obtained as follows:

(1) Assume a wall heat load to the liquid region.

(2) Calculate the liquid length and downstream gas-side boundary conditions (sec. 3.5.2) for several film-coolant flowrates; use the fin analysis to select the coolant flow consistent with the liquid-region temperature limit.

(3) Select an axial wall-temperature distribution (neglect radial variations) between the film boiling or detonation limit at the downstream end of the liquid region and the structural temperature limit at the throat or the end of the interegen section; calculate the wall heat transfer to the liquid region on the basis of this temperature distribution and the boundary conditions of step (2). Repeat steps (1) through (3) until the assumed and caluclated liquid-region heat loads agree.

(4) Calculate the wall-thickness variation downstream of the liquid region on the basis of temperature gradients and local axial heat loads of step (3).

3.3.1.1.2 Heat Sink Chamber

The wall thickness of a heat-sink chamber shall provide heat capacity adequate for the chamber to operate over the required duty cycle.

Determine heat-sink chamber wall thicknesses by standard two-dimensional conduction network analyses. Avoid using excess material whose temperature is essentially unperturbed at a time when the inner surface reaches its structural limit.

3.3.1.2 WALL CONTOUR

The chamber internal contour shall minimize the throat region surface area and promote laminarization of the boundary layer. For an interegen design, the contour shall also minimize the length of the conduction path from the throat to the liquid film and the combustion gas velocity in the liquid region.

Relatively large contraction ratios (4.0 or greater) and steep convergence angles (40° or greater) coupled with small throat radii of curvature are recommended, especially for interegen designs, for which such a contour acts as a heat flux reducer to help prevent film boiling in the liquid region. These contour features help to promote boundary-layer reverse transition when $P_{ch} \times F < 200\ 000\ lbf^2/in.^2$ (sec. 2.5.1). It is further recommended that the initial expansion angle from the throat be as large as possible consistent with performance constraints; this design will provide for a minimum conduction path from that part of the heat-source region downstream of the throat and for minimum surface area in this region.

3.3.1.3 HOT RESTART

Soak temperatures in the liquid region of an interegen or film-cooled heat sink chamber designed for multiple firing applications must be low enough to prevent detonation or sustained film boiling on restart.

The thickness of the chamber wall in the liquid region should be increased above that required for steady-state operation if control of soak temperatures is indicated by comparison of transient thermal analyses with allowable restart temperatures. The additional thickness will distribute the stored energy over a greater mass, thereby lowering the soak temperature. An alternate method is to use more film cooling, thereby reducing the stored energy. Demonstrated allowable restart temperatures for MMH and A-50 are 900°F and 700°F, respectively.

3.3.2 Structural Design

3.3.2.1 MATERIAL PROPERTIES

Material selection shall be based primarily on cycle life requirements and secondarily on providing high thermal conductivity (interegen) or heat capacity-thermal conductivity product (heat sink).

With N_2O_4/hydrazine-type propellants, beryllium is recommended for chambers that are operated with either reduced wall temperatures or very limited thermal cycling.

Copper and bimetallic copper chambers with Inconel liners should be used for applications where duty cycles and temperature gradients may result in low-cycle fatigue failure of beryllium. Film cooling should be used to control beryllium temperature gradients for thermal cycling and to extend the duration capability of copper chambers. In the absence of restart requirements, beryllium chambers may be designed for 1800°F operation and copper chambers for 1100°F.

OFHC copper should be specified and allowance made for an 0.050 in. skim cut from all surfaces after receipt in order to remove surface contamination. If hydrogen brazing is to be used, cycle the copper through a simulated braze ($\approx$ 1800°F for 30 min.); examine the specimen for blistering, porosity, or excessive growth in any dimension before considering the copper to be acceptable.

3.3.2.1.1 Beryllium Alloys

A beryllium alloy shall provide low-temperature elongation and low-cycle fatigue characteristics consistent with design strain levels and thermal cycle requirements.

For applications where low-cycle fatigue limits the design, specify a 2-percent-BeO alloy or an aircraft-brake-grade alloy and request special process controls to provide maximum elongation. A room-temperature hoop elongation of 3.0 percent is readily obtained, and 4.5 percent is possible with special processing. For good high-temperature strength in hot-pressed beryllium, the Fe/(Al + Si) impurity ratio should be controlled; a value of 1.4 for this ratio is recommended. Low-cycle-fatigue data are required to define allowable strains for various types of thermal cycles.

Surface treatment of beryllium is necessary to eliminate microcracks induced by machining that may act as stress risers and cause material fracture. Final machining cuts should be held to 1 to 2 mils. Following machining, the surface cracks (twinning) should be removed by acid etching of the machined surfaces. Acid used for rough etching should be 10 to 20% concentration of H_2SO_4. Finish etching should be done with 25% HNO_3 containing 0.25% HF.

3.3.2.2 CHAMBER WALL

3.3.2.2.1 Low-Cycle Fatigue

The chamber shall not fail from thermally induced low-cycle fatigue.

In the absence of specific fatigue data, the allowable total strain range (elastic plus plastic) should be predicted by use of the fatigue equation given in reference 109. In the limiting case of a single restart following complete cooldown (essentially complete strain reversal), the operating thermal strain should be less than the worst (hoop or longitudinal) room-temperature elongation. Thermal strains should be kept at or below allowables by limiting wall thickness and utilizing film coolant to control gas-side surface temperatures.

3.3.2.2.2 Thermal Stress

The chamber shall withstand all thermally induced stresses.

Thermally induced stresses are a structural problem primarily with graphite. Most graphite chambers should be supported (e.g., in a metal case) so that the graphite is in compression as it is heated. AXF-5Q, with its higher tensile strength (table VII), could be designed for tensile loading; however, such a design is difficult to achieve, because the allowable tensile strain of graphite is small (0.4 to 0.8%). The support structure should fit as closely as possible. For workhorse chambers, a watercooled metal case is recommended, or the graphite thickness should be great enough to insulate the case. For long firing durations, an insulator should be used between the graphite and the case. Asbestos/phenolic or a high-density ceramic-fiber composite such as Fiberfrax is recommended for the insulator. The former should be tape-wrapped or molded and cured under high pressure (> 200 psi) to obtain a minimum density of 1.70 gm/cm^3. Elastomeric fillers should not be used, and the graphite heat sink should be fitted to the insulator with as small a gap as practical.

3.3.2.3 ATTACHMENTS

3.3.2.3.1 Interface Characteristics

Injector/chamber interface materials and configurations shall limit post-fire heat soakback to the injector to acceptable levels.

Insulators may be used as the injector-to-chamber seal to control soakback to the injector. Nondegradable insulation such as mica is recommended for extended duty cycles; mica may also be used beneath bolt heads. Rubber-impregnated asbestos such as Raybestos or Durabala is recommended for single starts and short duty cycles. Metallic crush gaskets are not recommended; they require too high a bearing load to seal, they yield at soakback temperatures, and they are expensive. In graphite-lined chambers, locate the seal outboard of the graphite liner on the chamber case. Gaskets of Grafoil, or a combination of pyrolytic graphite (with the "c" direction normal to the interface) and Grafoil, are recommended. The injector should be recessed into the chamber wall and provision made for axial thermal expansion of the graphite liner by installing crushable washers or spacers of Grafoil, porous carbon, or carbon felt at the upstream end.

Heat soak may also be controlled by providing excess mass in the flange or forward chamber wall to act as a heat sink, or by using a reduced-thickness wall section to force more heat loss from the chamber and nozzle.

3.3.2.3.2 Flange Design

The design of the forward attachment flange shall prevent the loss of sealing due to thermal distortion or local yielding of the flange, bolts, or seal.

The flange should be located remote from the hottest portion of the chamber or have sufficient mass either to maintain a lower temperature or avoid rotation. If distortion of the flange cannot be prevented, coil springs or Belleville washers should be used beneath the bolt heads to ensure that bolt loads are maintained. Gaskets should be preyielded by tightening bolts to the required torque levels, loosening, and retorquing.

3.3.2.3.3 Attachment of Brittle Chambers

Attachment of brittle chambers (e.g., those of beryllium) shall minimize stress concentrations.

For injector attachment, use separate slip ring bearing on a segmented retaining ring to engage a small flange or lip on the chamber, as illustrated in figure 10; corner radii should be generous. This approach eliminates drilled holes and minimizes discontinuities and thermal stress concentrations due to the flange. If a bolted attachment is used, through-holes are recommended; drilled and tapped holes should not be used.

For nozzle attachment, use separate retaining rings or the lamp-base threads shown in figure 10.

3.4 ADIABATIC-WALL CHAMBERS

3.4.1 Thermal Design

3.4.1.1 MATERIALS

Adiabatic-wall chambers shall not be subject to throat area decrease or increase beyond acceptable limits.

The reactivity of the chamber wall material with the propellant combustion products must be determined by theoretical and preferably also by experimental means. A plot of carbon corrosion characteristics vs propellant characteristics, as shown in figure 11, should be used to determine if material regression or carbon buildup will occur. In the former case, the regression rate can be minimized by one or both of the following steps:

(1) Use a mixture ratio at the wall that minimizes the carbon reaction.

(2) Apply a PG coating on the inner surfaces of the chamber to a thickness of 0.025 in. or less. The inner surface must be smooth prior to PG application.

The best coating adherence is obtained by matching the thermal expansion coefficients of the PG coating and the substrate in the deposition plane, and by using a substrate with an elastic modulus slightly lower than that of the coating. Fibrous-graphite composites best meet these requirements.

Free-standing PG chambers can be used in applications requiring simple geometric shapes with large transition radii (0.5 in. or larger), small expansion ratios (sea level), and chamber pressures of 100 psi or less. Structural overwraps of graphite filaments (roving) can extend the pressure capability somewhat. The ratio of wall thickness to radius of curvature should not be more than 0.06. Caution should be exercised in using free-standing PG without performing a rigorous stress analysis to include thermal as well as residual stresses in the PG. If the above stated conditions cannot be met, fiber-reinforced graphite should be used.

If the thermochemical analysis indicates a potential for carbon buildup, no corrective action can be recommended at this time other than to change the fuel or to provide a more nearly compatible boundary layer by mixture-ratio control.

3.4.2 Structural Design

3.4.2.1 CHAMBER WALL

3.4.2.1.1 Pyrolytic Graphite

A pyrolytic graphite chamber shall not be subject to excessive thermal stresses resulting from the anisotropic nature of the material.

The differences in thermal expansion in the normal-to-deposit direction ("c" axis) and parallel-to-deposit axis must be considered in the design of pyrolytic graphite structures. When it is not practical to design the structure to preclude excessive stresses induced by the high thermal expansion in the "c" direction, the structures must be reinforced in the high-stress areas. Graphite roving in a carbonized phenolic matrix is recommended. See also section 3.4.2.2.2.

3.4.2.1.2 Fibrous-Graphite Composite

The design of a laminated fibrous-graphite composite chamber shall preclude loading of the chamber in interlaminar shear or cross-laminate tension.

Several factors enter into the selection of fabric or laminate orientation. A small angle of 5° to 10° with the chamber inner surface is considered best for adiabatic-wall chambers; however, compromises will have to be made, their nature depending on the fabrication method used. For tape-wrapped components, it may be necessary to go to an angle of 30° to 45° with the surface immediately downstream of the throat. To obtain sufficient shear area in that region, the chamber wall may have to be made thicker than in other regions. If a flange is incorporated at the injector end, the layers of fabric should be curved around the corner as illustrated in figure 12(b).

If the laminate orientation cannot be selected in a manner that will avoid excessive shear or block tension, a three-dimensional reinforcement should be used.

3.4.2.2 ATTACHMENTS

3.4.2.2.1 Interface Characteristics

The attachment design shall restrict heat flow to the chamber/injector interface, especially during coast periods.

The distance between the combustion zone and the injector connection should be made as large as possible. Figures 12(a) and (b) show two examples of possible solutions. The chamber wall thickness downstream of the injector should also be made as thin as structural requirements will allow in order to provide a thermal barrier. Furthermore, film cooling should be employed to keep the attachment area cool during operation.

3.4.2.2.2 Attachment Method

The chamber-to-injector attachment shall accommodate the thermal expansion of the chamber.

The attachment area must be designed to permit thermal expansion of the fibrous graphite chamber without imposing excessive bending loads. External hoop support should be avoided entirely, or a low-modulus external structure or sliding joint should be incorporated. Figure 12(b) shows an attachment design in which the chamber is clamped in the axial direction only and thermal expansion is in no way hindered. An example of a sliding joint is shown in figure 12(a).

3.4.3 Fabrication

The design of fibrous-graphite composite chambers shall call for fabrication methods that will minimize the possibility of wrinkles in the reinforcement.

The attainment of a satisfactory chamber is, to a large extent, dependent on the chamber geometry. A minimum of configuration transitional changes, use of relatively large radii at the transitions, and uniform, relatively thin (less than 0.3 in.) chamber walls have been found to enhance the possibility of obtaining satisfactory components. When the configuration permits, shingle or rosette layup in female molds rather than on male mandrels is recommended, since wrinkles can be eliminated completely and strength improved.

Tape wrapping generally is the least expensive fabrication method but also most susceptible to wrinkling. Wrinkling can be kept to a minimum by sufficiently high debulking (85% minimum) prior to cure. Tape widths should be less than 5.0 in. and chamber wall thickness less than 0.5 in., except possibly in the region of the throat and immediately downstream, where a greater thickness may be required to obtain sufficient laminate overlap.

Filament winding graphite yarn under tension on a removable mandrel is another method recommended for obtaining wrinkle-free reinforcement.

3.5 HEAT TRANSFER TO THE CHAMBER WALL

Predictions of convective heat transfer shall account for variations in gas composition and properties, chemical reactions, and mass addition from the wall

The convective heat flux to the chamber wall, without mass addition to the boundary layer from the wall, should be calculated as

$$\dot{q}_c = \rho\, u_e\, St\, (H_{aw} - H_w) \tag{6}$$

where

St = Stanton number for enthalpy difference = $h_g/(\rho\, u_e)$

H_{aw} = adiabatic wall (recovery) enthalpy

H_w = enthalpy of combustion gas at the chamber wall

with the density and all properties in the Stanton number prediction based on either the Eckert reference temperature (ref. 80) or the arithmetic mean of the adiabatic and non-adiabatic wall temperatures. With film cooling, all properties inlcuding H_w are based on the local mixture ratio (sec. 3.5.2). The magnitude of the Lewis number Le should always be checked, and if it is not near unity the heat flux determined from equation (6) is multiplied by the term

$$\left[1 + (Le - 1) \sum_{j=1}^{N} H_j^{o}\, (C_{j,aw} - C_{j,w})/(H_{aw} - H_w)\right]^{2/3}$$

where

Le = Lewis number

H_j^o = heat of formation, j^{th} species

$C_{j,aw}$ = species mass fraction, adiabatic wall temperature

$C_{j,w}$ = species mass fraction, wall temperature

With mass addition from the wall, as with transpiration cooling or reactive walls, the convective heat flux across the boundary layer as defined above is not equal to the heat flux to the wall. Part of the former must go to raising the enthalpy of the mass added to the boundary layer to the enthalpy H_w, thus

$$\dot{q}_w = \dot{q}_c - (\rho v)_w (H_w - H_c) \tag{7}$$

where

$\dot{q}_w$ = convective heat flux to or from chamber wall

v = velocity of transpired gas normal to wall

H_c = enthalpy of coolant

Evaluation of the Stanton number and of the adiabatic wall conditions with film cooling are considered in sections 3.5.1 and 3.5.2, respectively.

3.5.1 Evaluation of Stanton Number

Predictions of Stanton number shall account for the effects of flow acceleration.

Predictions of turbulent-flow Stanton number should be based on a pipe-flow correlation with variable coefficient:

$$St = C_g \, Re^{-0.2} \, Pr^{-0.6} \tag{8}$$

where

C_g = $C_g(x)$ = Stanton number correlation coefficient as a function of contour distance from film-coolant injection point

Pr = Prandtl number

with the variations in the correlating-coefficient obtained from test data on a system that corresponds as closely as possible to the specified chamber contour, injector, and propellant combination. If data for a specific configuration are not available, the C_g values of figure 16 are recommended. Boundary-layer analyses in the convergent section are not recommended, because they underestimate the effect of acceleration on the Stanton number. Such analyses may be used downstream of the throat, where acceleration effects are less significant, with the initial conditions providing agreement with the throat Stanton number defined above.

For low-thrust, low-pressure applications ($P_{ch} \times F < 200\,000$ lbf²/in.²), acceleration-induced reverse transition and laminarization must be considered. The following table provides a guide for the Reynolds numbers (properties based on the Eckert reference temperature) that characterize the upper limit of the laminarized regime and the lower limit of the turbulent regime (fig. 13).

Location	Convergence angle	Contraction ratio	Limit* Values for Re	
			Laminarized	Turbulent
Throat	30°	7.75	0.5×10^6	1.0×10^6
	45°	9.76	0.9	2.1
	60°	4.29	0.9	2.1
Upstream (c = 1.23 to 1.34)	30°	7.75	0.75	1.5
	60°	4.29	1.3	2.6

*Upper limit for laminarized regime, lower limit for turbulent

Note that acceleration effects are stronger upstream of the throat, near the start of the throat curvature. The variation of the acceleration parameter K (eq. (4)) should be calculated for the specific contour being considered. If $K \geq 3.3 \times 10^{-6}$ over a significant portion of the convergent section, complete laminarization will occur near the throat; the length over which this limiting K value must be maintained is not known, but may be the order of 100 times the momentum thickness at the point where the critical K value is first attained. On the basis of the above table, assume the local turbulent limit occurs at twice

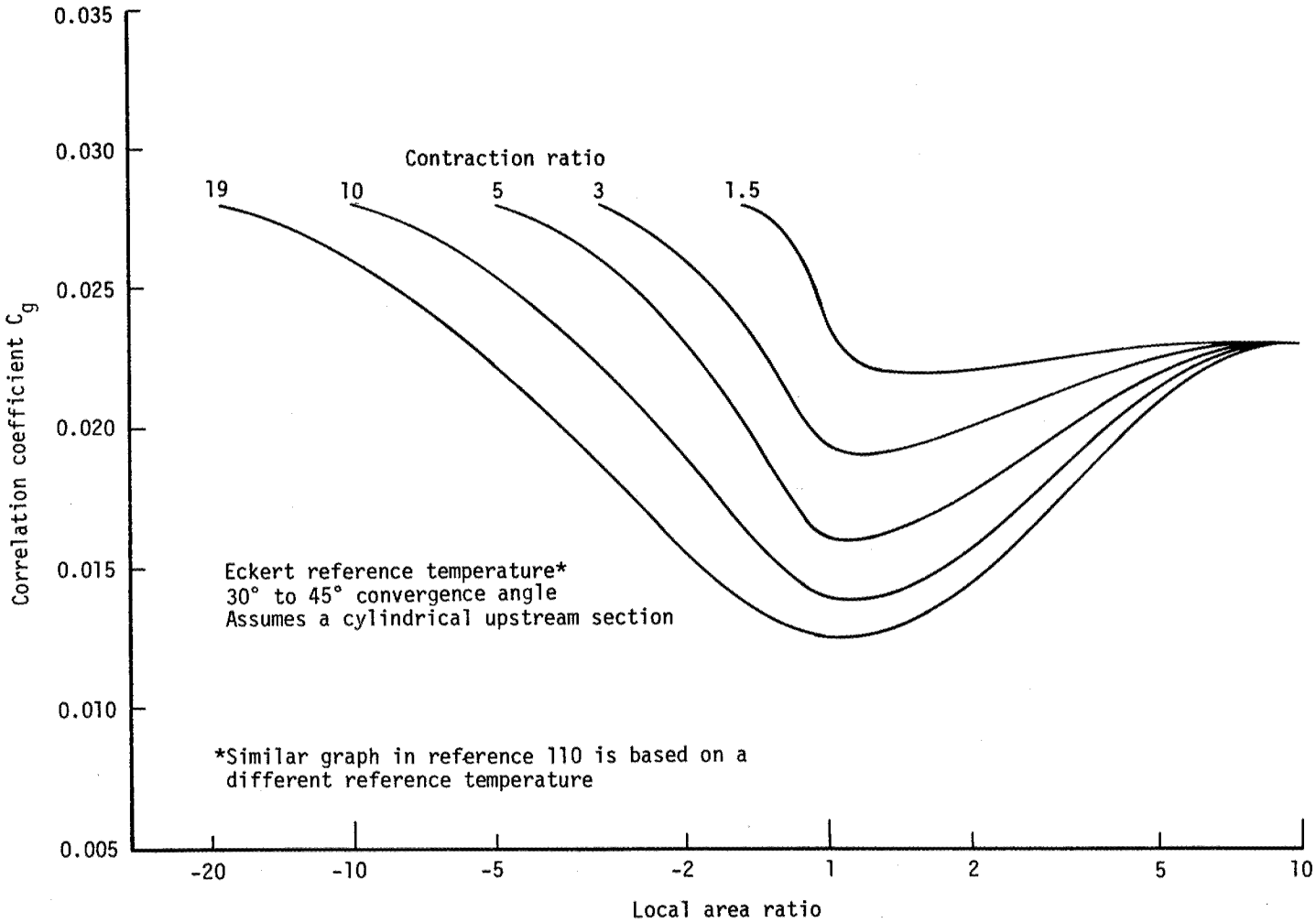

Figure 16. — Effect of acceleration on correlation coefficient for turbulent Stanton number.

the Reynolds number associated with laminarization limit. Laminarization or partial reverse transition must be verified experimentally for each design.

Stanton numbers in the laminarized regime may be calculated from the pipe-flow equation

$$St = 0.318\, Re^{-0.5}\, Pr^{-0.6} \tag{9}$$

or by laminar-boundary-layer theory, with the boundary-layer development starting where the pressure gradient first becomes significant as predicted in reference 96. A boundary-layer analysis based on local similarity is recommended; the required similar solutions are provided in reference 111. In the reverse-transition region, assume that the Stanton number increases linearly with Reynolds number between the laminarized and turbulent end points.

Reference 83 may also be used to predict the occurrence of reverse transition and laminarization and the corresponding reduction in Stanton number from turbulent values.

3.5.2 Film Cooling Analysis

Predictions of film-coolant flow shall account for flow turning and acceleration, coolant injection configuration, freestream turbulence, injector-induced mixing, and liquid film instability.

Gas film cooling.—For this analysis, the entrainment model of Appendix A is recommended. In this model, the entrainment flux of core flow into a mixing layer containing all the film coolant is equal to the product of the core axial mass velocity and an entrainment fraction. The coolant effectiveness is defined in terms of total enthalpies and is a function of the entrainment flow, coolant flow, and a variable shape factor for the mixing layer profile; the mixture ratio at the wall is obtained from the effectiveness through a mass-transfer/energy-transfer analogy. In this model, the recovery of kinetic energy offsets additional mixing in the expansion section and allows the analyst to predict the low adiabatic wall temperatures sometimes there. Adiabatic wall temperatures may be obtained from a reactive thermochemical analysis (e.g., ref. 112), or from the nonreactive model included in Appendix A.

The entrainment fraction is written as the product $\psi_r \psi_m(x)$, in which ψ_r is the entrainment fraction for plane, unaccelerated flow with continuous-slot injection (ref. 76). Therefore, the empirical parameter $\psi_m(x)$ must account for rocket turbulence levels, coolant injection configuration, core injector effects, and flow turning and acceleration. Section 2.5.2 indicates that these effects are very significant, so the realistic evaluation of ψ_m is the key to predicting coolant flow requirements. For evaluating individual

phenomena, use the acceleration correlation of reference 103 and the turning correlations of reference 105. In the absence of data from which to infer an overall ψ_m for a specific type of design, the results of reference 81 for hydrogen film cooling are recommended. These results indicate a preferred value of ψ_m = 3 to 4 at the injection point, the value decaying linearly with axial distance in the convergent section to a value of about 1.75 at the throat. Further decay of ψ_m occurs downstream of the throat as indicated in figure 17.

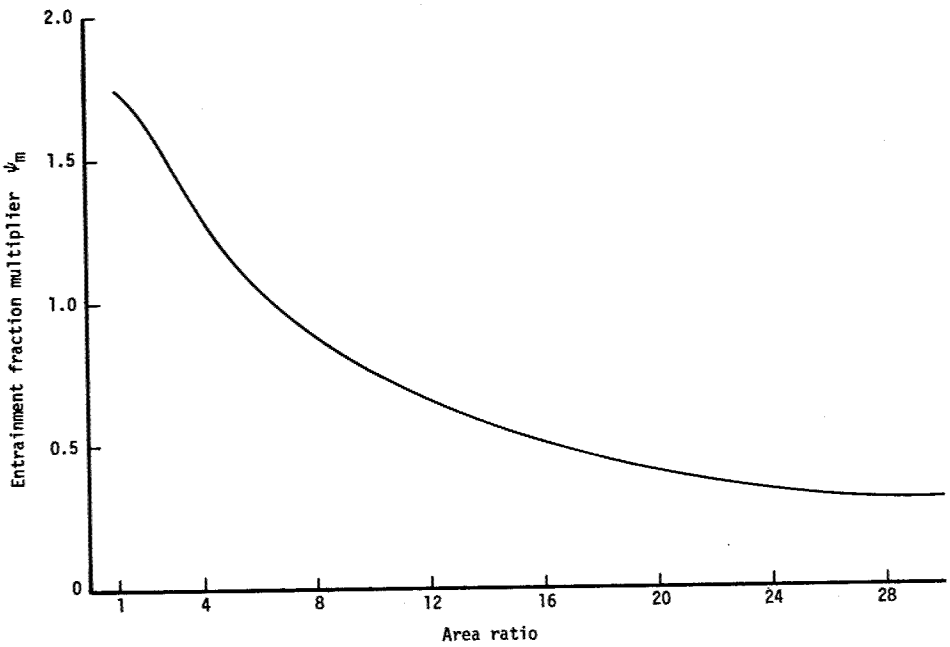

Figure 17. – Entrainment fraction multiplier ψ_m as a function of area ratio (in expansion section).

Liquid film cooling. – For this analysis, the model of Appendix B is recommended. In this model, the interaction of the unstable liquid film with the core flow is treated by a modification and extension of the concepts of reference 107; the modified model includes an empirical factor δ to account for coolant injection effects in rocket applications. For orifice injection parallel to the core flow, a δ of 1.0 to 1.6 based on the data of reference 51 is recommended; for swirl injection, δ may be as low as 0.4. Adiabatic wall temperatures downstream of the liquid film are determined by a mixing-layer entrainment model similar to that recommended above for gas film cooling, with the entrainment fraction equal to $\psi_L \psi_m(x)$, ψ_L being similar to ψ_r. Rocket data analyses with ψ_m = 1 (i.e., a uniform entrainment fraction) indicate ψ_L = 0.025 to 0.06. Immediately downstream of the liquid film, the coolant vapor at the wall is superheated without decomposition. After a critical

wall temperature for monopropellant coolants is reached (e.g., about 550°F for MMH), decomposition begins. The coolant vapor fraction then decreases as determined by the empirical constant ξ, which has a value of approximately 3000 sec^{-1} for MMH.

3.5.3 Film Coolant Injection

Film-coolant injection techniques shall provide uniform circumferential coverage and minimize mixing of injectant and core flow.

Orifices for injection of liquid film coolant should have a uniform peripheral spacing not exceeding 0.3 in. If this spacing cannot be achieved with practical orifice diameters (about 0.015 in. or greater), the following alternatives are recommended:

(1) Provide a circumferential velocity component or swirl to the film coolant unless the injector is baffled, or

(2) Utilize impinging pairs of film cooling orifices to provide tangential-fan flow patterns.

Liquid film coolant injected axially should impinge on the chamber wall at an angle of 25° to 35°.

Gaseous film coolant should be injected parallel to the chamber wall through slots; the rib thickness between slots should be a minimum consistent with structural requirements. The effective slot height (flow area/chamber circumference) should provide a coolant/core velocity ratio of 0.9 to 1.15.

APPENDIX A

ANALYTICAL MODEL FOR GAS FILM COOLING

(1) Entrainment flow ratio

$$\frac{W_E}{W_c} = \frac{W - W_c}{W_c} \left[2 \frac{\psi_r \bar{x}}{r_i - s_i} - \left(\frac{\psi_r \bar{x}}{r_i - s_i} \right)^2 \right]$$

where, in any consistent set of units,

W_E = entrainment flowrate

W_c = film-coolant flowrate

W = total flowrate in chamber

$$\bar{x} = \int_{x_i}^{x} \frac{r_i}{r} \frac{(\rho_e u_e)_{2D}}{(\rho_e u_e)_{1D}} \psi_m \, dx, \text{ effective contour distance}$$

$$\psi_r = \frac{0.1 \, (u_c/u_e)}{\left(\frac{\rho_c}{\rho_e}\right)^{0.15} \left(\frac{\rho_c u_c s_i}{\mu_c}\right)^{0.25} f}, \text{ reference entrainment fraction}$$

ρ = density

u = axial velocity

r = chamber radius

s = mixing layer height

x = distance along chamber contour

μ = dynamic viscosity

ψ_m = empirical entrainment fraction multiplier

f = $f(u_c/u_e)$ from figure A-1

and subscripts

c = film coolant

e = core stream

i = at injection point

1D = one-dimensional

2D = two-dimensional

(2) Effectiveness based on total enthalpy

$\eta = \eta\ (W_i / W_c)$ from figure A-2

(3) Adiabatic wall conditions

$$H_{aw} = H_{o,e} - \eta\ (H_{o,e} - H_c) - (1 - Pr_w^{1/3})\ (H_{o,e} - H_c)$$

$$(MR)_w = \frac{1 + (MR)_c}{1 + \eta \left(\frac{1 + (MR)_c}{1 + (MR)_c} - 1 \right)} - 1$$

$$T_{aw} = T\ \left((MR)_w, H_{aw} \right) \qquad \text{Reactive model}$$

$$T_{aw} = T_{o,e} - \frac{\eta\ C_{p,c}\ (T_{o,e} - T_c) + (1 - Pr_w^{1/3})\ (H_{o,e} - H_c)}{\eta\ C_{p,c} + (1 - \eta)\ C_{p,e}} \qquad \text{Non-reactive model}$$

where, in any consistent set of units,

H = enthalpy

Pr = Prandtl number

MR = mixture ratio

T = temperature

C_p = specific heat at constant pressure

and subscripts

aw = adiabatic wall

o = total

w = wall

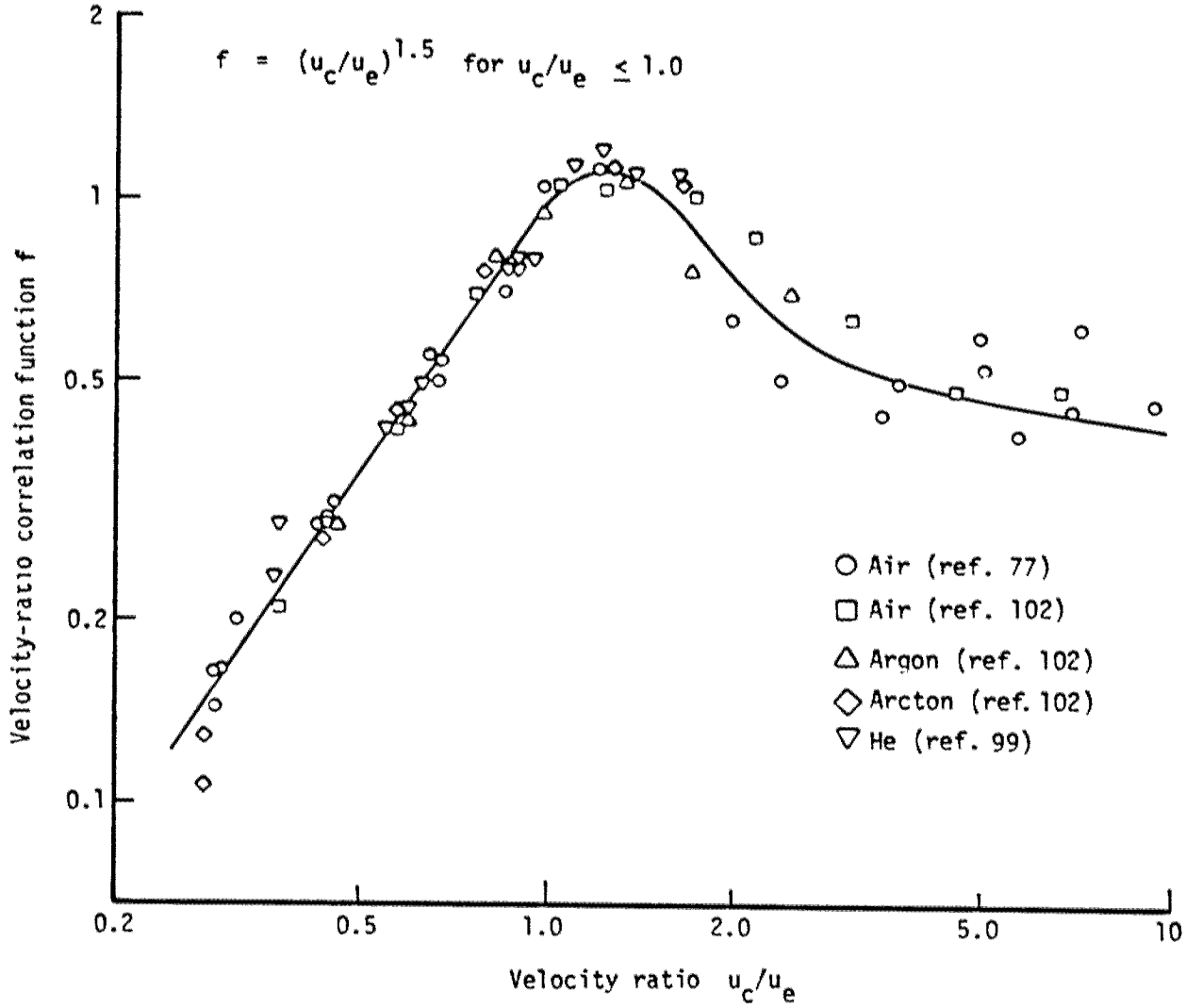

Figure A-1. — Velocity-ratio correlation function f vs velocity ratio.

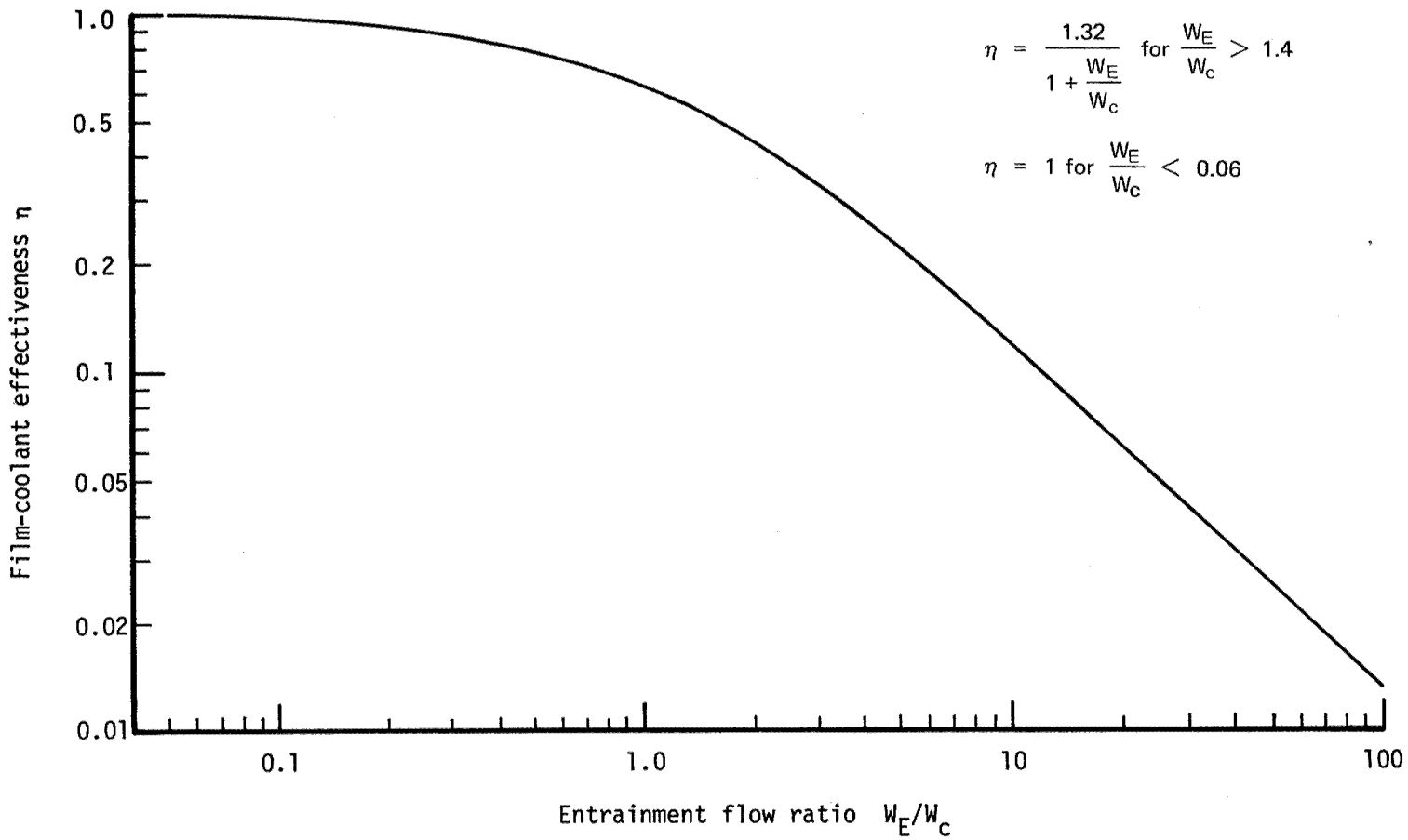

Figure A-2. — Film-coolant effectiveness η as a function of entrainment flow ratio.

APPENDIX B

ANALYTICAL MODEL FOR LIQUID FILM COOLING

(1) Liquid film length

The analytical expression presented below is based largely on empirical correlations. The validity of the mathematical expression for a correlation depends on the use of explicit numerical values for physical quantities (length, density, velocity, etc.) in specific units; these units are set forth in the definition of the symbol for a physical quantity. In the expression for any parameter or derived quantity (e.g., X_e), units are disregarded and only numerical values of the units specified for the physical quantities are used.

$$L = \frac{1}{A} \ln \left(1 + \frac{A\, W_c}{V} \right)$$

where

L = liquid film length, in.

A = $A(X_e)$ from figure B-1 = liquid entrainment parameter, in.$^{-1}$

X_e = $\delta(\rho_e/g)^{0.5}\ u_e(T_e/T_{if})^{0.25}/\sigma$, liquid entrainment correlation parameter

δ = empirical entrainment augmentation factor

ρ = density, lbm/ft^3

g = $32.174 \frac{\text{lbm}}{\text{lbf}} \frac{\text{ft}}{\text{sec}^2}$

u = velocity, ft/sec

T = temperature, °R

σ = surface tension, lbf/ft

W_c = film coolant flowrate, lbm/sec

V = $\pi D_{av} \frac{(\rho_e\, u_e)_{av}}{144}$ St B a, surface vaporization rate, lbm/in. - sec)

D = diameter of chamber, in.

144 = conversion factor, $in.^2/ft^2$

St = smooth-wall Stanton number without mass addition

$$B = \frac{H_{o,e} - H_c + \dot{q}_w / \left[(\rho_c u_c)_{av} \, St \, a \right]}{H_{c,sv} - H_c}$$

H = enthalpy, Btu/lbm

$H_c = H_c(T_{if})$

$\dot{q}_w$ = heat flux from the wall, $Btu/(ft^2 \cdot sec)$

a = $a(X_c, X_f)$ from figure B-1 = heat-transfer augmentation factor for liquid surface roughness

$X_f = \sigma X_c$, liquid film surface-roughness parameter

where subscripts c, o, e, and w have the meanings given in Appendix A, and subscripts

if = liquid film interface

av = average

sv = saturated vapor

Include the heat flux $\dot{q}_w$ from the wall to the liquid for hot restart and interegen applications. The liquid film interface temperature T_{if} is the saturation temperature corresponding to the partial pressure of the vapor P_v

$$P_v = \frac{P_{ch}}{1 + \dfrac{(MW)_c}{B\,(MW)_c}}$$

where

P = pressure

MW = molecular weight

and subscripts

v = vapor

ch = chamber

(2) Downstream effectiveness

$$\eta = \frac{1}{\theta\left(1 + \frac{W_E}{W_c}\right)}$$

(3) Entrainment flow ratio

$$\frac{W_E}{W_c} = \frac{W - W_c}{W_c}\left[2\psi_L \frac{\bar{x}}{r_i}\sqrt{1 - \frac{(W_E)_L}{W - W_c}} - \left(\psi_L \frac{\bar{x}}{r_i}\right)^2\right] + \frac{(W_E)_L}{W_c}$$

$\bar{x}$ as in Appendix A, except that integration starts at x = L, end of liquid film; r_i as in Appendix A

ψ_L = empirical entrainment fraction (similar to ψ_r, Appendix A)

$$\frac{(W_E)_L}{W_c} = \frac{1}{0.6\eta_L} - 1$$

$$\eta_L = \frac{B}{1 + B}$$

(4) Shape factor θ for mixing-layer profile

$$\theta = 0.6 + 0.263\,\frac{W_E - (W_E)_L}{W_c}, \text{ for } W_E < (W_E)_L + 0.6W_c$$

$$\theta = 0.758, \text{ for } W_E \geqslant (W_E)_L + 0.6W_c$$

(5) Downstream adiabatic wall conditions

$$H_{aw} = H_{o,e} - \eta\,(H_{o,e} - H_c) - (1 - Pr_w^{1/3})\,(H_{o,e} - H_e)$$

(a) Reactive model

$$H_{aw} = f_v\,\eta\left[H_{c,sv} + C_{p,v}\,(T_{aw} - T_{if})\right] + (1 - f_v\eta)\,H$$

$f_v = \exp(-\xi\tau)$ = fraction of coolant remaining as vapor

ξ = film-coolant decomposition rate constant

$$\tau = \int_1^x dx/u_c = \text{core flow transit time}$$

$$H = H((MR)_f, T_{aw})$$

$$(MR)_f = \frac{(1-\eta)(MR)_c}{1-\eta+\eta(1-f_v)(1+(MR)_c)}$$ reactive mixture ratio at the wall excluding coolant vapor

(b) Non-reactive model

$$T_{aw} = \frac{H_{aw} - \eta H_{c,sv} + f_v \eta C_{p,v} T_{if} + \eta(1-f_v) C_{p,d} T_d + (1-\eta)(C_{p,e} T_{o,e} - H_{o,e})}{f_v \eta C_{p,v} + \eta(1-f_v) C_{p,d} + (1-\eta) C_{p,e}}$$

where subscript d refers to decomposition products.

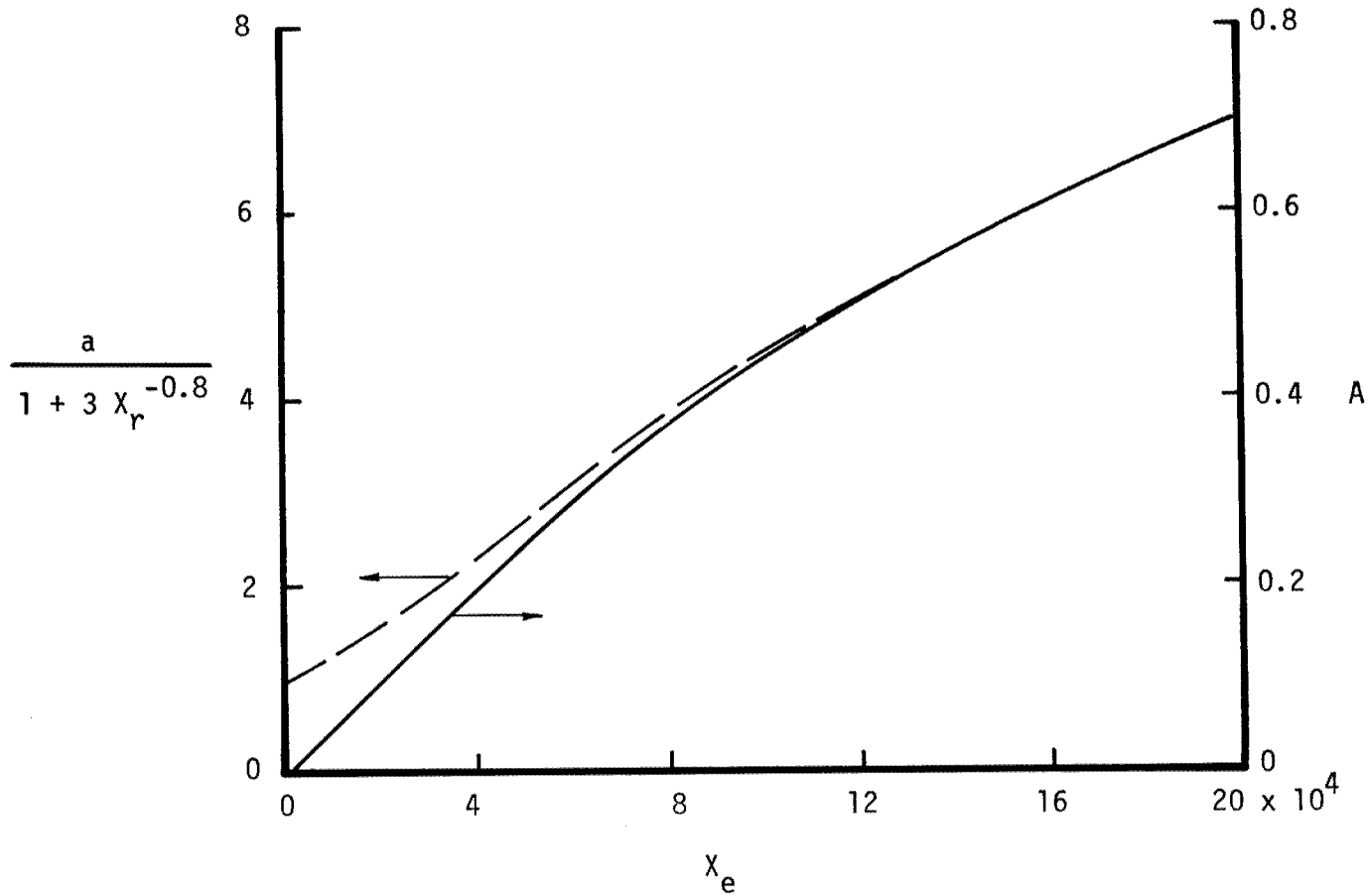

Figure B-1. — Liquid entrainment parameters A and a as functions of entrainment correlation parameter X_e.

APPENDIX C

Conversion of U.S. Customary Units to SI Units

Physical quantity	U.S. customary unit	SI unit	Conversion factor[a]
Angle	degree	radian	1.745×10^{-2}
Chamber pressure times thrust	$lbf^2/in.^2$	N^2/cm^2	3.066
Density	$lbm/in.^3$	kg/m^3	2.768×10^4
	gm/cm^3	kg/m^3	1.00×10^3
Energy	Btu	J	1.054×10^3
Enthalpy, specific	Btu/lbm	J/kg	2.324×10^3
Force	lbf	N	4.448
Heat flux	$\frac{Btu}{ft^2 \cdot sec}$	$\frac{W}{m^2}$	1.135×10^4
Heat-transfer coefficient	$\frac{Btu}{ft^2 \cdot sec \cdot {}^\circ F}$	$\frac{W}{m^2 \cdot K}$	2.043×10^4
Length	ft	m	3.048×10^{-1}
	in.	cm	2.54
	mil	μm	2.54×10^1
Mass	lbm	kg	4.536×10^{-1}
Modulus (compressive; elastic; tensile)	psi ($lbf/in.^2$)	N/cm^2	6.895×10^{-1}
Molecular weight	lbm/(lbm-mole)	kg/(kg-mole)	1.
Pressure	mm Hg	N/cm^2	1.333×10^{-2}
	psi	N/cm^2	6.895×10^{-1}

(continued)

Conversion of U.S. Customary Units to SI Units (concluded)

Physical quantity	U.S. customary unit	SI unit	Conversion factor[a]
Specific heat	Btu/(lbm·°F)	J/(kg·K)	4.184×10^{3}
Strength (compressive; flexural; shear; tensile)	psi	N/cm^2	6.895×10^{-1}
Surface tension	lbf/ft	N/cm	1.459×10^{-1}
Temperature	°F	K	$K = \frac{5}{9}(°F + 459.67)$
	°R	K	$K = \frac{5}{9}(°R)$
Temperature difference	°F	K	$K = \frac{5}{9}(°F)$
Thermal expansion coefficient	in./(in.·°F)	m/(m·K)	1.8
Thermal conductivity	$\frac{Btu}{hr\cdot ft\cdot °F}$ or	$\frac{J}{sec\cdot m\cdot K}$	1.730
	$\frac{Btu\cdot ft}{hr\cdot ft^2\cdot °F}$		
	$\frac{Btu\cdot in}{hr\cdot ft^2\cdot °F}$	$\frac{J}{sec\cdot m\cdot K}$	1.444×10^{-1}
Thermal resistance	$\frac{°F\cdot sec}{Btu}$	$\frac{K}{W}$	5.269×10^{-4}
Thrust	lbf	N	4.448
Viscosity, dynamic	$\frac{lbm}{hr\cdot ft}$	$\frac{N\cdot sec}{m^2}$	4.134×10^{-4}
Volume	$in.^3$	cm^3	1.639×10^{1}

[a]Multiply value given in U.S. customary unit by conversion factor to obtain equivalent value in SI unit. For a complete listing of conversion factors for basic physical quantities, see Mechtly, E. A.: The International System of Units. Physical Constants and Conversion Factors. Second Revision, NASA SP-7012, 1973.

APPENDIX D

GLOSSARY

Term	Definition
adiabatic wall temperature	the temperature of the combustion chamber wall when there is no heat transfer between the wall and the exhaust gas
B-stage	intermediate state in the polymerization of a thermosetting resin; in this stage the resin is dry and relatively stiff at room temperature but softens when heated
barrier cooling	means of reducing the severity of gas-side heating by changing the O/F ratio near the wall to provide a zone of low-temperature gases
boundary layer	film of fluid next to a bounding surface such as the combustion chamber or nozzle wall; its thickness usually is taken as the radial distance from the surface to the point at which fluid velocity reaches 99 percent of freestream velocity
bird-cage attachment	chamber-to-injector attachment in which bolts extend the length of the chamber from the injector to a separate retaining ring at the aft end
contraction ratio	ratio of injector face area to throat area
coupon	piece of material, representative of the material used in a part, that accompanies the parent part during processing and subsequently is used as a test specimen to evaluate properties of material in the finished part
debulking	process of compacting prepreg by applying pressure before initiating cure
Eckert reference temperature	$T_{ref} = 0.5\,(T_e + T_w) + 0.22\,(T_{aw} - T_e)$ (ref. 80)
endurance limit	maximum alternating stress at which a material presumably can endure an infinite number of cycles
exfoliated laminate	plies of the laminate stripped from the surface
film cooling	means of reducing the heat transfer to the gas-side wall of the combustion chamber by maintaining a thin layer of fluid over the wall
fractographic analysis	examination of a fractured surface under a very high magnification to determine the nature of the fracture

Term	Definition
interegen	coined word meaning internally regenerative
laminarization	process by which a turbulent boundary layer reverts to laminar-like characteristics as a result of flow acceleration
Lewis number (Le)	$\frac{\text{Mass diffusivity}}{\text{Thermal diffusivity}}$, $Le = \mathcal{D} C_p \rho / k$
liquid length	distance along chamber wall that film coolant remains in liquid state
low-cycle fatigue	life-cycle capability determined by the plastic strain range; generally less than 10^4 cycles
Mach number	ratio of the speed of flow to the speed of sound in the fluid
momentum thickness	thickness of the potential flow with a momentum equal to that lost in the boundary layer as a result of wall shear forces
nucleate boiling	the formation and breaking away of bubbles from active nuclei on a submerged heated surface; the rising bubbles stir the liquid so that heat transfer from the surface to the liquid is much greater than that due to normal convection
pack cementation	method of applying coating by packing article to be coated in a powder mixture and heating to reaction temperature
Prandtl number (Pr)	$\frac{\text{Momentum diffusivity}}{\text{Thermal diffusivity}}$, $Pr = C_p \mu / k$
prepreg	reinforcing material impregnated with the full complement of resin when received from supplier
pyrolysis	chemical decomposition by heat
reverse transition	transition from a turbulent to a laminar boundary layer as a result of flow acceleration (laminarization)
Reynolds number (Re)	$\frac{\text{Inertial force}}{\text{Viscous force}}$, $Re = \rho u_e D / \mu$
rosette layup	spiral arrangement of plies in which plies are laid up at an angle with the inner surface in both radial and axial directions
shingle layup	geometric arrangment of plies in which the plies overlap each other as in roof or wall coverings

Term	Definition
staging (of polymers)	increasing the molecular weight of the resin without effecting a cure
Stanton number (St)	$\frac{\text{Heat transferred to fluid}}{\text{Heat transported by fluid}}$ (1) For temperature difference: $St = h_g/(\rho\, u_e\, C_p)$ (2) For enthalpy difference: $St = h_g/(\rho\, u_e)$
storable propellant	propellant with a vapor pressure such that the propellant can be stored in a specified environment (earth or space) at moderate ullage pressures without significant loss over a specified period of time
weave, 8-harness	weave pattern of a fabric in which each fill yarn goes alternately over seven and under one warp yarn, staggered one warp yarn for each fill yarn
weave, square or plain	weave pattern of a fabric in which each fill yarn goes alternately over and under the warp yarns

Symbol	Definition
a, b, c	empirical constants in equation (1)
ACS	attitude control system
C_g	Stanton number correlation coefficient
C_j	species mass fraction
C_{ox}	concentration of oxidizing species in the combustion products
C_p	specific heat at constant pressure
c^*	characteristic exhaust velocity
$\mathcal{D}$	diffusion coefficient
D	chamber diameter
F	thrust
H	static enthalpy
H_{aw}	adiabatic wall (recovery) enthalpy

Symbol	Definition
H_o	total enthalpy
H_j^o	heat of formation, j^{th} species
h_g	convective-heat-transfer coefficient
ID	inner diameter
K	flow acceleration parameter, defined in equation (4)
k	thermal conductivity
L^*	characteristic length; ratio of combustion chamber volume to throat area
Le	Lewis number (q.v.)
LEM	lunar excursion module
M	Mach number (q.v.)
MR	mixture ratio, i.e., ratio of mass of oxidizer to mass of fuel at combustion
N	number of species
OAMS	orbital attitude and maneuvering system
OD	outer diameter
P	pressure
PBPS	post boost propulsion system
Pr	Prandtl number (q.v.)
$\dot{q}_c$	convective heat flux
$\dot{q}_w$	heat flux to or from the chamber wall
r	local chamber radius
R_u	radius of curvature of chamber wall upstream of nozzle throat
Re	Reynolds number (based on local chamber diameter) (q.v.)

Symbol	Definition
RCS	reaction control system
SM	service module (Apollo)
SPS	service propulsion system (Apollo)
St	Stanton number (q.v.)
T	static temperature
T_d	decomposition product temperature corresponding to saturated vapor enthalpy
T_o	total temperature
u	gas axial velocity
v	gas velocity normal to the chamber wall
W_c	film coolant flowrate
x	distance along chamber contour
α	coefficient of thermal expansion
β	angle between the chamber centerline and the wall tangent
γ	isentropic flow coefficient
δ	liquid entrainment augmentation factor for rocket application
ϵ	local area ratio
μ	dynamic viscosity
ρ	density
ψ_L	liquid-film-cooling empirical entrainment fraction, similar to ψ_r
ψ_m	entrainment fraction multiplier
ψ_r	reference entrainment fraction, i.e., gas-film-cooling entrainment fraction for straight, unaccelerated flow with continuous-slot injection

Symbol	Subscripts
aw	adiabatic wall
c	coolant
ch	chamber
e	core or free stream
j	species index
L	at the end of the liquid film
t	throat
w	at the chamber wall

Material[1]	Identification
A-50	50/50 mixture of UDMH and hydrazine, propellant grade per MIL-P-27402
A-286	austenitic, heat-resistant, iron-base alloy
acrylonitrile rubber	copolymer of acrylonitrile and butadiene
AG Carb	trade name of Aerojet-General Corp. for carbon/graphite composites
AG Carb 101	trade name of Aerojet-General Corp. for a carbon/graphite composite initially molded from WCA graphite-fabric reinforcement and FM 5228 phenolic resin, followed by carbonization, resin-pitch impregnation, and final graphitization
Arcton	trade name of Imperial Chemical Industries for a fluorocarbon (e.g., dichlorodifluoromethane)
ATJ	molded, extremely fine-grain, premium qualtiy bulk graphite that can be machined within small tolerances; manufactured by Union Carbide Corp.
AXF-5Q	high-strength, fine-grain, homogeneous graphite manufactured by Poco Graphite, Inc.
BA-1014	propellant: 67% N_2H_4, 24% MMH, 9% H_2O (by weight)

[1]Additional information on metallic materials herein can be found in the 1972 SAE Handbook, SAE, Two Pennsylvania Plaza, New York, N.Y.; in MIL-HDBK-5B Metallic Materials and Elements for Aerospace Vehicle Structures, Dept. of Defense, Washington, D.C., Sept. 1971; and in Metals Handbook (8th ed.), Vol. 1: Properties and Selection of Metals, Am. Society for Metals (Metals Park, OH), 1961.

Material	Identification
C-103	columbium-base alloy, Cb-10Hf-1Ti
C-129Y	high-strength columbium-base alloy with hafnium, tungsten, and yttrium as the major alloying elements
Carb-I-Tex	trade name for graphite-fabric-reinforced carbon/carbon manufactured by the Carborundum Co.
CHY	special grade of graphite developed by Union Carbide Corp. for application of vapor-deposited SiC
CTF	chlorine trifluoride
Durabala	compressed asbestos gasket material with a synthetic rubber binder; manufactured by the Durabala Manufacturing Co.
Durak KA	pack-cementation silicide coating manufactured by Chromizing Co., Div. of Chrome-Alloy American Corp. (Gardenia, CA)
elastomer	polymeric material that at room temperature can be stretched to approximately twice its length and on release return quickly to its original length
epoxy	thermosetting resin widely utilized as an adhesive and as a binder in the fabrication of glass-filament/resin composites
Fiberfrax	high-temperature fibrous insulation manufactured by Carborundum Co.
FLOX	mixture of liquid fluorine and liquid oxygen
fluorinated oxidizer	any fluorine-based oxidizer, e.g., OF_2, FLOX, N_2F_4
G-90	extruded medium-grain graphite manufactured by Carborundum Co.
Grafoil	trade name of Union Carbide Corp. for a low-density, anisotropic form of graphite
GRB silicon carbide	silicon carbide composite containing graphite particles; manufactured by the Carborundum Co.
green Refrasil	high-purity-silica fabric preimpregnated with resin that has not been staged
H-205-85	molded, fine-grain graphite; manufactured by Great Lakes Carbon Co.
Haynes 25, 188, L-605	designation of certain colbalt- and nickel-base high-temperature alloys manufactured by Stellite Division of Cabot Corporation

Material	Identification
hydrazine or hydrazine type	N_2H_4 or its derivatives (e.g., UDMH, MMH)
IRFNA	inhibited red fuming nitric acid, propellant grade per MIL-P-7254
Inconel	nickel alloys manufactured by International Nickel Co.
HLM-85	extruded medium-grain graphite manufactured by Great Lakes Carbon Corp.
JTA	trade name of Union Carbide Corp. for a high-density oxidation-resistant graphite/zirconium containing silicon and boron
KT silicon carbide	pure, high-density, self-bonded silicon carbide produced by the Carborundum Co.
Le Carbone P-2239	molded medium-density bulk graphite marketed by Société Le Carbone-Lorraine, Paris, France (affiliated with Advanced Carbon Products, Brisbane, CA)
LF_2	liquid fluorine
LPG	liquified petroleum gas, e.g., propane or butane
M-20	propellant: 80% N_2H_4, 20% MMH (by weight)
Marquardt RM 005	special SiC vapor-deposited coating (the Marquardt Corp.)
MHF-3, -5	mixed hydrazine fuels; -3 or -5 refers to a specific blend of hydrazine and MMH
micro-balloon	hollow spheres, usually phenolic resin or glass, used as filler in phenolic-resin-impregnated materials to obtain lower density
MMH	monomethylhydrazine, propellant grade per MIL-P-27404
MON	mixed oxides of nitrogen (10% NO – 90% N_2O_4)
OFHC	oxygen-free, high-conductivity
PG	pyrolytic graphite
phenolic	short term for a family of phenol-aldehyde thermosetting resins
polyamide	nylon-like polymer characterized by the presence of the amide or thioamide group

Material	Identification
polyimide	family of high-molecular-weight resins suitable for structural use at temperatures up to 700°F
prepreg	see listing under "Term"
Pyrocarb	trade name of HITCO for carbon/carbon composites
Pyrochrome	coating for control of emissivity and oxidation of a surface; distributed by Thermal Engineering and Equipment Co. (Los Angeles, CA)
P-2239	see Le Carbone P-2239
R508C	silicide coating manufactured by HiTemCo
R512A	slurry-applied silicide coating manufactured by HiTemCo
Raybestos	rubber-impregnated asbestos manufactured by Raybestos Manhattan, Inc.
Refrasil	trade name of HITCO for fibrous silica of high-purity SiO_2
RTV	trade name of General Electric for a two-part, room-temperature-vulcanizing dimethyl siloxane rubber
SCb-291	columbium-base refractory alloy, Cb-10Ta-10W; manufactured by Wah Chang-Teledyne, Inc.
Silastic	trade name of Dow Corning Corp. for silicone rubber
SX-4	trade name of Speer Carbon Corp. for graphite with low coefficient of thermal expansion
thermosetting resin	resin system that reacts when heated such that the material is crosslinked and irreversibly "set"
TZM	molybdenum alloy, Mo-0.5Ti-0.08Zr-0.3C; manufactured by Climax Moly Corp.
UT-6	high-modulus bulk graphite manufactured by Ultra Carbon Corp. (Bay City, MI)
UDMH	unsymmetrical dimethylhydrazine, propellant grade per MIL-P-25604

ABBREVIATIONS

Abbreviation	Identification
AFML	Air Force Materials Laboratory
AFRPL	Air Force Rocket Propulsion Laboratory
AIAA	American Institute of Aeronautics and Astronautics
AIChE	American Institute of Chemical Engineers
ARS	American Rocket Society
ASME	American Society of Mechanical Engineers
BLIMP	Boundary Layer Integral Matrix Procedure
CPIA	Chemical Propulsion Information Agency
IAS	Institute of the Aeronautical Sciences
JANNAF	Joint Army-Navy-NASA Air Force
JPL	Jet Propulsion Laboratory
MDAC	McDonnell Douglas Astronautics Company
MIT	Massachusetts Institute of Technology
SAE	Society of Automotive Engineers

REFERENCES

1. Anon.: Study to Determine the Thermophysical Properties of Ablative Materials. Rep. 04812-6002-R000, Systems Group, TRW, Inc., February 1967.

2. Hughes, T. A.: Ablative Thrust Chamber Study. Rep. 213/SA3-F, vol. 4, Aerojet-General Corp., October 1964.

3. Hines, W. S.; et al.: Development of Injector Chamber Compatibility Analysis, Final Report. AFRPL-TR-70-12, Rocketdyne Div., North American Rockwell Corp., March 1970.

4. Hines, W. S.; et al.: Extension of a Thrust Chamber Compatibility Model. AFRPL-TR-72-19, Rocketdyne Div., North American Rockwell Corp., March 1972.

5. Powars, C. A.; and Kendall, R. M.: User's Manual, Aerotherm Chemical Equilibrium (ACE) Computer Program. Aerotherm Corp., May 1969.

6. Anon.: User's Manual, Aerotherm Charring Material Thermal Response and Ablation Program, Version 3. AFRPL-TR-70-92, vol. I, Aerotherm Corp., April 1970.

7. Anon.: User's Manual, Aerotherm Axisymmetric Transient Heating and Material Ablation Computer Program (ASTHMA 3). AFRPL-TR-72-24, Aerotherm Corp., January 1972.

8. Friedman, H. S.; Hines, W. S.; and Cunial, G. D.: Designer's Guide and Computer Program for Ablative Materials in Liquid Rocket Thrust Chambers. AFRPL-TR-67-159, Rocketdyne Div., North American Aviation, Inc., June 1967.

9. Munson, T. R.; and Spindler, R. J.: Transient Thermal Behavior of Decomposing Materials, Part I: General Theory and Application to Convective Heating. Paper 62-30, IAS 30th Annual Meeting, January 1962.

10. Tick, S. J.; Huson, G. R.; and Griese, R.: Design of Ablative Thrust Chambers and Their Materials. J. Spacecraft Rockets, vol. 2, no. 3, May-June 1965, pp. 325-331.

11. DeAcetis, J.; and Swope, L. M.: Evaluation of the Regression Rates of Solid Rocket Nozzle Materials as a Function of Exhaust Gas Environments, Chamber Pressure, and Material Variations. CPIA Publ. 111, vol. III, 1966, p. 233.

12. Bartz, D. R.: A Simple Equation for Rapid Estimation of Rocket Nozzle Convective Heat Transfer Coefficients. Jet Propulsion, vol. 27, no. 1, January 1957, pp. 49-51.

13. Carter, W. A.; and Bell, G. S.: Development and Demonstration of a N_2O_4/N_2H_4 Injector (U). AFRPL-TR-69-231, TRW, Inc., October 1969. (CONFIDENTIAL)

14. Seely, J. H.; Duckering, R. E.; and Bazinet, G. D.: Development and Demonstration of an Advanced N_2O_4/N_2H_4 PBPS Axial Engine Assembly (U). AFRPL-TR-71-76, Aerojet Liquid Rocket Co., July 1971. (CONFIDENTIAL)

15. Anon.: Materials Survey for the Apollo Lunar Module Descent Engine Ablative Chamber, Injector Compatibility Improvement Study. Rep. 11602-6022-RO-00, Systems Group, TRW, Inc., March 1969.

16. Pavli, A. J.: Experimental Evaluation of Several Advanced Ablative Materials as Nozzle Sections of a Storable-Propellant Rocket Engine. NASA TMX-1559, April 1968.

17. Mitchell, B. J.; and Tempesta, F. L.: Ablative Plastics Characterization. Part II: Additional Arc-Heater Screening and Trajectory Simulation. AFML-TR-67-176, AVCO Corporation, October 1968.

18. Anon.: AJ10-138 Engine Uprating for Stage II. Part I: Thrust Chamber Assembly Verification Program. Rep. 2752-F-1, Aerojet-General Corp., November 1969.

19. Horgan, L. M.; Bartel, E. H.; and Hall, R. B.: Experiments in Fiber Orientation of Ablative Materials for Thrust Chambers (U). NWC-TP 4586, Naval Weapons Center, December 1969. (CONFIDENTIAL)

20. Bartlett, R. C.; et al.: Chamber Technology for Space Storable Propellants. Rep. R-6561-2, Rocketdyne Div., North American Aviation, Inc., September 1966.

21. Winter, J. M.; and Peterson, D. A.: Development of Improved Throat Inserts for Ablative Rocket Engines. NASA TN D-4964, July 1969.

22. Winter, J. M.; and Peterson, D. A.: Experimental Evaluation of 7.82-Inch (19.8-Cm) Diameter Throat Inserts in a Storable-Propellant Rocket Engine. NASA TM X-1463, April 1968.

23. Crump, D. N.; et al.: Improved Throat Inserts for Ablative Thrust Chambers. NASA CR-54984, TRW, Inc., September 1967.

24. Fio Rito, R. J.: Ablatively Cooled Pulse Rocket Engine Design. J. Spacecraft Rockets, vol. 2, no. 5, September - October 1965, pp. 758-764.

25. Anon.: MX Half Scale Analog Motor SS-001, Final Report. MX-A112-06, Aerojet Solid Propulsion Co., August 1975.

26. Batchelor, J. D.; et al.: Feasibility Demonstration of Pyrolytic Graphite Coated Nozzles. RPL-TR-65-57, Atlantic Research Corp., March 1965.

27. Zorich, D. R.; and Ellison, J. R.: High-Temperature Evaluation of a Pyrolytic Graphite Coated Nozzle Insert (U). AFRPL TR-69-103, Air Force Rocket Propulsion Laboratory, May 1969. (CONFIDENTIAL)

*28. Anon.: Apollo Service Module Engine Block II Development Test Report: Analysis of Chamber Blistering. Rep. 3865-454, Aerojet-General Corp., November 1967.

*29. Senneff, J. M.: Development of a Light Weight Ablative Thrust Chamber. Bell Aerosystems, A Textron Company, no date.

*Dossier for design criteria monograph "Liquid Rocket Engine Self-Cooled Combustion Chambers." Unpublished Collected source material available for inspection at NASA Lewis Research Center, Cleveland, Ohio

30. Campbell, J. G.; et al.: Spacecraft Engine Thrust Chamber Cooling. Rep. 6069, The Marquardt Corp., July 1964.

31. Anon.: Elevated-Temperature Properties of Carbonaceous and Silica Fabric-Reinforced Phenolic Composites. Rep. MF-540, Aerojet-General Corp., June 1964.

32. Pears, C. D.; et al.: The Thermal and Mechanical Properties of Five Ablative Reinforced Plastics from Room Temperature to 750°F. AFML-TR-65-133, Southern Research Institute (Birmingham, AL), April 1965.

33. Warga, J. J.; et al.: Deviation Nozzle Program. AFRPL-TR-68-81, Aerojet-General Corp., June 1968.

34. Warga, J. J.: Investigation of Effects of Ablative Discrepancies on Nozzle Performance Reliability. NASA CR-72702, Aerojet-General Corp., January 1970.

35. Fore, D. W.; et al.: Final Report – Columbium Combustion Chamber Development Program. Rep. A-1072, The Marquardt Corp., September 1967.

36. Aves, W. L.; and Bourland, G. W.: Investigation and Development of Techniques to Extend the Utility of Pack Processes and Compositions for Coating Molybdenum and Columbium Alloys. AFML-TR-65-272, LTV Aerospace Corp., August 1965.

37. Hallowell, J. B.; Maykuth, D. J.; and Ogden, H. R.: Coatings for Tantalum Base Alloys. ASD-TDR-63-232, Battelle Memorial Inst., April 1968.

38. Perkins, R. A.; and Packer, C. M.: Coatings for Refractory Metals in Aerospace Environments. AFML-TR-65-351, Lockheed Missiles and Space Co., September 1965.

39. Anon.: Present Status and Future Requirements for Coatings on Superalloys, Refractory Metals, and Graphite Materials. MAB Rep. 234 Materials Advisory Board, National Research Council, 1968.

40. Balling, N. R.; et al.: Evaluation Testing of Protective Coating on Refractory Metals. Interim Report 07587-6004-T000, Systems Group, TRW, Inc., October 1968.

41. Gadd, J. D.; and Jeffreys, R. A.: Advancement of High-Temperature Protective Coatings for Columbium Alloys. ASD-TDR-62-934, Tapco Div., TRW, Inc., November 1962.

42. Boyd, B. R.; et al.: Low Thrust Throttleable Engine for the Lunar Manned Flying System. Final Report 4491-6001-R0000, Systems Group, TRW, Inc., May 1966.

43. Anon.: Model 8414 Low Thrust Throttleable Engine Performance Evaluation Program, Final Report, Rep. 8414-933004, Bell Aerosystems Co., March 1966.

*44. Anon.: Interview on Radiation-Cooled Chambers with Personnel at the Marquardt Corporation. Sec. 7.3,Rep. 12021F-1A, Aerojet-General Corp., March 1969, pp. 137-140.

*Dossier for design criteria monograph "Liquid Rocket Engine Self-Cooled Combustion Chambers." Unpublished. Collected source material available for inspection at NASA Lewis Research Center, Cleveland, Ohio.

45. Anon.: Maneuvering Satellite Propulsion System Demonstration (U). Final Report – Part II. RPL-TDR-64-121, Bell Aerosystems Co., July 1964. (CONFIDENTIAL)

46. Coulbert, C. D.: Development in Radiation Cooled Thrust Chambers. Chem. Eng. Prog. Symposium Series, no. 52, vol. 60, AIChE, 1964, pp. 105-115.

47. Anon.: Study of Spacecraft Attitude Control Propulsion Devices (U). Rep. 8214-933001, Bell Aerosystems Co., December 1962. (CONFIDENTIAL)

48. Anon.: Experimental Auxiliary Rocket Engine. Rep. 8374-933004, Bell Aerosystems Co., January 1966.

49. Anon.: Preliminary Investigation of Beryllium Thrust Chambers in the 100-Pound-Thrust Class. Part I: Experimental Results. NAA-R R-15074, Rocketdyne Div., North American Aviation, Inc., October 1965.

50. Campagna, F. E.: Development and Demonstration of a Beryllium Rocket Engine (U). Vol. I, AFRPL-TR-66-251, Rocketdyne Div., North American Aviation, Inc., November 1966. (CONFIDENTIAL)

51. Barsic, N.; and McFarland, B. L.: Advanced Experimental Thrust Chamber Program (Phases III and IV). Final Report. NAA-R R-7281, Rocketdyne Div., North American Rockwell Corp., July 9, 1968.

52. Glenn, L. A.; and McFarland, B. L.: Advanced Experimental Thrust Chamber Program (Phases I and II). Final Report. NAA-R R-6857, Rocketdyne Div., North American Aviation Inc., April 10, 1967.

53. Anon.: High Energy Propellant Beryllium Thrust Chamber Program (U). Vol. II, AFRPL-TR-68-1, Rocketdyne Div., North American Rockwell Corp., January 1968. (CONFIDENTIAL)

54. Arndt, F. E.; and Williams, R. M.: Space Storable Thruster Investigation. NASA CR-72495, Systems Group, TRW, Inc., Aug. 1, 1969.

55. Jones, R. E.: PBPS Engine Development Program and System Design, Final Report. AFRPL-TR-69-88, Aerojet-General Corp., April 1969.

*56. Anon.: Attitude Control System Thrustor Hipermet 100. Technical Brief, Aerojet General Corp., October 1967.

57. Anon.: Flox-Diborane Technology – Boundary Reactions. Final Report. Rep. AGC R659-F, Aerojet-General Corp., September 1969.

58. Campagna, F. E.: High-Energy-Propellant Beryllium Thrust Chamber Program (Phase I Report). AFRPL-TR-67-150, Rocketdyne Div., North American Aviation, Inc., May 1967.

59. Campagna, F. E.: Development and Demonstration of a Beryllium Rocket Engine. Properties of Beryllium for Rocket Engine Design. Vol. II, AFRPL-TR-66-251, Rocketdyne Div., North American Aviation, Inc., November 1966.

*Dossier for design criteria monograph "Liquid Rocket Engine Self-Cooled Combustion Chambers." Unpublished Collected source material available for inspection at NASA Lewis Research Center, Cleveland, Ohio

60. Anon.: Improved Spartan Monopropellant and Bipropellant Reaction Control System Technology Programs. Rep. MDAC-A68-8042, Aerojet-General Corp., Feb. 27, 1969.

61. Anon.: Mariner-Mars 1971 Rocket Engine Assembly, Type-Approval Test Program Final Report. R-8357, Rocketdyne Div., North American Rockwell Corp., Sept. 29, 1970.

62. French, G. C.: A Study of the Durability of Beryllium Rocket Engines, Final Test Report. R-9556, Rocketdyne Div., Rockwell International, June 1974.

63. Chazen, J. L.: Space Shuttle Hypergolic Bipropellant RCS Engine Study, Final Report. Rep. 8701-910041, Bell Aerospace Div. of Textron, Inc., May 1974.

64. Senneff, J. M.: Space Shuttle Orbit Maneuvering Engine Reusable Thrust Chamber Program, Final Report. NASA CR-144632, Bell Aerospace Div. of Textron, Inc., May 1975.

65. Stechman, R. C.: Performance and Verification of the Space Shuttle Reaction Control Thrusters. Paper No. 75-1300, AIAA 11th Propulsion Conference (Anaheim, CA), Sept. 29-Oct. 1, 1975.

66. Dickson, J. C.: Fluorinated Oxidizer Thrust Chamber Materials Evaluation Program. RPL-TR-66-322, Aerojet-General Corp., December 1966.

67. Schindler, R. C.; and Williams, C. W.: Development and Demonstration of Ablative Thrust Chamber Assemblies Using LF_2/N_2H_4 Blend Propellants (U). Phase I, AFRPL-TR-67-52, Aerojet-General Corp., March 1967. (CONFIDENTIAL)

68. Schindler, R. C.; and Kiser, H. V.: Development and Demonstration of Ablative Thrust Chamber Assemblies Using LF_2/N_2H_4 Blend Propellants (U). AFRPL-TR-69-2, Aerojet-General Corp., February 1969. (CONFIDENTIAL)

69. Dickson, J. C.; and Schindler, R. C.: Development and Demonstration of Passively Cooled Thrust Chamber Assemblies for Fluorinated Propellants (U). AFRPL-TR-70-24, Aerojet-General Corp., February 1970. (CONFIDENTIAL)

70. Coulbert, C. D.; and Fio Rito, R. J.: Space Storable Thrustor Investigation. NASA CR-72526, The Marquardt Corp., June 1969.

71. Campbell, J. G.; and Hass, M. L.: Free Standing Pyrolytic Graphite Thrust Chambers for Space Operation and Attitude Control. AFRPL-TR-68-44, vol. I, The Marquardt Corp., September 1968.

72. Campbell, J. G.; et al.: Freestanding Pyrolytic Graphite Thrust Chambers for Space Operation and Attitude Control (U). AFRPL-TR-67-98, The Marquardt Corp., May 1967. (CONFIDENTIAL)

73. Coulbert, C. D.; et al.: Advanced Pyrolytic Spacecraft Thrust Chamber Materials. Rep. PR 5033-5Q, The Marquardt Corp., November 1968.

74. Campbell, J. G.: Test and Evaluation of a Passively Cooled Thrust Chamber for Fluorinated Propellants (U). AFRPL-TR-69-232, The Marquardt Corp., December 1969. (CONFIDENTIAL)

75. Anon.: Refractory Composite Materials for Spacecraft Thrust Chambers. Final Report for the Period of 23 July 1969 to 22 February 1970. Rep. S-989, The Marquardt Corp., May 1971.

76. Ewen, R. L.: Hydrogen Film/Conductive Cooling. NASA CR-120926, Aerojet Liquid Rocket Co., November 1972.

77. Seban, R. A.: Heat Transfer and Effectiveness for A Turbulent Boundary Layer with Tangential Fluid Injection. J. Heat Transfer, Trans. ASME, Series C, vol. 82, 1960, pp. 303-312.

78. Brokaw, R. S.: The Lewis Number. Prog. in Int. Res. on Thermodynamic and Transport Properties, Joseph F. Masi and Donald H. Tsai, eds., Academic Press, Inc., 1962, pp. 271-278.

79. Bartz, D. R.: Turbulent Boundary-Layer Heat Transfer from Rapidly Accelerating Flow of Rocket Combustion Gases and of Heated Air. Advances in Heat Transfer, vol. 2, Academic Press, Inc., 1965, pp. 1-108.

80. Eckert, E. R. G.: Engineering Relations for Heat Transfer and Friction in High-Velocity Laminar and Turbulent Boundary Layer Flow Over Surfaces with Constant Pressure and Temperature. Trans. ASME, vol. 78, 1956, pp. 1273-1283.

81. Schoenman, L.: Hydrogen-Oxygen Auxiliary Propulsion for the Space Shuttle. Vol. I: High Pressure Thrustors. NASA CR-120895, Aerojet Liquid Rocket Co., Jan. 30, 1972.

82. Ewen, R. L.: Improvement of the Titan III Second Stage Thermal Model and Application to the First Stage. Rep. ADR-9734-069, Aerojet Liquid Rocket Co., August 1973.

83. von Glahn, U. H.: Correlation of Gas-Side Heat Transfer for Axisymmetric Rocket Engine Nozzles. NASA TM X-1748, February 1969.

84. Mayer, E.: Analysis of Convective Heat Transfer in Rocket Nozzles. ARS J., vol. 31, no. 7, July 1961, pp. 911-917.

85. Ambrok, G. S.: Approximate Solution of Equations for the Thermal Boundary Layer with Variations in Boundary Layer Structure. Soviet Physics (Technical Physics), vol. 2, 1957, pp. 1979-1986.

86. Elliott, D. G.; Bartz, D. R.; and Silver, S.: Calculation of Turbulent Boundary Layer Growth and Heat Transfer in Axisymmetric Nozzles. Tech. Rep. 32-387, Jet Propulsion Lab., Calif. Inst. Tech., Feb. 15, 1963.

87. Patankar, S. V.; and Spalding, D. B.: Heat and Mass Transfer in Boundary Layers. CRC Press (Cleveland, OH), 1968.

88. Herring, H. J.; and Mellor, G. L.: A Method of Calculating Compressible Turbulent Boundary Layers. NASA CR-1144, Princeton Univ., September 1968.

89. Evans, R. M.: BLIMP-J User's Manual. Boundary Layer Integral Matrix Procedure for JANNAF. NASA CR-144046, Rep. UM-75-64, Aerotherm Div., Acurex Corp., July 1975.

90. Back, L. H.: Massier, P. F.; and Gier, H. L.: Convective Heat Transfer in a Convergent-Divergent Nozzle. Tech. Rep. 32-415, Jet Propulsion Lab., Calif. Inst. Tech., Nov. 15, 1963.

91. Back, L. H.; Massier, P. F.; and Cuffel, R. F.: Some Observations on Reduction of Turbulent Boundary Layer Heat Transfer in Nozzles. AIAA J., vol. 4, no. 12, December 1966, pp. 2226-2229.

92. Back, L. H.; Massier, P. F.; and Cuffel, R. F. : Flow Phenomena and Convective Heat Transfer in a Conical Supersonic Nozzle. J. Spacecraft Rockets, vol. 4, no. 8, August 1967, pp. 1040-1047.

93. Moretti, P. M.; and Kays, W. M.: Heat Transfer to a Turbulent Boundary Layer with Varying F Freestream Velocity and Varying Surface Temperature – An Experimental Study. Int. J. Heat Mass Transfer, vol. 8, September 1965, pp. 1187-1202.

94. Launder, B. E.: Laminarization of the Turbulent Boundary Layer by Acceleration. Rep. 77, Gas Turbine Laboratory, MIT, November 1964.

95. Nash-Webber, J. L.: Wall Shear-Stress and Laminarization in Accelerated Turbulent Compressible Boundary Layers. Rep. 94, Gas Turbine Laboratory, MIT, April 1968.

96. Schoenman, L.; and Block, P.: Laminar Boundary-Layer Heat Transfer in Low-Thrust Rocket Nozzles. J. Spacecraft Rockets, vol. 5, no. 9, September 1968, pp. 1082-1089.

97. Boldman, D. R.; et al.: Laminarization of a Turbulent Boundary Layer as Observed from Heat Transfer and Boundary Layer Measurements in Conical Nozzles. NASA TN D-4788, September 1968.

98. Kays, W. M.: Convective Heat and Mass Transfer. McGraw-Hill Book Co., (New York), 1966, pp. 96-97.

99. Hatch, J. E.; and Papell, S. S.: Use of a Theoretical Flow Model to Correlate Data for Film Cooling or Heating an Adiabatic Wall by Tangential Injection of Gases of Different Fluid Properties. NASA TN D-130, November 1959.

100. Stollery, J. L.; and El-Ehwany, A. A. M.: A Note on the Use of a Boundary Layer Model for Correlating Film Cooling Data. Int. J. Heat Mass Transfer, vol. 8, January 1965, pp. 55-65.

101. Carlson, L. W.; and Talmor, E.: Gaseous Film Cooling at Various Degrees of Hot-Gas Acceleration and Turbulence Levels. Int. J. Heat Mass Transfer, vol. II, November 1968, pp. 1695-1713.

102. Pai, B. R.; and Whitelaw, J. H.: The Influence of Density Gradients on the Effectiveness of Film Cooling. ARC CP 1013, Aeronautical Research Council, Imperial College of Science and Technology (London, England), December 1967.

103. Rousar, D. C.; and Ewen, R. L.: Hydrogen Film Cooling Investigation. NASA CR-121235, Aerojet Liquid Rocket Co., August 1973.

104. Williams, J. J.: The Effect of Gaseous Film Cooling on the Recovery Temperature Distribution in Rocket Nozzles. PhD Thesis, University of California at Davis, May 1969.

105. Rousar, D. C.; and Ewen, R. L.: Combustion Effects on Film Cooling. NASA CR-135052, Aerojet Liquid Rocket Co., Feb. 24, 1977.

106. Gater, R. A.; L'Ecuyer, M. R.; and Warner, C. F.: Liquid-Film Cooling: Its Physical Nature and Theoretical Analysis. Rep. TM-65-6, Jet Propulsion Center, Purdue University, October 1965.

107. Gater, R. A.; and L'Ecuyer, M. R.: A Fundamental Investigation of the Phenomena that Characterized Liquid-Film Cooling. Rep. TM-69-1, Jet Propulsion Center, Purdue University, January 1969.

108. Stechman, R. C.; Oberstone, J.; and Howell, J. C.: Film Cooling Design Criteria for Small Rocket Engines. Paper No. 68-617, AIAA 4th Propulsion Joint Specialist Conference, (Cleveland, OH), June 1968.

109. Manson, S. S.: Thermal Stress and Low-Cycle Fatigue. McGraw-Hill Book Co. (New York), 1966.

110. Anon.: Liquid Rocket Engine Fluid-Cooled Combustion Chambers. NASA Space Vehicle Design Criteria Monograph, NASA SP-8087, April 1972.

111. Back, L. H.; and Witte, A. B.: Prediction of Heat Transfer from Laminar Boundary Layers with Emphasis on Large Freestream Velocity Gradients and Highly Cooled Wall. Rep. 32-728, Jet Propulsion Lab., Calif. Inst. Tech., June 1, 1965.

112. Svehla, R. A.; and McBride, B. J.: FORTRAN IV Computer Program for Calculation of Thermodynamic and Transport Properties of Complex Chemical Systems. NASA TN D-7056, January 1973.

NASA SPACE VEHICLE DESIGN CRITERIA MONOGRAPHS ISSUED TO DATE

ENVIRONMENT

SP-8005	Solar Electromagnetic Radiation, Revised May 1971
SP-8010	Models of Mars Atmosphere (1974), Revised December 1974
SP-8011	Models of Venus Atmosphere (1972), Revised September 1972
SP-8013	Meteoroid Environment Model–1969 (Near Earth to Lunar Surface), March 1969
SP-8017	Magnetic Fields–Earth and Extraterrestrial, March 1969
SP-8020	Surface Models of Mars (1975), Revised September 1975
SP-8021	Models of Earth's Atmosphere (90 to 2500 km), Revised March 1973
SP-8023	Lunar Surface Models, May 1969
SP-8037	Assessment and Control of Spacecraft Magnetic Fields, September 1970
SP-8038	Meteoroid Environment Model–1970 (Interplanetary and Planetary), October 1970
SP-8049	The Earth's Ionosphere, March 1971
SP-8067	Earth Albedo and Emitted Radiation, July 1971
SP-8069	The Planet Jupiter (1970), December 1971
SP-8084	Surface Atmospheric Extremes (Launch and Transportation Areas), Revised June 1974
SP-8085	The Planet Mercury (1971), March 1972
SP-8091	The Planet Saturn (1970), June 1972
SP-8092	Assessment and Control of Spacecraft Electromagnetic Interference, June 1972

SP-8103	The Planets Uranus, Neptune, and Pluto (1971), November 1972
SP-8105	Spacecraft Thermal Control, May 1973
SP-8111	Assessment and Control of Electrostatic Charges, May 1974
SP-8116	The Earth's Trapped Radiation Belts, March 1975
SP-8117	Gravity Fields of the Solar System, April 1975
SP-8118	Interplanetary Charged Particle Models (1974), March 1975
SP-8122	The Environment of Titan (1975), July 1976

STRUCTURES

SP-8001	Buffeting During Atmospheric Ascent, Revised November 1970
SP-8002	Flight-Loads Measurements During Launch and Exit, December 1964
SP-8003	Flutter, Buzz, and Divergence, July 1964
SP-8004	Panel Flutter, Revised June 1972
SP-8006	Local Steady Aerodynamic Loads During Launch and Exit, May 1965
SP-8007	Buckling of Thin-Walled Circular Cylinders, Revised August 1968
SP-8008	Prelaunch Ground Wind Loads, November 1965
SP-8009	Propellant Slosh Loads, August 1968
SP-8012	Natural Vibration Modal Analysis, September 1968
SP-8014	Entry Thermal Protection, August 1968
SP-8019	Buckling of Thin-Walled Truncated Cones, September 1968
SP-8022	Staging Loads, February 1969
SP-8029	Aerodynamic and Rocket-Exhaust Heating During Launch and Ascent, May 1969
SP-8030	Transient Loads From Thrust Excitation, February 1969
SP-8031	Slosh Suppression, May 1969

SP-8032	Buckling of Thin-Walled Doubly Curved Shells, August 1969
SP-8035	Wind Loads During Ascent, June 1970
SP-8040	Fracture Control of Metallic Pressure Vessels, May 1970
SP-8042	Meteoroid Damage Assessment, May 1970
SP-8043	Design-Development Testing, May 1970
SP-8044	Qualification Testing, May 1970
SP-8045	Acceptance Testing, April 1970
SP-8046	Landing Impact Attenuation for Non-Surface-Planing Landers, April 1970
SP-8050	Structural Vibration Prediction, June 1970
SP-8053	Nuclear and Space Radiation Effects on Materials, June 1970
SP-8054	Space Radiation Protection, June 1970
SP-8055	Prevention of Coupled Structure-Propulsion Instability (Pogo), October 1970
SP-8056	Flight Separation Mechanisms, October 1970
SP-8057	Structural Design Criteria Applicable to a Space Shuttle, Revised March 1972
SP-8060	Compartment Venting, November 1970
SP-8061	Interaction with Umbilicals and Launch Stand, August 1970
SP-8062	Entry Gasdynamic Heating, January 1971
SP-8063	Lubrication, Friction, and Wear, June 1971
SP-8066	Deployable Aerodynamic Deceleration Systems, June 1971
SP-8068	Buckling Strength of Structural Plates, June 1971
SP-8072	Acoustic Loads Generated by the Propulsion System, June 1971
SP-8077	Transportation and Handling Loads, September 1971

SP-8079	Structural Interaction with Control Systems, November 1971
SP-8082	Stress-Corrosion Cracking in Metals, August 1971
SP-8083	Discontinuity Stresses in Metallic Pressure Vessels, November 1971
SP-8095	Preliminary Criteria for the Fracture Control of Space Shuttle Structures, June 1971
SP-8099	Combining Ascent Loads, May 1972.
SP-8104	Structural Interaction With Transportation and Handling Systems, January 1973
SP-8108	Advanced Composite Structures, December 1974

GUIDANCE AND CONTROL

SP-8015	Guidance and Navigation for Entry Vehicles, November 1968
SP-8016	Effects of Structural Flexibility on Spacecraft Control Systems, April 1969
SP-8018	Spacecraft Magnetic Torques, March 1969
SP-8024	Spacecraft Gravitational Torques, May 1969
SP-8026	Spacecraft Star Trackers, July 1970
SP-8027	Spacecraft Radiation Torques, October 1969
SP-8028	Entry Vehicle Control, November 1969
SP-8033	Spacecraft Earth Horizon Sensors, December 1969
SP-8034	Spacecraft Mass Expulsion Torques, December 1969
SP-8036	Effects of Structural Flexibility on Launch Vehicle Control Systems, February 1970
SP-8047	Spacecraft Sun Sensors, June 1970
SP-8058	Spacecraft Aerodynamic Torques, January 1971
SP-8059	Spacecraft Attitude Control During Thrusting Maneuvers, February 1971

SP-8065	Tubular Spacecraft Booms (Extendible, Reel Stored), February 1971
SP-8070	Spaceborne Digital Computer Systems, March 1971
SP-8071	Passive Gravity-Gradient Libration Dampers, February 1971
SP-8074	Spacecraft Solar Cell Arrays, May 1971
SP-8078	Spaceborne Electronic Imaging Systems, June 1971
SP-8086	Space Vehicle Displays Design Criteria, March 1972
SP-8096	Space Vehicle Gyroscope Sensor Applications, October 1972
SP-8098	Effects of Structural Flexibility on Entry Vehicle Control Systems, June 1972
SP-8102	Space Vehicle Accelerometer Applications, December 1972

CHEMICAL PROPULSION

SP-8089	Liquid Rocket Engine Injectors, March 1976
SP-8087	Liquid Rocket Engine Fluid-Cooled Combustion Chambers, April 1972
SP-8113	Liquid Rocket Engine Combustion Stabilization Devices, November 1974
SP-8120	Liquid Rocket Engine Nozzles, July 1976
SP-8107	Turbopump Systems for Liquid Rocket Engines, August 1974
SP-8109	Liquid Rocket Engine Centrifugal Flow Turbopumps, December 1973
SP-8052	Liquid Rocket Engine Turbopump Inducers, May 1971
SP-8110	Liquid Rocket Engine Turbines, January 1974
SP-8081	Liquid Propellant Gas Generators, March 1972
SP-8048	Liquid Rocket Engine Turbopump Bearings, March 1971
SP-8101	Liquid Rocket Engine Turbopump Shafts and Couplings, September 1972
SP-8100	Liquid Rocket Engine Turbopump Gears, March 1974

SP-8088	Liquid Rocket Metal Tanks and Tank Components, May 1974
SP-8094	Liquid Rocket Valve Components, August 1973
SP-8097	Liquid Rocket Valve Assemblies, November 1973
SP-8090	Liquid Rocket Actuators and Operators, May 1973
SP-8119	Liquid Rocket Disconnects, Couplings, Fittings, Fixed Joints, and Seals, September 1976
SP-8123	Liquid Rocket Lines, Bellows, Flexible Hoses, and Filters, April 1977
SP-8112	Pressurization Systems for Liquid Rockets, October 1975
SP-8080	Liquid Rocket Pressure Regulators, Relief Valves, Check Valves, Burst Disks, and Explosive Valves, March 1973
SP-8064	Solid Propellant Selection and Characterization, June 1971
SP-8075	Solid Propellant Processing Factors in Rocket Motor Design, October 1971
SP-8076	Solid Propellant Grain Design and Internal Ballistics, March 1972
SP-8073	Solid Propellant Grain Structural Integrity Analysis, June 1973
SP-8039	Solid Rocket Motor Performance Analysis and Prediction, May 1971
SP-8051	Solid Rocket Motor Igniters, March 1971
SP-8025	Solid Rocket Motor Metal Cases, April 1970
SP-8093	Solid Rocket Motor Internal Insulation, December 1976
SP-8115	Solid Rocket Motor Nozzles, June 1975
SP-8114	Solid Rocket Thrust Vector Control, December 1974
SP-8041	Captive-Fired Testing of Solid Rocket Motors, March 1971

NASA-Langley, 1978